



# Contrôle et stabilité Entrée-Etat en dimension infinie du profil du facteur de sécurité dans un plasma Tokamak

Federico Bribiesca Argomedo

## ► To cite this version:

Federico Bribiesca Argomedo. Contrôle et stabilité Entrée-Etat en dimension infinie du profil du facteur de sécurité dans un plasma Tokamak. Autre. Université de Grenoble, 2012. Français. NNT : 2012GRENT023 . tel-00920942

**HAL Id: tel-00920942**

**<https://theses.hal.science/tel-00920942>**

Submitted on 19 Dec 2013

**HAL** is a multi-disciplinary open access archive for the deposit and dissemination of scientific research documents, whether they are published or not. The documents may come from teaching and research institutions in France or abroad, or from public or private research centers.

L'archive ouverte pluridisciplinaire **HAL**, est destinée au dépôt et à la diffusion de documents scientifiques de niveau recherche, publiés ou non, émanant des établissements d'enseignement et de recherche français ou étrangers, des laboratoires publics ou privés.

## THÈSE

Pour obtenir le grade de

## DOCTEUR DE L'UNIVERSITÉ DE GRENOBLE

Spécialité : **Automatique et Productique**

Arrêté ministériel : 7 août 2006

Présentée par

**Federico BRIBIESCA ARGOMEDO**

Thèse dirigée par **Christophe PRIEUR**  
et coencadrée par **Emmanuel WITRANT**

préparée au sein du laboratoire **GIPSA-Lab**,  
et de l'école doctorale **Électronique, Électrotechnique, Automatique et  
Traitement du Signal**.

## Infinite Dimensional Control and Input-to-State Stability of the Safety Factor Profile in a Tokamak Plasma

*Contrôle et Stabilité Entrée-État en Dimension Infinie du Profil  
du Facteur de Sécurité dans un Plasma Tokamak*

Thèse soutenue publiquement le **12 septembre 2012**,  
devant le jury composé de :

**Thierry GALLAY**, Président

Professeur, UJF, Institut Fourier (Grenoble, France)

**Hans ZWART**, Rapporteur

Professeur, Université de Twente (Enschede, Pays-Bas)

**Jacques BLUM**, Rapporteur

Professeur, Université de Nice-Sophia-Antipolis, Laboratoire J.-A. Dieudonné  
(Nice, France)

**Jonathan B. LISTER**, Examineur

Matre d'enseignement et de recherche, CRPP, EPFL (Lausanne, Suisse)

**Sylvain BRÉMOND**, Examineur

Chef du Groupe Pilotage Asservissement et Scénarios, IRFM, CEA Cadarache  
(Saint Paul lez Durance, France)

**Christophe PRIEUR**, Directeur de thèse

Directeur de Recherche, CNRS, GIPSA-Lab (Grenoble, France)

**Emmanuel WITRANT**, Co-Encadrant de thèse

Maître de Conférences, UJF, GIPSA-Lab (Grenoble, France)





# Résumé détaillé en français

## Contexte et motivation

Dans la recherche de sources d'énergie sûres et propres qui n'utilisent pas de combustibles fossiles, un grand effort a été consacré au développement de la fusion thermonucléaire contrôlée. Elle consiste en la fusion à très haute température de deux noyaux atomiques légers en produire un plus lourd. En particulier, les expériences actuelles (et planifiées) sont basées sur la fusion de deux isotopes d'hydrogène: deutérium et tritium. L'abondance naturelle du deutérium et la possibilité de produire du tritium à partir de lithium (qui est assez abondant) impliquent que les réserves potentielles de combustible pour la production d'énergie par fusion pourraient satisfaire la demande énergétique globale pendant des milliers d'années (aux niveaux actuels) [[Wesson, 2004](#)].

Comme toutes les sources d'énergie nucléaire, l'absence d'émissions de carbone est un avantage important de la fusion nucléaire. De plus, la sûreté inhérente à la réaction de fusion (au contraire de la fission nucléaire) et le traitement comparativement simple des déchets radioactifs (puisque seulement les composants structurels qui se trouvent proches de la réaction de fusion sont activés et doivent être stockés pendant quelques décennies avant d'être recyclés) font de cette forme de production d'énergie une alternative très intéressante.

Bien que l'idée de la fusion nucléaire soit très attractive, produire et maintenir la réaction n'est pas simple. Pour fusionner deux noyaux atomiques (avec une charge électrique positive), la force électrostatique qui les sépare doit être vaincue (barrière de Coulomb). Cela est fait en réchauffant le combustible à des températures très élevées (ce qui a pour effet de ioniser les atomes d'hydrogène, formant un plasma). Une fois que les atomes ont assez d'énergie pour surpasser la barrière de Coulomb il faut encore qu'une proportion suffisante d'atomes soit fusionnée pour produire un gain net d'énergie. Pour faire cela (d'une façon techniquement faisable) deux approches principales ont été développées:

- réchauffer le combustible pour obtenir un plasma à haute densité avec un temps de confinement relativement court (principe du confinement inertiel)

- 
- réchauffer le combustible pour obtenir un plasma de basse densité mais avec un temps de confinement assez long (principe du confinement magnétique).

En vue du projet ITER [ITER Organization, 2010] en cours de construction à Cadarache, le confinement magnétique et, particulièrement, les tokamaks seront l'objet de cette thèse.

Un tokamak consiste d'une chambre toroïdale recouverte de bobines magnétiques qui génèrent un champ magnétique très fort avec des composantes poloïdales et toroïdales. Dans cette chambre, le plasma de deuterium-tritium circule pour que la réaction de fusion ait lieu (une explication détaillée de la physique des tokamaks est donnée dans [Wesson, 2004]).

L'opération des tokamaks présente plusieurs problèmes de contrôle très importants, voir par exemple [Pironti and Walker, 2005], [Walker et al., 2006], [Walker et al., 2008], [Ariola and Pironti, 2008]. La plupart de la littérature sur le contrôle des tokamaks portait sur un ou plusieurs paramètres scalaires (par exemple la forme, la position, le courant total, la densité moyenne). En particulier [Ariola and Pironti, 2008] étudie la plupart de ces problèmes.

Pour travailler dans des modes dits avancés dans un tokamak (voir par exemple [Taylor, 1997], [Gormezano, 1999], [Wolf, 2003]) il est désirable d'avoir un contrôle plus fin de certaines variables. En particulier, le contrôle des profils de température et courant peut s'avérer nécessaire. étant donné le degré d'incertitude dans la reconstruction en ligne des profils et mesures, aussi bien que dans la modélisation des phénomènes de transport à l'intérieur du plasma, le contrôle des profils internes devient assez difficile et requiert des approches de contrôle très robustes.

## Problème de contrôle et travaux précédents

Dans cette thèse, on s'intéresse au contrôle du profil de facteur de sécurité. Le facteur de sécurité est déterminé par la relation entre les deux composantes du champ magnétique. Cette variable physique est liée à l'apparition de plusieurs phénomènes dans le plasma. En particulier des instabilités magnétohydrodynamiques (MHD). Il est particulièrement important d'avoir un profil de facteur de sécurité adéquat pour l'opération avancée du tokamak (produisant un haut degré de confinement et stabilité MHD). Pour faire cela, on tâchera de contrôler le profil de flux magnétique poloidal (et en particulier son gradient). Ceci est un problème difficile à cause de plusieurs facteurs:

- l'évolution de la variable physique à contrôler est gouvernée par la diffusion résistive du flux magnétique, qui est modélisée par une équation aux dérivées partielles de

---

type parabolique, avec des coefficients répartis et variant rapidement dans le temps qui dépendent de la solution d'une autre équation liée au transport de la chaleur;

- bien que l'action soit distribuée dans le domaine spatial, des contraintes de forme non-linéaires sont imposées (avec seulement quelques paramètres disponibles pour la commande);
- des termes sources non-linéaires sont présents dans l'équation d'évolution (en particulier un courant auto-induit appelé courant de bootstrap);
- des incertitudes importantes existent sur la plupart de mesures, estimations et modèles.

Le problème de control du profil de flux magnétique poloidal est fortement lié au problème de contrôle du profil de courant (via les équations de Maxwell). Quelques travaux existants montrent la possibilité de contrôler des paramètres de forme du profil de courant. Par exemple, pour Tore Supra: [Wijnands et al., 1997] caractérise la forme du profil de courant par l'inductance interne et le facteur de sécurité au centre du plasma; [Barana et al., 2007] où le contrôle de la largeur du dépôt de courant par l'antenne hybride est montré et validé expérimentalement. [Imbeaux et al., 2011] propose un contrôle discret temps-réel du profil de facteur de sécurité en régime stationnaire, en considérant quelques modes possibles d'opération. D'autres travaux considèrent la nature distribuée du système et utilisent des modèles discrétisés identifiés autour d'un point d'opération. Quelques exemples de ces approches peuvent être trouvés dans [Laborde et al., 2005], où un modèle basé sur une projection de Galerkin est utilisé pour contrôler des profils multiples sur JET; [Moreau et al., 2009], où un modèle d'ordre réduit est utilisé pour contrôler quelques points sur le profil de facteur de sécurité; [Moreau et al., 2011], où l'application de ces méthodes d'identification et de contrôle à plusieurs tokamaks est présentée; ou encore [Ou et al., 2010], où un régulateur robuste est construit, basé sur une décomposition de type Galerkin en supposant des coefficients de diffusion fixes qui sont seulement multipliés par une variable scalaire.

Des contributions spécifiques de la communauté automatique ont commencé à apparaître aussi, basées sur des modèles simplifiés qui capturent la nature distribuée du système. Quelques exemples sont [Ou et al., 2008], où un contrôle optimal est développé pour le profil de courant de DIII-D; [Felici and Sauter, 2012], où des techniques d'optimisation non-linéaire sont utilisées pour trouver des trajectoires optimales pour la commande en boucle ouverte des profils du plasma. Pour des exemples en boucle fermée, [Ou et al., 2011] et d'autres travaux utilisent un modèle décrit par des équations aux dérivées partielles (EDPs) pour construire un régulateur optimale pour le profil de courant en considérant des profils fixes pour les actionneurs et profils de diffusion. D'autres approches EDP liés à Tore Supra peuvent être mentionnés: [Gahlawat et al.,

---

2011], où des polynômes de type somme de carrés sont utilisés pour construire une fonction de Lyapunov en considérant les profils de diffusion constants, [Gaye et al., 2011], où un contrôleur de type modes glissants est construit pour le système en dimension infinie, avec des profils de diffusion constants.

## Principales contributions

Les principales contributions de cette thèse sont:

- l'illustration de quelques méthodes de contrôle qui résultent de la discrétisation du modèle distribué avant la conception d'une loi de commande et ses limites inhérents;
- l'utilisation d'un modèle simplifié, physiquement pertinent, en dimension infinie pour le développement d'une loi de commande distribuée pour la stabilisation du gradient du flux magnétique poloïdal (et donc du facteur de sécurité) à l'aide des antennes hybrides (LH) avec une attention particulière aux effets de la variation temporelle des coefficients et à la possible extension à d'autres sources non-inductives arbitraires;
- la prise en considération des profils de diffusion variants dans le temps dans la conception de la loi de contrôle, garantissant la stabilité du système et sa robustesse par rapport à plusieurs sources communes d'erreur et à des dynamiques non-modélisées;
- l'inclusion de couplages négligés entre le courant total du plasma et le contrôle du profil de flux magnétique;
- l'application de méthodes d'optimisation en temps-réel qui incluent des contraintes non-linéaires imposées par les profils de dépôt de courant tout en gardant la stabilité et robustesse garanties de façon théorique;
- la validation de l'approche de contrôle proposée en utilisant le code METIS [Artaud, 2008] (un module du code CRONOS, adapté à des simulations en boucle-fermée [Artaud et al., 2010]) pour la configuration Tore Supra;
- l'addition (en simulation) des délais de reconstruction des profils dans la boucle de contrôle;
- l'extension de l'approche de contrôle proposée à TCV en utilisant des actionneurs de fréquence cyclotronique-électronique (FCE) et la simulation en utilisant le code RAPTOR [Felici et al., 2011].

---

# Plan

Cette thèse est organisée comme suit:

- le Chapitre 2 contient le modèle distribué qui est utilisé tout au long de cette thèse aussi que les principales hypothèses physiques nécessaires pour les simplifications réalisées.
- Le Chapitre 3 présente deux approches de contrôle basées sur la discrétisation spatiale du système distribué présenté dans le Chapitre 2. La première approche néglige la nature temps-variante du système et met simplement à jour un régulateur linéaire quadratique en utilisant les valeurs estimées de certains variables physiques (principalement la résistivité du plasma). La deuxième approche prend en compte le caractère temps-variant des profils de diffusivité et utilise des inégalités linéaires matricielles avec une structure linéaire à paramètres variants polytopique pour calculer des régulateurs qui stabilisent le système pour des variations extrêmes des paramètres (les sommets du polytope). Bien que cette approche prenne en compte les variations des profils de diffusivité, l'extension au contrôle du gradient du profil de flux magnétique n'est pas directe.
- Le Chapitre 4 contient la contribution principale de cette thèse: une fonction de Lyapunov stricte développée pour le système distribué en boucle-ouverte, ce qui permet de construire des lois de commande fortement contraintes qui préservent la stabilité du système tout en modifiant le gain entrée-état entre les différentes perturbations et le gradient du profil de flux magnétique. Quelques fonctions de Lyapunov alternatives sont présentées avec leurs inconvénients pour motiver la forme finale choisie pour la fonction de Lyapunov utilisée dans la suite de la thèse.
- Le Chapitre 5 contient l'extension du schéma de contrôle proposé, basé sur la fonction de Lyapunov construite, pour prendre en compte l'important couplage qui existe entre la puissance hybride et le courant total du plasma dans le tokamak. Des simulations avancées en utilisant le code METIS sont présentées pour illustrer la robustesse du schéma de contrôle par rapport aux différences entre le modèle de référence et le modèle réel, ainsi que d'autres actionneurs qui agissent en tant que source de perturbations (représentée, par exemple, par une injection de puissance à la fréquence cyclotronique-ionique) et délais de reconstruction des profils. Finalement, la flexibilité de l'approche est illustrée avec une application à TCV en utilisant les antennes cyclotroniques-électroniques et simulée sur le code RAPTOR [Felici et al., 2011].



<i>Variables</i>	<i>Description</i>	<i>Unités</i>
$\psi$	Profil de flux magnétique poloïdal	$Tm^2$
$\phi$	Profil de flux magnétique toroïdal	$Tm^2$
$q$	Profil de facteur de sécurité $q \doteq d\phi/d\psi$	
$R_0$	Localisation du centre magnétique	$m$
$B_{\phi_0}$	Champ magnétique toroïdal au centre du plasma	$T$
$\rho$	Rayon équivalent des surfaces magnétiques	$m$
$a$	Petit rayon de la dernière surface magnétique fermée	$m$
$r$	Variable spatiale normalisée $r \doteq \rho/a$	
$t$	Temps	$s$
$V$	Volume du plasma	$m^3$
$F$	Fonction diamagnétique	$Tm$
$C_2, C_3$	Coefficients géométriques	
$\eta_{\parallel}$	Resistivité parallèle	$\Omega m$
$\eta$	Coefficient de diffusivité normalisé $\eta_{\parallel}/\mu_0 a^2$	
$\mu_0$	Permeabilité du vide: $4\pi \times 10^{-7}$	$Hm^{-1}$
$\bar{n}$	Densité électronique moyenne	$m^{-3}$
$j_{ni}$	Densité de courant non-inductive effective	$Am^{-2}$
$j$	Densité de courant non-inductive effective normalisée $\mu_0 a^2 R_0 j_{ni}$	
$I_p$	Courant total du plasma	$A$
$V_{loop}$	Tension par tour	$V$
$\eta_{lh}$	Efficacité du coupleur hybride	$Am^{-2}W^{-1}$
$P_{lh}$	Puissance de l'antenne hybride	$W$
$N_{\parallel}$	Indice de réfraction parallèle de l'onde hybride	
$I_{\Omega}$	Courant ohmique	$A$
$V_{\Omega}$	Tension ohmique	$V$

Table 1: Définition des variables physiques

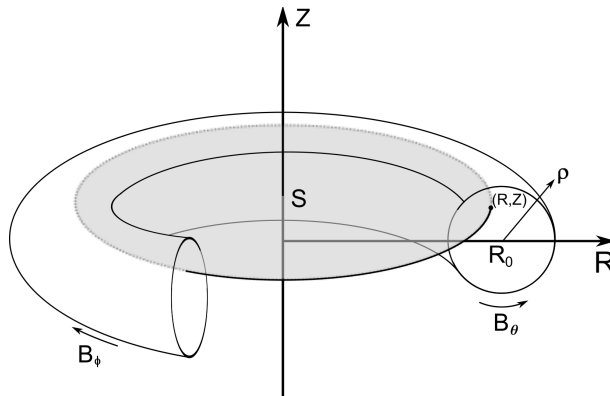


Figure 1: Coordonées  $(R, Z)$  et surface  $S$  utilisées pour définir le flux magnétique toroïdal  $\psi(R, Z)$ .

---

## Modèle de référence

Le flux magnétique toroïdal  $\psi(R, Z)$  est défini comme le flux par radian du champ magnétique  $\mathbf{B}(R, Z)$  qui passe à travers un disque centré sur l'axe toroïdal à une hauteur  $Z$ , ayant un rayon  $R$  et une surface  $\mathbf{S}$ , comme le montre la Fig. 1. Un modèle 1D simplifié pour ce profil de flux magnétique poloïdal est considéré. Sa dynamique est donnée par [Blum, 1989]:

$$\frac{\partial \psi}{\partial t} = \frac{\eta_{\parallel} C_2}{\mu_0 C_3} \frac{\partial^2 \psi}{\partial \rho^2} + \frac{\eta_{\parallel} \rho}{\mu_0 C_3^2} \frac{\partial}{\partial \rho} \left( \frac{C_2 C_3}{\rho} \right) \frac{\partial \psi}{\partial \rho} + \frac{\eta_{\parallel} V_{\rho} B_{\phi_0}}{F C_3} j_{ni} \quad (0.0.1)$$

où  $\rho \doteq \sqrt{\frac{\phi}{\pi B_{\phi_0}}}$  est un rayon équivalent qui indice les surfaces magnétiques,  $\phi$  est le flux magnétique toroïdal,  $B_{\phi_0}$  le champ magnétique toroïdal au centre du plasma,  $\eta_{\parallel}$  est la résistivité parallèle du plasma, le terme source  $j_{ni}$  représente le profil de densité de courant généré par les sources de courant non-inductives,  $\mu_0$  est la perméabilité du vide,  $F$  est la fonction diamagnétique,  $V_{\rho}$  est la dérivée spatiale du volume de plasma contenu dans la surface magnétique d'indice  $\rho$ . Les principales variables physiques sont présentées dans le Tableau 1. Les coefficients  $C_2$  and  $C_3$  sont définis comme:

$$\begin{aligned} C_2(\rho) &= V_{\rho} \left\langle \frac{\|\rho\|^2}{R^2} \right\rangle \\ C_3(\rho) &= V_{\rho} \left\langle \frac{1}{R^2} \right\rangle \end{aligned}$$

où  $\langle \cdot \rangle$  représente une moyenne sur la surface isoflux d'indice  $\rho$ . En négligeant l'effet diamagnétique provoqué par les courants poloidaux et en utilisant une approximation cylindrique de la géométrie du plasma ( $\rho \ll R_0$ , où  $R_0$  est le rayon majeur du plasma) les coefficients peuvent être simplifiés comme:

$$F \approx R_0 B_{\phi_0}, \quad C_2 = C_3 = 4\pi^2 \frac{\rho}{R_0}, \quad V_{\rho} = 4\pi^2 \rho R_0$$

En définissant une variable spatiale normalisée  $r = \frac{\rho}{a}$ , où  $a$  (supposé constante) est le rayon équivalent de la dernière surface magnétique fermée, le modèle simplifié est obtenu comme dans [Witrant et al., 2007; Artaud et al., 2010]:

$$\frac{\partial \psi}{\partial t}(r, t) = \frac{\eta_{\parallel}(r, t)}{\mu_0 a^2} \left( \frac{\partial^2 \psi}{\partial r^2} + \frac{1}{r} \frac{\partial \psi}{\partial r} \right) + \eta_{\parallel}(r, t) R_0 j_{ni}(r, t) \quad (0.0.2)$$

avec conditions aux bords:

$$\frac{\partial \psi}{\partial r}(0, t) = 0 \quad (0.0.3)$$

et

$$\frac{\partial \psi}{\partial r}(1, t) = -\frac{R_0 \mu_0 I_p(t)}{2\pi} \quad \text{ou} \quad \frac{\partial \psi}{\partial t}(1, t) = V_{loop}(t) \quad (0.0.4)$$

où  $I_p$  est le courant total du plasma et  $V_{loop}$  est la tension par tour toroïdal, avec condition initiale:

$$\psi(r, t_0) = \psi_0(r)$$

---

# Principaux résultats

## Chapitre 3

Dans ce chapitre, on considère le problème de contrôle d’une version discrétisée du modèle de diffusion du flux magnétique. Ce modèle a été discrétisé spatialement, pour la commande, en utilisant un schéma de différences finies. La discrétisation complète (en temps et espace) du système utilisé à des fins de simulation est détaillé dans [Witrant et al., 2007]. Dans un premier pas, on se concentrera sur le contrôle du profil de flux magnétique. Après discrétisation, deux approches différentes sont présentées.

Dans la première section, on vise à contrôler un modèle linéaire temps-variant avec un régulateur linéaire quadratique mis à jour à chaque pas de temps. Ceci est fait pour tester l’efficacité d’une approche quasi-statique pour la conception d’un contrôle par retour d’états. Des contraintes de forme sont rajoutées en linéarisant les profils de dépôt de courant autour d’un équilibre en considérant trois paramètres disponibles (correspondant aux trois paramètres habituels dans une distribution gaussienne) pour le contrôle de la forme du dépôt de courant non-inductif. Cette section est basée sur [Bribiesca Argomedeo et al., 2010].

Dans la deuxième section, un régulateur linéaire à paramètres variants polytopique a été conçu pour prendre en compte le comportement transitoire des coefficients de diffusion dans la construction de la loi de commande (sur le système discrétisé). A travers un changement de variables, le caractère temps-variant de la matrice  $B$  est enlevé pour nous permettre de formuler une loi de commande qui permet de stabiliser le système (étendu avec un intégrateur à la sortie) composée d’une combinaison linéaire de régulateurs calculés pour les variations extrêmes des paramètres. Cette section est basée sur [Bribiesca Argomedeo et al., 2011].

## Chapitre 4

Dans ce chapitre, la notion de stabilité entrée-état sera le cadre choisi pour étudier la stabilité et robustesse d’une équation de diffusion dans un domaine circulaire sous une condition de symétrie. L’intérêt d’étudier cette équation est illustré par l’application proposée, où une équation similaire provient d’une équation physique en 2D moyennée sur des surfaces isoflux. La stabilité entrée-état veut dire, principalement, garantir un gain borné entre une norme des entrées (qui peuvent être aussi des perturbations) et la norme des états du système. Une référence complète sur des résultats de stabilité entrée-état (ISS), en dimension finie, peut être trouvé dans [Sontag, 2008]. Des propriétés de type ISS en dimension infinie peuvent se trouver dans [Jayawardhana et al., 2008]. Néanmoins on a préféré une approche basée sur des fonctions de Lyapunov qui permet

---

le traitement de perturbations et erreurs assez générales.

Bien que l'utilisation de fonctions de Lyapunov dans un cadre en dimension infinie ne soit pas nouveau (voir par exemple [Baker and Bergen, 1969]), il est encore un sujet de recherche actif. Quelques résultats pour des équations paraboliques sont [Cazenave and Haraux, 1998], où une fonction de Lyapunov est utilisée pour prouver l'existence d'une solution globale pour l'équation de la chaleur; [Krstic and Smyshlyaev, 2008], où une fonction de Lyapunov est construite pour l'équation de la chaleur avec des paramètres déstabilisants inconnus. Les approches de type Lyapunov sont aussi utilisées pour d'autres types d'équations, par exemple [Coron and d'Andréa Novel, 1998] pour la stabilisation d'une poutre rotative; dans [Coron et al., 2008] pour l'analyse de stabilité de systèmes quasi-linéaires hyperboliques et, dans [Coron et al., 2007] pour la construction de lois de commande stabilisantes pour un système de lois de conservation. En particulier, dans [Mazenc and Prieur, 2011] et [Prieur and Mazenc, 2012] l'intérêt d'utiliser une fonction de Lyapunov stricte pour obtenir des propriétés de type ISS est abordé dans le cas parabolique et hyperbolique, respectivement. L'utilisation de normes  $L^2$  à poids ou d'expressions similaires n'est pas nouveau et quelques exemples sont [Peet et al., 2009] (pour des systèmes à retards) et [Gahlawat et al., 2011] (où un poids est utilisé pour le contrôle de l'équation du flux magnétique dans un tokamak, mais pas son gradient). Quelques travaux sur d'équations de réaction-diffusion dans des domaines cylindriques en 2D sont, par exemple, [Vazquez and Krstic, 2006] et [Vazquez and Krstic, 2010], où des lois de commande frontière sont développées pour la stabilisation de boucles de convection thermique. Cependant, dans ce deux cas, le domaine considéré n'inclut pas le point  $r = 0$ .

Dans ce chapitre, on développe une fonction de Lyapunov stricte pour l'équation de diffusion avec un ensemble admissible de coefficients de diffusion. Notre contribution principale est que les coefficients peuvent être distribués et temps-variants sans imposer des contraintes sur la vitesse de variation des coefficients. Ceci représenté un avantage sur d'autres méthodes qui considèrent des profils de diffusivité distribués ou temps-variants mais pas simultanément. Des exemples de ces approches peuvent être trouvés dans [Smyshlyaev and Krstic, 2004], [Smyshlyaev and Krstic, 2005], [Vazquez and Krstic, 2008]. D'autre part, des résultats de stabilité et robustesse sont obtenus pour une loi de commande simple qui considère les sources d'erreur suivantes:

- *perturbations sur l'état*: représentant, par exemple, des dynamiques non-modélisées;
- *erreurs d'actuation*: représentant des erreurs dans les modèles d'actionneur (similaire au concept de fragilité de la commande);
- *erreurs d'estimation dans l'état et coefficients de diffusivité* : correspondant par exemple à des mesures discrétisées ou des modèles incertains ou bruit de mesure.

---

## Chapitre 5

Les principaux objectifs de ce chapitre sont:

- l'introduction d'un modèle simplifié pour l'évolution de la condition au bord (fonction du courant total de plasma) qui considère le couplage entre la puissance hybride et le courant du plasma;
- l'utilisation de ce modèle simplifié pour explorer le possible impact des couplages sur la stabilité du système (voir Figure 2);
- l'implémentation de la loi de commande développée dans le Chapitre 4 en simulation, avec le code METIS;
- la simulation de l'effet des délais de reconstruction de jusqu'à 100ms (basés sur la période de calcul dans [Blum et al., 2012]);
- l'extension de la loi de commande du Chapitre 4 en simulation avec le code RAPTOR à des scénarios TCV.

Dans la première section de ce chapitre, on présente un modèle étendu pour le système qui prend en compte l'équation de diffusion résistive qui gouverne le flux magnétique poloïdal (système en dimension infinie) et aussi les couplages qui existent entre la puissance hybride injectée au système et la condition au bord donnée par le courant total du plasma (système dynamique en dimension finie). Le comportement dynamique du système en dimension finie est approximé en utilisant un modèle de transformateur comme proposé dans [Kazarian-Vibert et al., 1996].

Puisque l'antenne LH est utilisée comme entrée de commande pour le système en dimension infinie et les valeurs des paramètres ingénieur sont calculés seulement par leur impact sur ce sous-système, il est nécessaire maintenant d'étudier leur impact sur le système interconnecté. Cela pourrait être difficile car dans le Chapitre 4 on n'a pas obtenu des inégalités ISS pour le système par rapport aux perturbations sur la condition au bord (seulement  $D^1$ ISS). Cependant, avec l'introduction d'une hypothèse physique (liée à la densité totale de courant sur la dernière surface magnétique fermée) on peut développer des inégalités ISS (plus fortes). Le système interconnecté est représenté sur la Figure 2.

Basé sur le temps de calcul pris par la reconstruction des profils dans [Blum et al., 2012], la loi de commande proposée a été testée en simulation sur METIS, avec des paramètres de Tore Supra et avec un délai de reconstruction de 100 ms pour le calcul de la commande. Les résultats sont présentés sur la Figure 3. Les paramètres de l'algorithme de commande ont été choisis pour éviter des dépassements et oscillations dans la réponse du système. Le gain a été limité pour éviter des problèmes dus au retard. Malgré ce

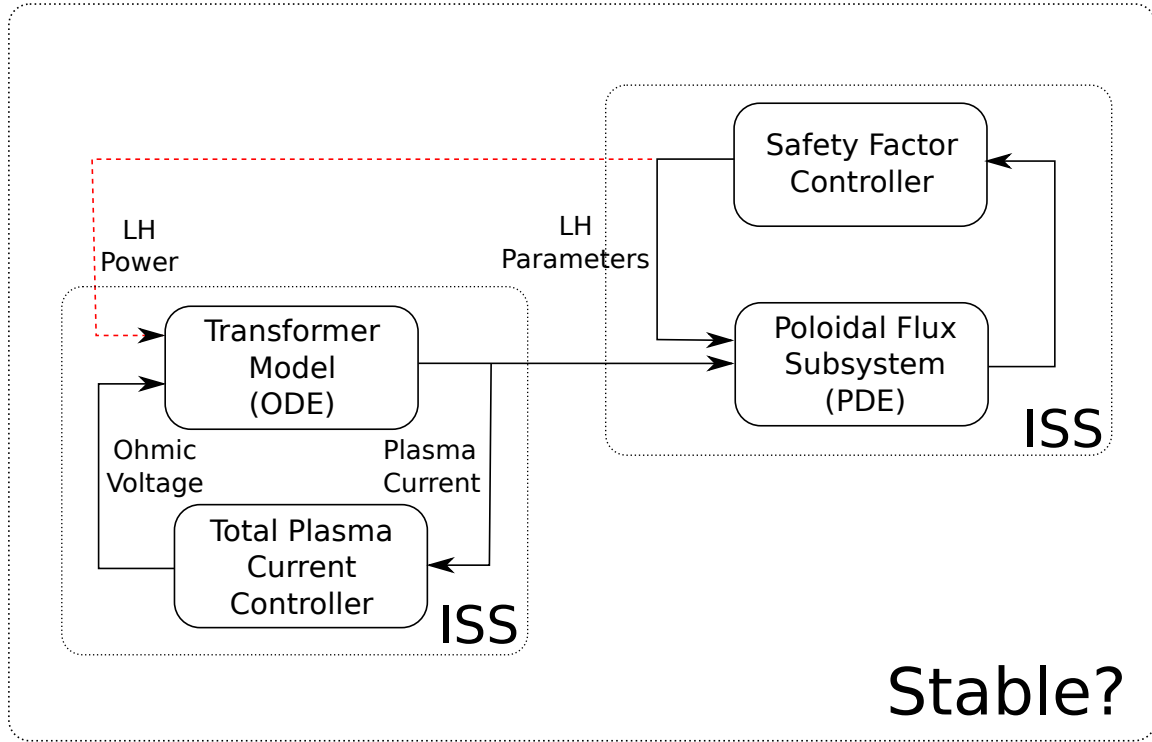
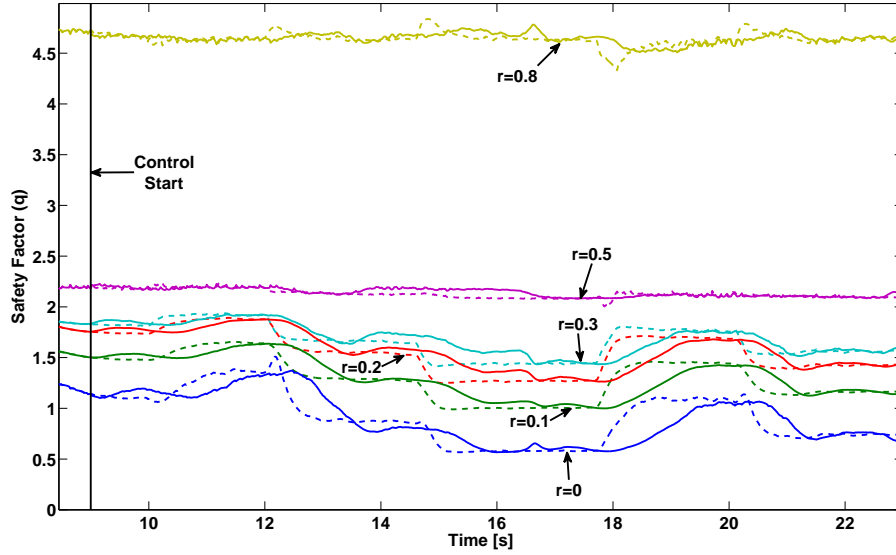


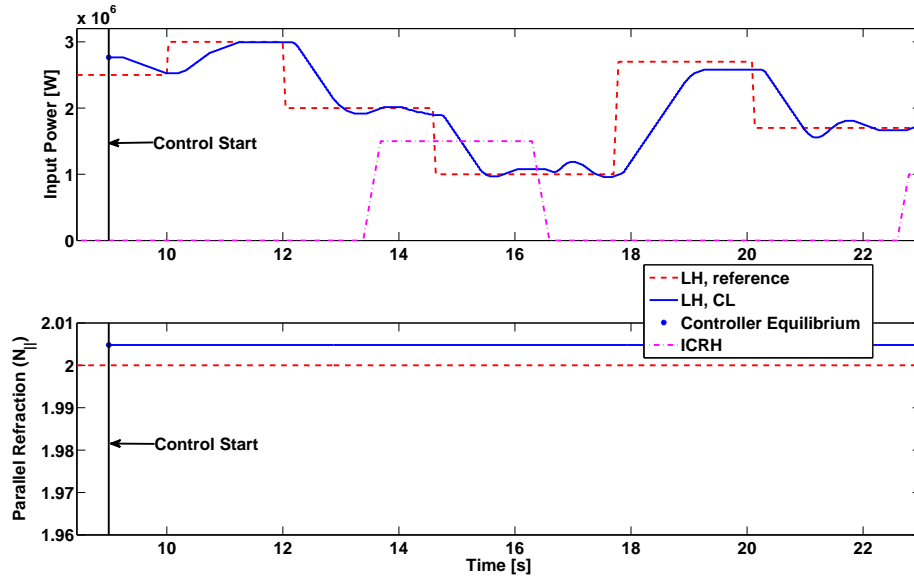
Figure 2: Diagramme de couplage entre les systèmes en dimension finie et infinie.

retard, la poursuite est satisfaisante même en présence de perturbations dans la forme de puissance FCI (à la fréquence cyclotronique-ionique). Le gain peut encore être augmenté, mais, vu l'important délai rajouté dans la boucle, une dégradation de la performance est presque inévitable.

Simulation sur TCV: une perturbation qui ne peut pas être directement compensée par les actionneurs disponibles. Dans ce cas, elle est composée par une combinaison de chauffage électronique-cyclotronique à  $r = 0.2$ , et une entrée de courante électronique-cyclotronique (ECCD), à  $r = 0.4$ . Cette combinaison ne peut pas être rejetée avec les deux actionneurs disponibles (ECCD à  $r = 0$  et  $r = 0.4$ ). Néanmoins, si l'on compare la réponse en boucle ouverte (Figure 4) et la boucle fermée (Figure 5), l'action de la boucle fermée a un impact positif sur la réponse du système. A la fin de la simulation, la réduction de l'erreur entre la référence et le facteur de sécurité obtenu dans la Figure 5 (b) par rapport à 4 (b) est assez évident.

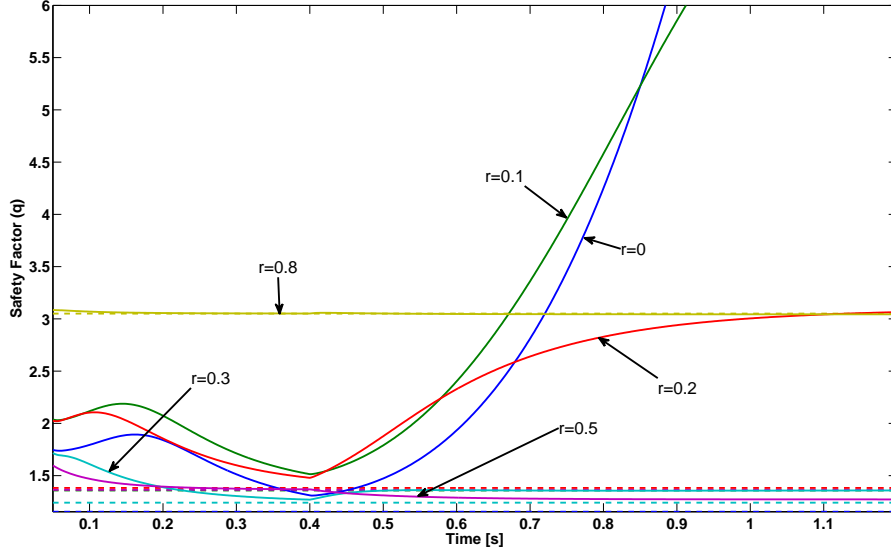


(a) Suivi du facteur de sécurité. Trait discontinu: reference pour  $q$ ; trait solide: valeur de  $q$  obtenue.

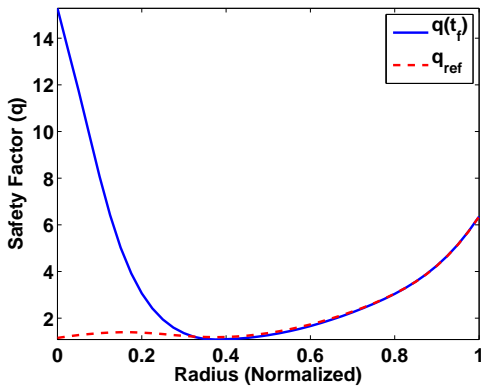


(b) Action et perturbation PFCI (ICRH).

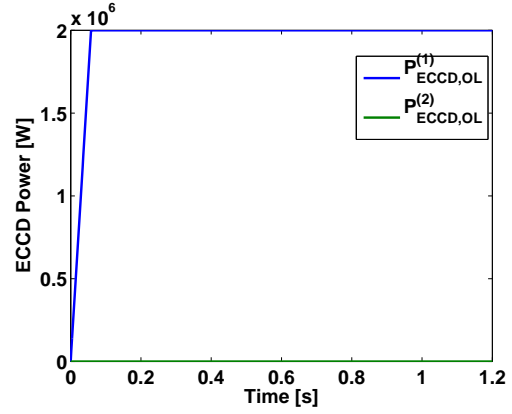
Figure 3: Suivi du facteur de sécurité et évolution des paramètres des antennes.



(a) Suivi du facteur de sécurité. Trait discontinu: référence pour  $q$ ; trait solide: valeur de  $q$  obtenue.



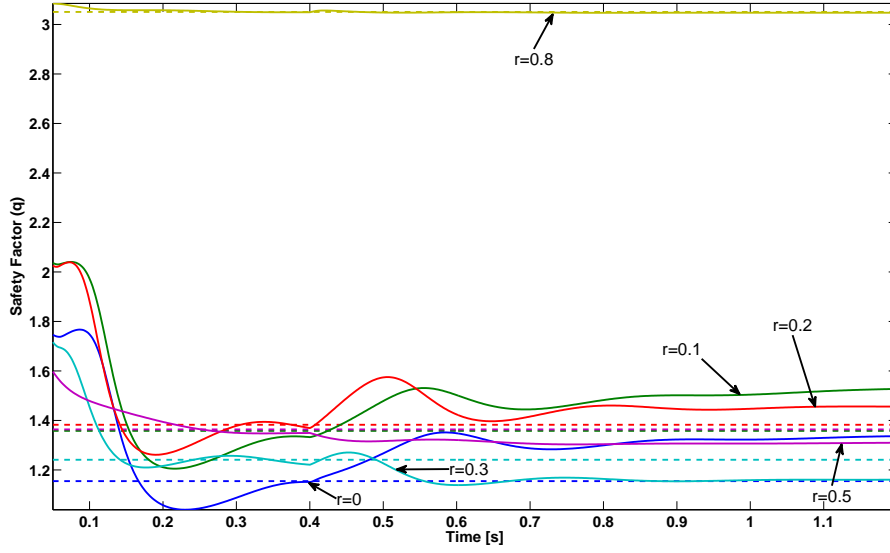
(b) Facteur de sécurité final et référence.



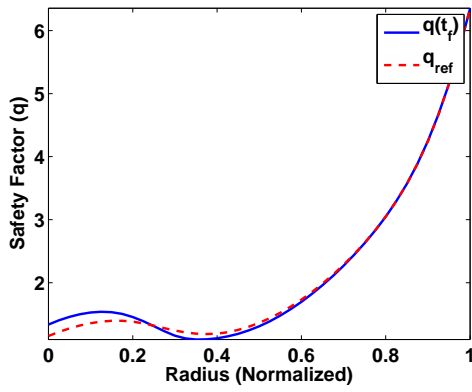
(c) Puissance FCE appliquée.

Figure 4: Profil de facteur de sécurité et puissance FCE en boucle ouverte avec perturbations FCE en courant et chauffage à  $r = 0.4$  et  $r = 0.2$ , respectivement, pour  $t \geq 0.4$  s.

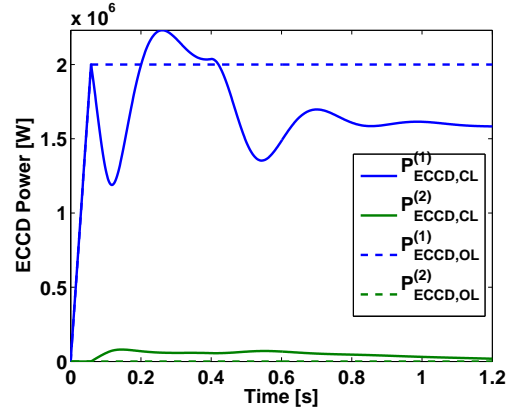




(a) Suivi du facteur de sécurité. Trait discontinu: référence pour  $q$ ; trait solide: valeur de  $q$  obtenue.



(b) Facteur de sécurité final et référence.



(c) Puissance FCE appliquée.

Figure 5: Profil de facteur de sécurité et puissance FCE en boucle fermée avec perturbations FCE en courant et chauffage à  $r = 0.4$  et  $r = 0.2$ , respectivement, pour  $t \geq 0.4$  s.

# Contents

<b>1</b>	<b>Introduction</b>	<b>21</b>
<b>2</b>	<b>Reference Model and Control Problem Formulation</b>	<b>27</b>
2.1	Poloidal Magnetic Flux in a Tokamak . . . . .	27
2.1.1	Actuator Constraints . . . . .	33
2.2	Control Problem . . . . .	33
2.2.1	Why not study directly the evolution of the safety factor? . . . .	34
2.3	Key Challenges . . . . .	34
<b>3</b>	<b>Finite-Dimensional Control</b>	<b>37</b>
3.1	LQR Controller . . . . .	38
3.1.1	Optimal and Pseudo-Optimal Profile Regulation Without Con- straints . . . . .	39
3.1.2	Pseudo-optimal Profile Regulation Under Shape Constraints . . .	41
3.1.3	Simulation Results . . . . .	42
3.1.4	Summary and Conclusions on LQR control . . . . .	45
3.2	Polytopic LPV . . . . .	46
3.2.1	LPV Model . . . . .	47
3.2.2	Controller Synthesis Results . . . . .	48
3.2.3	Validation . . . . .	52
3.2.4	Summary and Conclusions on the Polytopic Approach . . . . .	55
3.3	Motivation for an Infinite-Dimensional Approach . . . . .	55

<b>4</b>	<b>Infinite-Dimensional Control</b>	<b>57</b>
4.1	Some Possible Lyapunov Functions . . . . .	60
4.1.1	First Candidate Lyapunov Function . . . . .	60
4.1.2	Second Candidate Lyapunov Function . . . . .	61
4.2	Selected Control Lyapunov Function and Nominal Stability . . . . .	63
4.2.1	Candidate Control Lyapunov Function . . . . .	63
4.2.2	Some Implications . . . . .	66
4.3	Input-to-State Stability and Robustness . . . . .	67
4.3.1	Disturbed Model . . . . .	67
4.4	D <sup>1</sup> -Input-to-State Stability . . . . .	71
4.4.1	Strict Lyapunov Function and sufficient conditions for D <sup>1</sup> -Input-to-State Stability . . . . .	71
4.5	Application to the Control of the Poloidal Magnetic Flux Profile in a Tokamak Plasma . . . . .	74
4.5.1	Illustration of Stability: Numerical computation of the Lyapunov function . . . . .	74
4.5.2	Illustration of ISS property: Tokamak Simulation with Unconstrained Controller . . . . .	77
4.5.3	Exploiting the Lyapunov Approach: Tokamak Simulation with Constrained Control . . . . .	78
<b>5</b>	<b>Controller Implementation</b>	<b>84</b>
5.1	Total Plasma Current Dynamic Model . . . . .	86
5.1.1	Perfect Decoupling and Cascade Interconnection of ISS Systems . . . . .	87
5.1.2	Interconnection Without Perfect Decoupling . . . . .	88
5.2	Modified Lyapunov Function . . . . .	89
5.3	Simulation Results of Closed-loop Tracking with Approximated Equilibrium using METIS . . . . .	92
5.3.1	General Description . . . . .	93

---

5.3.2	First case: Independent $I_p$ control, large variations of $P_{th}$ , temperature profile disturbed by ICRH heating. . . . .	94
5.3.3	Second case: Independent $I_p$ control, large variations of $N_{  }$ , temperature profile disturbed by ICRH heating. . . . .	97
5.4	Some Preliminary Extensions . . . . .	97
5.4.1	Profile Reconstruction Delays . . . . .	99
5.4.2	Extension for TCV . . . . .	99
5.5	Summary and Conclusions . . . . .	105
<b>6</b>	<b>Conclusion and Perspectives</b>	<b>110</b>
<b>A</b>	<b>Proof of Theorem 2.1.2</b>	<b>114</b>
<b>B</b>	<b>Finding a Lyapunov Function</b>	<b>116</b>
B.1	Finding a Weighting Function . . . . .	116
B.1.1	Considered Set of Diffusivity Profiles . . . . .	116
B.1.2	Sufficient Conditions and Algorithm . . . . .	117
B.2	Numerical Application . . . . .	119
B.2.1	Weighting Function . . . . .	119
B.2.2	Simulations . . . . .	120
	<b>Bibliography</b>	<b>124</b>



# Chapter 1

## Introduction

### Context and Motivation

In the search for clean and safe energy sources that do not rely on fossil fuels, a great deal of effort has been dedicated to the development of controlled thermonuclear fusion. Consisting on the fusion at very high temperatures of two light atomic nuclei to form a heavier one, it is considered to be a promising energy source for the future. Current and planned experimental facilities rely mostly on two Hydrogen isotopes: Deuterium and Tritium. The natural abundance of Deuterium and the possibility of producing Tritium from readily available Lithium mean that easily available fuel reserves for this kind of energy production could amount, in all likelihood, to thousands of years of world energy consumption at current levels [[Wesson, 2004](#)]. Like all nuclear power sources, the absence of carbon emissions is a key advantage of using nuclear fusion. Furthermore, the inherent safety of the fusion reaction (as opposed to the fission one) and the comparatively easy treatment of radioactive byproducts (only structural components that are in close proximity to where the reaction takes place become activated and need to be stored for a few decades before being safely recycled) make this form of energy production extremely attractive.

However enticing the prospect of controlled nuclear fusion may be, achieving and maintaining the fusion reaction is not simple. To fuse two (positively charged) nuclei, the electrostatic force keeping them apart must be overcome (Coulomb barrier). This is done by taking the fuel to extremely high temperatures (which ionize the fuel atoms, forming a plasma). Once the fuel has enough kinetic energy to overcome this barrier, a question that remains is whether or not a significant amount of nuclei will fuse producing a net energy gain. To achieve this (in a technically feasible way), two main approaches have been explored:

- heating the fuel to obtain a high-density plasma (high fusion rate) and keeping it confined for a short period of time, which is the principle behind inertial confinement fusion, and
- heating the fuel to obtain a low-density plasma (low fusion rate) and keeping it confined for a long period of time, which is the principle behind magnetic confinement fusion.

In view of the ITER project [ITER Organization, 2010] currently under construction at Cadarache in southern France, magnetic confinement, and particularly the tokamak configuration will be the focus of this thesis.

A tokamak is a toroidal chamber lined with magnetic coils that generate a very strong magnetic field with both toroidal and poloidal components. In this chamber, the Tritium-Deuterium plasma circulates so that the fusion reaction can take place (a detailed account of tokamak physics can be found in [Wesson, 2004]). Tokamak operation presents several challenging control problems, an overview of which can be found in [Pironti and Walker, 2005], [Walker et al., 2006], [Walker et al., 2008] and [Ariola and Pironti, 2008]. Until recently, most of the literature considered the control of one or several scalar parameters of the plasma (for example: shape, position, total current, density). In particular, [Ariola and Pironti, 2008] addresses most of these problems.

When dealing with advanced tokamak scenarios (see for instance [Taylor, 1997], [Gormezano, 1999] and [Wolf, 2003]) it is desirable to have a finer degree of control on some variables. In particular, full profile control of the current density and temperature may be required. Given the high uncertainty in online profile reconstruction and measurements, as well as in modeling of transport phenomena inside the plasma, controlling these internal profiles is a very challenging task and necessitates robust feedback approaches.

## Problem Statement and Background

In this thesis, we are interested in the control of the *safety factor profile* or *q-profile*. The safety factor profile is determined by the relation between the two components of the magnetic field. This physical quantity has been found to be related to several phenomena in the plasma, in particular *magnetohydrodynamic* (MHD) instabilities. Having an adequate safety factor profile is particularly important to achieve advanced tokamak operation, providing high confinement and MHD stability. To achieve this, we focus in controlling the poloidal magnetic flux profile (and in particular, its gradient). This is a challenging problem for several reasons:

- The evolution of the physical variable to be controlled is governed by the resistive diffusion of the magnetic flux, which is a parabolic equation with spatially-distributed rapidly time-varying coefficients that depend on the solution of another partial differential equation related to heat transport;
- the control action is distributed in the spatial domain but nonlinear constraints are imposed on its shape (with only a few engineering parameters available for control, strong restrictions on the admissible shape are imposed);
- nonlinear source terms appear in the evolution equation (in particular the bootstrap current);
- important uncertainties exist in most measurements, estimations and models.

The problem of poloidal magnetic flux profile control is closely related, via the Maxwell equations, to the control of plasma current profile. Some previous works show the possibility of controlling profile shape parameters, for instance on Tore Supra: [Wijnands et al., 1997], where the current profile shape is characterized by its internal inductance and the central safety factor value and experimental results are presented; and [Barana et al., 2007], where the control of the width of the lower hybrid power deposition profile is shown and experimentally validated. Also, [Imbeaux et al., 2011] proposes a discrete real-time control of steady-state safety factor profile, considering some possible operating modes. Other works consider the distributed nature of the system and use discretized linear models identified around experimental operating point. Examples of such works can be found in [Laborde et al., 2005], where a model based on a Galerkin projection was used to control multiple profiles in JET, [Moreau et al., 2009], where a reduced order model is used to control some points in the safety factor profile, [Moreau et al., 2011], where the applicability of these identification and integrated control methods to various tokamaks is presented and in [Ou et al., 2010] where a robust controller is constructed based on a POD/Galerkin decomposition and assuming constant shape of the diffusivity profiles (varying only modulo a scalar variable).

Specific contributions from the automatic control research community have also started to appear, dealing with simplified control-oriented models that retain the distributed nature of the system. Some examples are [Ou et al., 2008], where an extremum-seeking open-loop optimal control is developed for the current profile in DIII-D; [Felici and Sauter, 2012], where nonlinear model-based optimization is used to compute open-loop actuator trajectories for plasma profile control. For closed-loop control examples, in [Ou et al., 2011] and related works, an infinite-dimensional model, described by partial differential equations (PDEs), is used to construct an optimal controller for the current profile, considering fixed shape profiles for the current deposited by the RF antennas and for the diffusivity coefficients. Other PDE-control approaches, related to Tore Supra, can be mentioned: [Gahlawat et al., 2011], where sum-of-square



polynomials are used to construct a Lyapunov function considering constant diffusivity coefficients; [Gaye et al., 2011], where a sliding-mode controller was designed for the infinite-dimensional system, considering time-invariant diffusivity coefficients.

A simplified control-oriented model of the poloidal magnetic flux diffusion based on that presented in [Witrant et al., 2007] is described in Chapter 2. This model is composed of a diffusion-like parabolic partial differential equation with time-varying distributed parameters. This type of differential equations (PDEs) (in particular diffusion or diffusion-convection equations) are used to model a wide array of physical phenomena ranging from heat conduction to the distribution of species in biological systems. While the diffusivity coefficients can be assumed to be constant throughout the spatial domain for most applications, spatially-distributed coefficients are needed when treating nonhomogeneous or anisotropic (direction-dependent) media. Unfortunately, extending existing results from the homogeneous to the nonhomogeneous case is not straightforward, particularly when the transport coefficients are time-varying.

## Main Contributions

The main contributions of this thesis are:

- the illustration of some control schemes that result from the discretization of the distributed model before designing a control law (lumped-parameter approach) and their inherent limits;
- the use of a physically relevant simplified infinite-dimensional model for the development of a distributed control law for the tracking of the gradient of the magnetic flux profile (safety factor profile) by means of LH current drive with particular care given to time-varying effects and possible extension to arbitrary non-inductive current sources;
- the consideration of time varying diffusivity coefficient profiles in the control design, guaranteeing the stability of the system and its robustness with respect to several common sources of errors and unmodeled dynamics;
- the inclusion of previously neglected couplings between the total plasma current control and the magnetic flux profile control;
- the application of real-time optimization that includes the nonlinear constraints imposed by the current deposit profiles while preserving the theoretical stability and robustness guarantees;

- the validation of the proposed control approach using the METIS code [Artaud, 2008] (a module of the CRONOS suite of codes, suitable for closed-loop control simulations [Artaud et al., 2010]) for Tore Supra;
- the addition (in simulation) of profile-reconstruction delays in the control loop;
- the extension of the control scheme to ECCD actuators and simulation using the RAPTOR code [Felici et al., 2011] for TCV parameters.

## Outline

This thesis is organized as follows:

- Chapter 2 presents the main distributed model that is used throughout this thesis along with the main physical hypotheses required for the model simplification.
- Chapter 3 presents two control approaches based on the spatial discretization of the distributed model presented in Chapter 2. The first approach disregards the time-varying nature of the system and simply updates an LQR (linear quadratic regulator) using the estimated values of some physical quantities (mainly the plasma resistivity). The second approach takes into account the time-varying character of the diffusivity profiles and uses linear matrix inequalities with a polytopic linear parameter-varying (LPV) structure to compute stabilizing controllers for the extreme variations of the parameters (the vertices of the polytope). Even though this approach takes into account the variation of the diffusivity coefficients, its extension to the control of the gradient of the poloidal flux profile is not straightforward (the proposed change of variables done to obtain a constant  $B$  matrix no longer holds and the problem becomes non-linear in the parameters).
- Chapter 4 presents the main contribution of this thesis. A strict Lyapunov function is derived for the open-loop distributed system, which allows to construct strongly constrained control laws that preserve the stability of the system while modifying the input-to-state gains between different disturbances and the gradient of the magnetic flux. Some alternative Lyapunov functions are presented with their drawbacks to motivate the final form chosen for the Lyapunov function used in the rest of the thesis.
- Chapter 5 presents the extension of the proposed control scheme based on the Lyapunov function to take into account important couplings between the LH power and the total plasma current in the tokamak. Advanced simulations using the METIS code are presented to illustrate the robustness of the control scheme with respect to differences between the reference model and the actual model, as well

as other actuators acting as source of disturbances (represented, for example, by the ICRH actuator) and profile-reconstruction delays. Finally, the flexibility of the proposed scheme to accomodate different actuator models and plasma shapes is illustrated with some simulations using the RAPTOR code [Felici et al., 2011] with TCV parameters.

## List of Related Publications by the Author:

### Journal Papers:

- Bribiesca Argomedo, F., Prieur, C., Witrant, E., and Brémond, S. (2012). A strict control Lyapunov function for a diffusion equation with time-varying distributed coefficients. To appear, IEEE Transactions on Automatic Control.
- Bribiesca Argomedo, F., Witrant, E., Prieur, C., Brémond, S., Nouailletas, R. and Artaud, J.F. (2012). Lyapunov-based distributed control of the safety factor profile in a tokamak plasma. Submitted for Publication.

### International Conference Papers:

- Bribiesca Argomedo, F., Witrant, E., Prieur, C., Georges, D., and Brémond, S. (2010). Model-based control of the magnetic flux profile in a tokamak plasma. In Proceedings of the 49th IEEE Conference on Decision and Control, pages 6926-6931, Atlanta, GA.
- Bribiesca Argomedo, F., Prieur, C., Witrant, E., and Brémond, S. (2011). Polytopic control of the magnetic flux profile in a tokamak plasma. In Proceedings of the 18th IFAC World Congress. Milan, Italy.
- Bribiesca Argomedo, F., Witrant, E., and Prieur, C. (2012).  $D^1$ -Input-to-State stability of a time-varying nonhomogeneous diffusive equation subject to boundary disturbances. In Proceedings of the American Control Conference, Montréal, Canada.

# Chapter 2

## Reference Model and Control Problem Formulation

### Contents

---

<b>2.1</b>	<b>Poloidal Magnetic Flux in a Tokamak . . . . .</b>	<b>27</b>
2.1.1	Actuator Constraints . . . . .	33
<b>2.2</b>	<b>Control Problem . . . . .</b>	<b>33</b>
2.2.1	Why not study directly the evolution of the safety factor? . . .	34
<b>2.3</b>	<b>Key Challenges . . . . .</b>	<b>34</b>

---

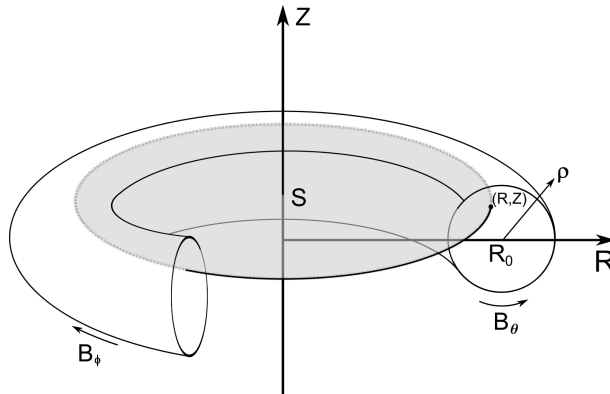
In this thesis, we are interested in controlling the safety factor profile in a tokamak plasma. As the safety factor scales as the ratio of the normalized radius to the poloidal magnetic flux gradient [Witrant et al., 2007], controlling this latter variable allows controlling the safety factor profile. In this chapter we present the reference dynamical model for the poloidal magnetic flux profile and its gradient (equivalent to the effective poloidal field magnitude, as defined in [Hinton and Hazeltine, 1976]), used throughout the following chapters, as well as the control problem under consideration. Some of the main difficulties encountered when dealing with this problem are also highlighted.

### 2.1 Poloidal Magnetic Flux in a Tokamak

The poloidal magnetic flux, denoted  $\psi(R, Z)$ , is defined as the flux per radian of the magnetic field  $\mathbf{B}(R, Z)$  through a disc centered on the toroidal axis at height  $Z$ , having a radius  $R$  and surface  $\mathcal{S}$ , as depicted in Fig. 2.1. A simplified one-dimensional model for this poloidal magnetic flux profile is considered. Its dynamics are given by the following

<i>Variables</i>	<i>Description</i>	<i>Units</i>
$\psi$	Poloidal magnetic flux profile	$Tm^2$
$\phi$	Toroidal magnetic flux profile	$Tm^2$
$q$	Safety factor profile $q \doteq d\phi/d\psi$	
$R_0$	Location of the magnetic center	$m$
$B_{\phi_0}$	Toroidal magnetic field at the center	$T$
$\rho$	Equivalent radius of the magnetic surfaces	$m$
$a$	Location of the last closed magnetic surface	$m$
$r$	Normalized spatial variable $r \doteq \rho/a$	
$t$	Time	$s$
$V$	Plasma Volume	$m^3$
$F$	Diamagnetic Function	$Tm$
$C_2, C_3$	Geometric coefficients	
$\eta_{\parallel}$	Parallel resistivity	$\Omega m$
$\eta$	Normalized diffusivity coefficient $\eta_{\parallel}/\mu_0 a^2$	
$\mu_0$	Permeability of free space: $4\pi \times 10^{-7}$	$Hm^{-1}$
$\bar{n}$	Electron average density	$m^{-3}$
$j_{ni}$	Non-inductive effective current density	$Am^{-2}$
$\dot{j}$	Normalized non-inductive effective current density $\mu_0 a^2 R_0 \dot{j}_{ni}$	
$I_p$	Total plasma current	$A$
$V_{loop}$	Toroidal loop voltage	$V$
$\eta_{lh}$	LH current drive efficiency	$Am^{-2}W^{-1}$
$P_{lh}$	Lower Hybrid antenna power	$W$
$N_{\parallel}$	Hybrid wave parallel refractive index	
$I_{\Omega}$	Ohmic current	$A$
$V_{\Omega}$	Ohmic voltage	$V$

Table 2.1: Variable definition


Figure 2.1: Coordinates  $(R, Z)$  and surface  $\mathbf{S}$  used to define the poloidal magnetic flux  $\psi(R, Z)$ .

equation [Blum, 1989]:

$$\frac{\partial \psi}{\partial t} = \frac{\eta_{\parallel} C_2}{\mu_0 C_3} \frac{\partial^2 \psi}{\partial \rho^2} + \frac{\eta_{\parallel} \rho}{\mu_0 C_3^2} \frac{\partial}{\partial \rho} \left( \frac{C_2 C_3}{\rho} \right) \frac{\partial \psi}{\partial \rho} + \frac{\eta_{\parallel} V_{\rho} B_{\phi_0}}{F C_3} j_{ni} \quad (2.1.1)$$

where  $\rho \doteq \sqrt{\frac{\phi}{\pi B_{\phi_0}}}$  is an equivalent radius indexing the magnetic surfaces,  $\phi$  is the toroidal magnetic flux,  $B_{\phi_0}$  the toroidal magnetic field at the center of the vacuum vessel,  $\eta_{\parallel}$  is the parallel resistivity of the plasma, the source term  $j_{ni}$  represents the current density profile generated by non-inductive current sources,  $\mu_0$  is the permeability of free space,  $F$  is the diamagnetic function,  $V_{\rho}$  is the spatial derivative of the plasma volume enclosed by the magnetic surface indexed by  $\rho$ . The main physical variables are summarized in Table 2.1. Coefficients  $C_2$  and  $C_3$  are defined as in [Blum, 1989]:

$$\begin{aligned} C_2(\rho) &= V_{\rho} \left\langle \frac{\|\rho\|^2}{R^2} \right\rangle \\ C_3(\rho) &= V_{\rho} \left\langle \frac{1}{R^2} \right\rangle \end{aligned}$$

where  $\langle \cdot \rangle$  represents the average on the flux surface indexed by  $\rho$ .

Neglecting the diamagnetic effect caused by poloidal currents and using a cylindrical approximation of the plasma geometry ( $\rho \ll R_0$ , where  $R_0$  is the major plasma radius) the coefficients in (2.1.1) simplify as follows:

$$F \approx R_0 B_{\phi_0}, \quad C_2 = C_3 = 4\pi^2 \frac{\rho}{R_0}, \quad V_{\rho} = 4\pi^2 \rho R_0$$

Defining a normalized spatial variable  $r = \frac{\rho}{a}$ , where  $a$  (assumed constant) is the equivalent (minor) radius of the last closed magnetic surface, the simplified model is obtained as in [Witrant et al., 2007; Artaud et al., 2010]:

$$\frac{\partial \psi}{\partial t}(r, t) = \frac{\eta_{\parallel}(r, t)}{\mu_0 a^2} \left( \frac{\partial^2 \psi}{\partial r^2} + \frac{1}{r} \frac{\partial \psi}{\partial r} \right) + \eta_{\parallel}(r, t) R_0 j_{ni}(r, t) \quad (2.1.2)$$

with the boundary conditions:

$$\frac{\partial \psi}{\partial r}(0, t) = 0 \quad (2.1.3)$$

and

$$\frac{\partial \psi}{\partial r}(1, t) = -\frac{R_0 \mu_0 I_p(t)}{2\pi} \quad \text{or} \quad \frac{\partial \psi}{\partial t}(1, t) = V_{loop}(t) \quad (2.1.4)$$

where  $I_p$  is the total plasma current and  $V_{loop}$  is the toroidal loop voltage, with initial condition:

$$\psi(r, t_0) = \psi_0(r)$$

**Remark 2.1.1.** *The validity of this model can be extended to other tokamaks by changing the definition of the coefficients  $C_2$ ,  $C_3$ ,  $F$  and  $V_{\rho}$ .*

For the purposes of this thesis,  $j_{ni}$  is considered as having three main components:

- the auto-generated bootstrap current  $j_{bs}$  (produced by trapped particles in the "banana" regime);
- the LHCD (*Lower Hybrid Current Drive*) current deposit  $j_{lh}$ ;
- the ECCD (*Electron Cyclotron Current Drive*) current deposit  $j_{eccd}$  (introduced as a disturbance in some examples).

We define  $\eta \doteq \eta_{\parallel}/\mu_0 a^2$  and  $j \doteq \mu_0 a^2 R_0 j_{ni}$  to simplify the notations. An equilibrium  $\bar{\psi}$ , if it exists, is defined as a stationary solution to:

$$0 = \left[ \frac{\eta}{r} [r\bar{\psi}_r]_r \right]_r + [\eta\bar{j}]_r \quad \forall r \in (0, 1) \quad (2.1.5)$$

with the boundary conditions:

$$\begin{aligned} \bar{\psi}_r(0) &= 0 \\ \bar{\psi}_r(1) &= -\frac{R_0 \mu_0 \bar{I}_p}{2\pi} \end{aligned} \quad (2.1.6)$$

for a given couple  $(\bar{j}, \bar{I}_p)$ . Where, to simplify the notation, for any function  $\xi$  depending on the independent variables  $r$  and  $t$ ,  $\xi_r$  and  $\xi_t$  are used to denote  $\frac{\partial}{\partial r}\xi$  and  $\frac{\partial}{\partial t}\xi$ , respectively.

**Remark 2.1.1.** When trying to find an equilibrium by solving (2.1.5)-(2.1.6) two cases have to be considered:

- there is no drift in  $\bar{\psi}$  (equivalent to  $V_{loop} = 0$  at all times using the alternative boundary condition  $\partial\psi/\partial t(1, t) = V_{loop}(t)$  in (2.1.4)) and therefore the solution of (2.1.5)-(2.1.6) verifies:

$$\frac{\eta}{r} [r\bar{\psi}_r]_r + \eta\bar{j} = 0 \quad (2.1.7)$$

in this case,  $\bar{\psi}$  (and its spatial derivative) is independent on the value of  $\eta$  and therefore the stationary solution exists (i.e. there is an equilibrium of the time-varying system) regardless of the variations in  $\eta$ . This is the case we directly address in this thesis.

- there is a radially constant drift in  $\bar{\psi}$  (equivalent to  $V_{loop} \neq 0$  for some times when using the alternative boundary condition) and therefore the solution of (2.1.5)-(2.1.6) verifies, for some  $c(t)$ :

$$\frac{\eta(r, t)}{r} [r\bar{\psi}_r(r, t)]_r + \eta(r, t)\bar{j}(r) = c(t) \quad (2.1.8)$$

in this case,  $\bar{\psi}_r$  does not correspond to an equilibrium since it will be a function of time and space (in particular, it will be a function of  $\eta(r, t)$  and  $c(t)$ ), we will call the corresponding  $\bar{\psi}(r, t)$  a pseudo-equilibrium of the system. It can be shown to verify:

$$\bar{\psi}_r(r, t) = \frac{1}{r} \int_0^r \left( \frac{\varrho}{\eta(\varrho, t)} c(t) - \varrho \bar{j}(\varrho) \right) d\varrho \quad (2.1.9)$$

with time-derivative:

$$\bar{\psi}_{rt}(r, t) = \frac{1}{r} \int_0^r \left( \frac{\varrho}{\eta(\varrho, t)} \dot{c}(t) - \frac{\varrho \dot{\eta}(\varrho, t)}{\eta^2(\varrho, t)} c(t) \right) d\varrho \quad (2.1.10)$$

this case is not extensively addressed in this thesis but the results presented in chapters 4 and 5 will not be severely affected as long as  $\dot{c}(t)$  and  $\dot{\eta}(r, t)$  are bounded in a suitable way. Since a pseudo-equilibrium will exist at each time, the robustness result presented in Theorem 4.3.2 can be applied, rewriting the evolution of the system around this pseudo-equilibrium (instead of an actual equilibrium) and considering  $w = -\bar{\psi}_{rt}(r, t)$  (the time-varying nature of the pseudo-equilibrium acts as a state-disturbance for the system).

Around the equilibrium (assumed to exist as per the previous remark) and neglecting the nonlinear dependence of the bootstrap current on the state, the dynamics of the system are given by:

$$\tilde{\psi}_t = \frac{\eta}{r} \left[ r \tilde{\psi}_r \right]_r + \eta \tilde{j}, \quad \forall (r, t) \in (0, 1) \times [0, T] \quad (2.1.11)$$

with boundary conditions:

$$\begin{aligned} \tilde{\psi}_r(0, t) &= 0 \\ \tilde{\psi}_r(1, t) &= -\frac{R_0 \mu_0 \tilde{I}_p(t)}{2\pi} \end{aligned} \quad (2.1.12)$$

and initial condition:

$$\tilde{\psi}(r, 0) = \tilde{\psi}_0(r) \quad (2.1.13)$$

where the dependence of  $\tilde{\psi} \doteq \psi - \bar{\psi}$ ,  $\tilde{j} \doteq j - \bar{j}$  and  $\eta$  on  $(r, t)$  is implicit;  $\tilde{I}_p \doteq I_p - \bar{I}_p$  and  $0 < T \leq +\infty$  is the time horizon.

As the safety factor profile depends on the magnetic flux gradient, our focus is on the evolution of  $z \doteq \partial \tilde{\psi} / \partial r$  (equivalent to deviations of the effective poloidal field magnitude around an equilibrium), with input  $u \doteq \tilde{j}$ , defined as:

$$z_t(r, t) = \left[ \frac{\eta(r, t)}{r} [r z(r, t)]_r \right]_r + [\eta(r, t) u(r, t)]_r, \quad \forall (r, t) \in (0, 1) \times [0, T] \quad (2.1.14)$$

with Dirichlet boundary conditions:

$$z(0, t) = 0$$



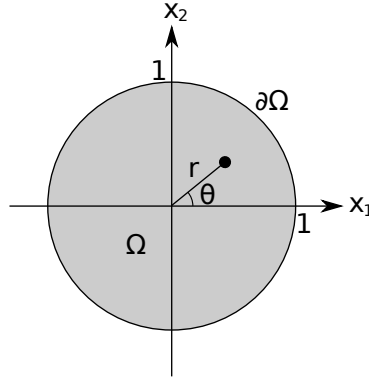


Figure 2.2: Coordinates  $(x_1, x_2)$ ,  $(r, \theta)$  and domain  $\Omega$  used to define the diffusion equation.

$$z(1, t) = -\frac{R_0 \mu_0 \tilde{I}_p(t)}{2\pi} \quad (2.1.15)$$

and initial condition:

$$z(r, 0) = z_0(r) \quad (2.1.16)$$

where  $z_0 \doteq \left[ \tilde{\psi}_0 \right]_r$ .

The following properties are assumed to hold in (2.1.14):

**P<sub>1</sub>:**  $K \geq \eta(r, t) \geq k > 0$  for all  $(r, t) \in [0, 1] \times [0, T]$  and some positive constants  $k, K$ .

**P<sub>2</sub>:** The two-dimensional Cartesian representations of  $\eta$  and  $u$  are in<sup>1</sup>  $C^{1+\alpha_c, \alpha_c/2}(\overline{\Omega} \times [0, T])$ ,  $0 < \alpha_c < 1$ , where  $\Omega \doteq \{(x_1, x_2) \in \mathbb{R}^2 \mid x_1^2 + x_2^2 < 1\}$  as shown in Fig. 2.2.

**P<sub>3</sub>:**  $\tilde{I}_p$  is in  $C^{(1+\alpha_c)/2}([0, T])$

For completeness purposes, the existence and uniqueness of sufficiently regular solutions (as needed for the Lyapunov analysis and feedback design purposes in the next chapters) to the evolution equation is stated, assuming that the properties  $P_1$ - $P_3$  are verified.

**Theorem 2.1.2.** *If Properties  $P_1$ - $P_3$  hold then, for every  $z_0 : [0, 1] \rightarrow \mathbb{R}$  in  $C^{2+\alpha_c}([0, 1])$  ( $0 < \alpha_c < 1$ ) such that  $z_0(0) = 0$  and  $z_0(1) = -R_0 \mu_0 \tilde{I}_p(0)/2\pi$ , the evolution equations (2.1.14)-(2.1.16) have a unique solution  $z \in C^{1+\alpha_c, 1+\alpha_c/2}([0, 1] \times [0, T]) \cap C^{2+\alpha_c, 1+\alpha_c/2}([0, 1] \times [0, T])$ .*

The proof of this result is given in Appendix A.

---

<sup>1</sup> Here  $C^{\alpha_c, \beta_c}(\overline{\Omega} \times [0, T])$  denotes the space of functions which are  $\alpha_c$ -Hölder continuous in  $\overline{\Omega}$ ,  $\beta_c$ -Hölder continuous in  $[0, T]$ .  $P_2$  can be strengthened by assuming that  $\eta$  and  $u$  are in  $C^{2,1}(\overline{\Omega} \times [0, T])$  which is the case for the physical application.

### 2.1.1 Actuator Constraints

It is important to notice that, although the system allows for in-domain actuation, strong shape constraints are imposed on the achievable current deposit profiles from the actuators as a result of the limited number of engineering parameters available in the antennas. For control design purposes, as discussed in [Witrant et al., 2007], it is assumed that the shape of LHCD deposit can be adequately approximated by a gaussian curve with parameters  $\mu$ ,  $\sigma$  and  $A_{lh}$  depending on the engineering parameters  $P_{lh}$  and  $N_{||}$  and the operating point :

$$j_{lh}(r, t) = A_{lh}(t)e^{-(r-\mu(t))^2/(2\sigma^2(t))}, \forall (r, t) \in [0, 1] \times [0, T] \quad (2.1.17)$$

Scaling laws for the shape parameters can be built based on suprathreshold electron emission, measured via hard X-ray measurements, see for instance [Imbeaux, 1999] and [Barana et al., 2006]. The total current driven by the LH antenna is then calculated using scaling laws such as those presented in [Goniche et al., 2005]. It should be noted that the methods presented in this thesis can easily be extended to other current deposit shapes (either for use in other tokamaks or to change the non-inductive current drives used).

## 2.2 Control Problem

The objective of this thesis is to control the safety factor profile  $q$  in a tokamak. This is done by controlling the poloidal magnetic flux profile  $\psi$ . In particular, the desired properties of the controller are:

- to guarantee the exponential stability, in a given topology, of the solutions of equation (2.1.14) to zero (or "close enough") by closing the loop with a controlled input  $u(\cdot, t)$ ;
- to be able to adjust (in particular, to accelerate) the rate of convergence of the system using the controlled input;
- to be able to determine the impact of a large class of errors motivated by the physical system and to propose a robust feedback design strategy. Actuation errors, estimation/measurement errors, state disturbances and boundary condition errors should be considered specifically.

### 2.2.1 Why not study directly the evolution of the safety factor?

A natural question that may arise at this point is why study the evolution of the poloidal magnetic flux profile instead of studying directly the safety factor profile. Assuming the safety factor profile is related to the magnetic flux profile as:

$$q(r, t) = -\frac{B_{\phi_0} a^2 r}{\psi_r(r, t)} \quad (2.2.1)$$

the evolution of the safety factor profile is then given by:

$$q_t(r, t) = \frac{B_{\phi_0} a^2 r}{\psi_r^2(r, t)} \psi_{rt}(r, t) = \frac{q^2(r, t)}{B_{\phi_0} a^2 r} \psi_{rt}(r, t)$$

and, from (2.1.2):

$$q_t(r, t) = -\frac{q^2(r, t)}{r} \left[ \frac{\eta(r, t)}{r} \left[ \frac{r^2}{q(r, t)} \right]_r \right] + \frac{q^2(r, t)}{B_{\phi_0} a^2 r} [\eta(r, t) u(r, t)]_r \quad (2.2.2)$$

or, in a more general form:

$$q_t(\rho, t) = -\frac{q^2(\rho, t)}{\mu_0 \rho} \left[ \frac{\eta_{\parallel}(\rho, t) \rho}{C_3^2(\rho)} \left[ \frac{C_2(\rho) C_3(\rho)}{q(\rho, t)} \right]_{\rho} \right] + \frac{q^2(\rho, t)}{\rho} \left[ \frac{\eta_{\parallel}(\rho, t) V_{\rho}}{F C_3(\rho)} j_{ni}(\rho, t) \right]_{\rho}$$

which can be obtained from (2.1.1) and the relation:

$$q(\rho, t) = -\frac{B_{\phi_0} \rho}{\psi_{\rho}(\rho, t)}$$

Equation (2.2.2) is nonlinear in  $q$  (making it difficult to extend results obtained around one equilibrium to other equilibria). This can be solved by working instead with the so-called rotational transform (denoted  $\iota$  in [Wesson, 2004], which is the inverse of the safety factor). Nevertheless, the boundary condition in the  $z$  variable (i.e. the total plasma current) can be directly (and precisely) measured using either a continuous Rogowski coil or several discrete magnetic coils around the plasma (see [Wesson, 2004]). Therefore, in this thesis we have chosen to control the safety factor profile by controlling the  $z$  variable.

## 2.3 Key Challenges

The problem under consideration poses several challenges that have to be addressed, some of which are:

- different orders of magnitude of the transport coefficients depending on the radial position that are also time varying;

- strong nonlinear shape constraints imposed on the actuators and saturations on the available parameters;
- robustness of any proposed control scheme with respect to numerical problems (in particular given the difference in magnitude of the transport coefficients) and disturbances;
- coupling between the control applied to the infinite-dimensional system and the boundary condition;
- the control algorithms must be implementable in real-time (restrictions on the computational cost).



# Chapter 3

## Finite-Dimensional Control

### Contents

---

<b>3.1</b>	<b>LQR Controller . . . . .</b>	<b>38</b>
3.1.1	Optimal and Pseudo-Optimal Profile Regulation Without Constraints . . . . .	39
3.1.2	Pseudo-optimal Profile Regulation Under Shape Constraints . .	41
3.1.3	Simulation Results . . . . .	42
3.1.4	Summary and Conclusions on LQR control . . . . .	45
<b>3.2</b>	<b>Polytopic LPV . . . . .</b>	<b>46</b>
3.2.1	LPV Model . . . . .	47
3.2.2	Controller Synthesis Results . . . . .	48
3.2.3	Validation . . . . .	52
3.2.4	Summary and Conclusions on the Polytopic Approach . . . . .	55
<b>3.3</b>	<b>Motivation for an Infinite-Dimensional Approach . . . . .</b>	<b>55</b>

---

In this chapter, we consider the problem of controlling a discretized version of model (2.1.2). The model was spatially discretized, for control purposes, using a finite-difference scheme. The full discretization (in space and time) of the system used for simulation purposes is detailed in [Witrant et al., 2007]. As a first step towards controlling the safety factor profile in the Tokamak, we focus on the control of the magnetic flux profile. After discretization, two different approaches are presented.

In the first section, the model is a linear time-varying system (LTV) and an LQR controller is implemented by solving at each sampling time the associated Algebraic Riccati Equation (ARE). This is done to test the efficiency of a quasi-static approach for the feedback control design problem. Shape constraints are introduced by linearizing the current deposit profiles close to an equilibrium and considering that three con-

trol parameters (corresponding to the three parameters in a gaussian distribution) are available to control the shape of the input current density. This section is based on [Bribiesca Argomedo et al., 2010].

In the second section, a Polytopic Linear Parameter-Varying (Polytopic LPV) controller was designed to adequately take into account the transient behaviour of the diffusion coefficients in the feedback design (albeit on the discretized system). Via a change of variables, the time-varying nature of the input matrix  $B$  is removed, allowing us to formulate a stabilizing control law for the system (extended with an output integrator) in the form of a linear combination of suitable controllers calculated for the extrema of the dynamic variation (in terms of a set of parameters). This section is based on [Bribiesca Argomedo et al., 2011]. For some comprehensive surveys on linear parameter-varying systems (LPV) control and gain scheduling controllers, see [Leith and Leithead, 2000] and [Rugh and Shamma, 2000]. For some applications of LPV/LMI gain-scheduling controls see [Wassink et al., 2005] and [Gilbert et al., 2010].

In both sections, the distributed model (2.1.2) is spatially discretized (in  $N+2$  points) using the midpoint rule to approximate the operators  $\frac{\partial^2}{\partial r^2}$  and  $\frac{1}{r} \frac{\partial}{\partial r}$ . The calculations are made to allow for a non-uniform spatial step distribution. Details of the process used for the discretization and relevant implementation details can be found in [Witrant et al., 2007].

When discretizing the PDE (2.1.2) and solving the finite dimensional system for the points  $r = 0$  and  $r = 1$  (using the boundary conditions), the dynamical behavior of the remaining states can be expressed as follows:

$$\dot{\psi} = A(t)\psi + B(t)j_{ni} + W(t) \quad (3.0.1)$$

where  $A(t)$  is an  $N \times N$  matrix that takes into account both the approximated differential operators and the influence of  $\eta_{||}/(\mu_0 a^2)$ .  $B(t)$  is an  $N \times N$  matrix representing  $\eta_{||} R_0$ .  $W(t)$  is an  $N \times 1$  column vector representing the effect of the PDE time-varying boundary conditions on the system. For the rest of this chapter we refer to  $\psi(r_i, \cdot)$  simply as  $\psi_i(t)$ .

### 3.1 LQR Controller

This section is based on the results presented in [Bribiesca Argomedo et al., 2010]. A particularity of this method is the computation of a pseudo-optimal regulator by considering the solution to an algebraic Riccati equation (ARE) in real time. The cost function used to build the dynamical version of this ARE, in the constrained version, depends on the evolution of three points in the magnetic flux profile (at the center, edge and mid-radius), as well as the integral of the error at those three points. Also, shape constraints are considered for the LHCD deposit. The regulator is then tested by numerical

simulation following the guidelines of [Witrant et al., 2007].

### 3.1.1 Optimal and Pseudo-Optimal Profile Regulation Without Constraints

Let us consider the system represented in (3.0.1). Our goal is to regulate the profile  $\psi(t)$  around a reference equilibrium  $\bar{\psi}$  (see Remark 2.1.1 for a discussion on the existence of such an equilibrium). Adding a full state integrator to the system, the extended system becomes:

$$\begin{bmatrix} \dot{\psi} \\ \dot{E} \end{bmatrix} = \begin{bmatrix} A(t) & 0 \\ -\mathbb{I} & -\lambda(t) \end{bmatrix} \begin{bmatrix} \psi \\ E \end{bmatrix} + \begin{bmatrix} B(t) \\ 0 \end{bmatrix} j_{ni} + \begin{bmatrix} W(t) \\ \bar{\psi} \end{bmatrix} \quad (3.1.1)$$

where  $E$  is the integral of the error. A new parameter  $\lambda_{max} \geq \lambda(t) \geq 0$  has been introduced as a "forgetting factor" for the integrator. The purpose of this term is to avoid high overshoots when changing the operating point by weighting down past accumulated errors. It is clear that, to avoid steady-state errors, we must have  $\lambda(t) \rightarrow 0$  as  $t \rightarrow \infty$ . This parameter is designed to vanish in finite time and its effect is illustrated in Figure 3.1.

**Remark 3.1.1.** *A bounded  $\lambda(t)$ , nonzero only when changing operating point and vanishing in finite time, allows us to preserve the overall stability of the system (provided that we change operating points only when we have already reached steady state).*

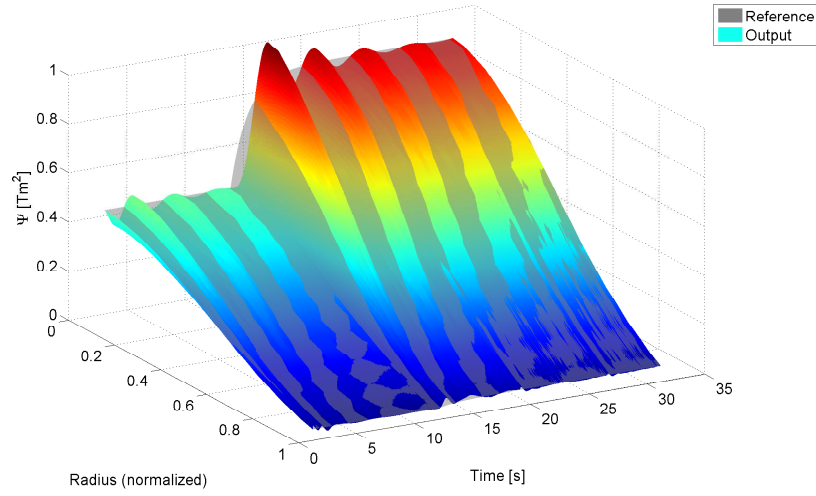
For the purposes of this section, we focus solely on the use of LHCD for the control of the system and, since we have not yet introduced any input constraints, we can consider controlling the system directly with the non-inductive input  $u \doteq j_{lh} + j_{bs}$ , ( $j_{ECCD}$  is not used). We express the extended system in the more compact form:

$$\dot{X} = A_e(t)X + B_e(t)u + W_e(t) \quad (3.1.2)$$

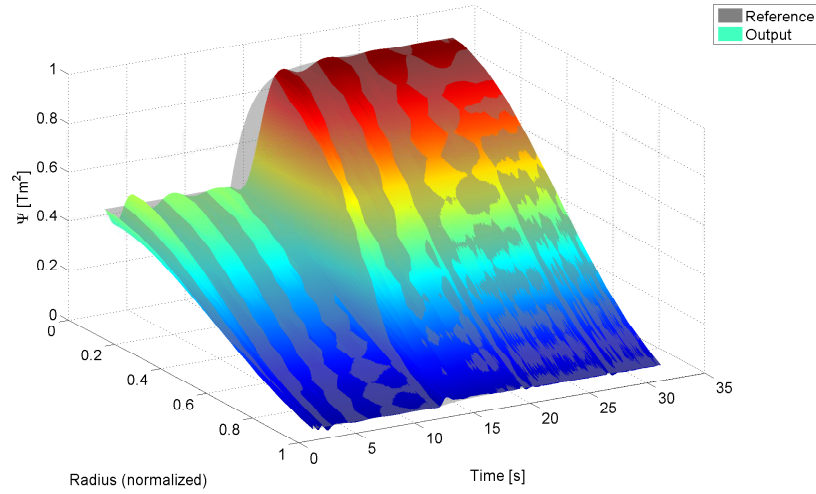
where

$$\begin{aligned} X &= \begin{bmatrix} \psi \\ E \end{bmatrix} \\ A_e(t) &= \begin{bmatrix} A(t) & 0 \\ -\mathbb{I} & -\lambda(t) \end{bmatrix} \\ B_e(t) &= \begin{bmatrix} B(t) \\ 0 \end{bmatrix} \\ W_e(t) &= \begin{bmatrix} W(t) \\ \bar{\psi} \end{bmatrix} \end{aligned}$$





(a) Response of the system with a pure integrator ( $\lambda = 0$ )



(b) Response of the system with  $(\lambda(t) = \min \{0.1|\dot{\Psi}_{ref}(t)|, 0.05\})$

Figure 3.1: Comparison of system responses without and with the effect of the parameter  $\lambda(t)$ .

Assuming, for control purposes that the matrices  $A_e$  and  $B_e$  are time-invariant and defining the variables  $(\tilde{X}, \tilde{u}, \tilde{W}_e)$  as follows:

$$\begin{aligned}\tilde{X} &\doteq X - \bar{X} \\ \tilde{u} &\doteq u - \bar{u} \\ \tilde{W}_e &\doteq W_e - \bar{W}_e\end{aligned}$$

the resulting state dynamics are:

$$\dot{\tilde{X}} = A_e \tilde{X} + B_e \tilde{u} + \tilde{W}_e(t) \quad (3.1.3)$$

Neglecting the term  $\widetilde{W}_e(t)$ , we now consider a feedback minimizing the cost function:

$$J = \frac{1}{2} \int_{t_0}^{\infty} \left( \widetilde{X}^T Q \widetilde{X} + \widetilde{u}^T R \widetilde{u} \right) dt \quad (3.1.4)$$

with  $Q = Q^T \geq 0$  and  $R = R^T > 0$ .

Since we assumed the matrices  $A$  and  $B$  are assumed to be constant and the optimization is done over an infinite horizon an algebraic Riccati equation (ARE) is considered (that can be solved in real time).

With these two assumptions, the resulting pseudo-optimal feedback (neglecting the disturbances) is:

$$\begin{aligned} \widetilde{u} &= -R^{-1} B_e^T P \widetilde{X} \\ 0 &= P A_e + A_e^T P - P B_e R^{-1} B_e^T P + Q \end{aligned} \quad (3.1.5)$$

Although this feedback has been found to adequately regulate the system under simulation, the inputs are not physically realizable (the current deposit from LHCD has a particular form constraint). The input shape constraints are taken into account in the next subsection.

### 3.1.2 Pseudo-optimal Profile Regulation Under Shape Constraints

To include the shape constraints, an equilibrium  $(\overline{X}, \overline{u}, \overline{W}_e)$ , obtained from experimental data is considered (therefore with  $j_{lh}$  respecting the shape constraints).

We neglect again the term  $\widetilde{W}_e(t)$  and consider the variations in the bootstrap current as a disturbance. Therefore, linearizing the gaussian shape constraint (2.1.17) with respect to variations of the equilibrium parameters  $\overline{u}_p = (\overline{\mu}, \overline{\sigma}, \overline{A}_{lh})$ , and defining  $\widetilde{u}_p$  as a variation of these parameters, the system can be approximated as:

$$\dot{\widetilde{X}} = A_e(t) \widetilde{X} + B_e(t) \nabla u|_{u=\overline{u}} \widetilde{u}_p$$

Defining  $B_p(t) \doteq B_e(t) \nabla u|_{u=\overline{u}}$  the system can be written as:

$$\dot{\widetilde{X}} = A_e(t) \widetilde{X} + B_p(t) \widetilde{u}_p \quad (3.1.6)$$

The function  $u(u_p)$  being a gaussian curve, the three vectors representing the partial derivatives of  $u$  with respect to the parameters are linearly independent, which implies

that the rank of  $B_p(t)$  is 3 (recall that  $B(t)$  is a diagonal matrix of rank  $N$  that accounts for  $\eta_{||}R_0$ ). In turn, this guarantees that the controllability matrix of the system has a rank  $\geq 3$ .

Building on the properties of the matrix  $A(t)$  we choose as a reference three points in the  $\psi$  profile:  $\psi_1$ ,  $\psi_N$  and  $\psi_{N/2}$  (in this chapter, the subscript  $N/2$  should be understood to represent the largest integer  $\leq N/2$ ). It can be checked that the pair  $(A_e(t), B_p(t))$  is stabilizable for all  $t \geq t_0$ . Changing the integrator in equation (3.1.1) to evolve as  $\dot{E} = -K\psi - \lambda(t)E$ , where  $K\psi = (\psi_1, \psi_{N/2}, \psi_N)^T$ , we can choose  $Q = C^T C \geq 0$  such that the pair  $(A_e(t), C)$  is observable (in our case, weighting only the three chosen states and their integral). The fact that the pair  $(A_e(t), B_p(t))$  is stabilizable and the pair  $(A_e(t), C)$  is observable for all  $t$  ensures the existence of a positive definite solution to the ARE for all  $t \geq t_0$  (see e.g. [Ni, 2008]).

**Remark 3.1.2.** *Even though the pair  $(A_e(t), B_p(t))$  is stabilizable and there exists a positive definite solution to the ARE at all times, the stability of the time-varying system is not guaranteed. In particular, having all closed-loop eigenvalues with negative real parts at all times is not a sufficient condition to determine the stability of such systems without an additional condition of slow-enough variation, see for instance [Rosenbrock, 1963], [Desoer, 1969], [Kamen et al., 1989], [Amato et al., 1993].*

Assuming again that the matrices  $A_e$  and  $B_e$  are not time-varying and using the same cost function (3.1.4) with the new value for  $Q$  and under analogous hypotheses, we can obtain a similar pseudo-optimal feedback for our constrained system:

$$\begin{aligned}\tilde{u}_p &= -R^{-1}B_p^T P \tilde{X} \\ 0 &= PA_e + A_e^T P - PB_p R^{-1} B_p^T P + Q\end{aligned}\tag{3.1.7}$$

### 3.1.3 Simulation Results

The proposed control laws were numerically simulated with global parameters obtained from Tore Supra shot TS-35109 ( $I_p = 0.6$  MA, power input around 1.8 MW) and a simulator built on [Witrant et al., 2007]. For all the simulations, the boundary conditions are (2.1.3) and the version of (2.1.4) depending on the total plasma current. The references were chosen from estimations drawn from the same experimental run TS-35109, so they represent realistic values.

#### a. Controller without shape constraints

The unconstrained controller (3.1.5) was tested by numerical simulation, with its output considered directly to be  $j_{ni}$ . First, the reference was set to  $\bar{\psi}$ . At time  $t = 20$  s

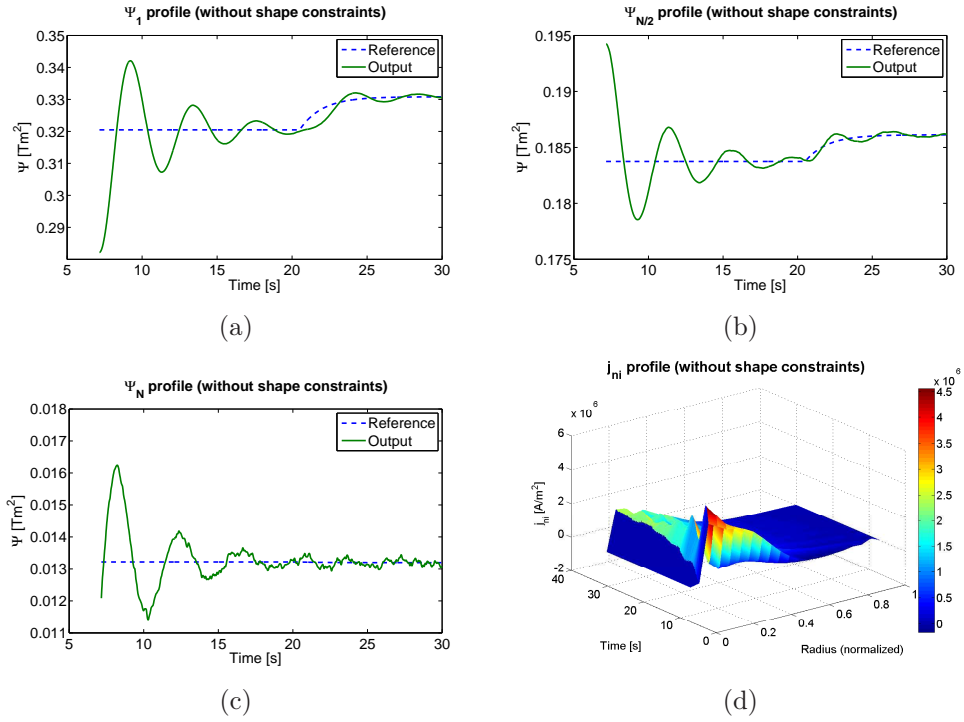


Figure 3.2: Regulation around  $\bar{\psi}$  with the unconstrained controller (plain line: numerical simulation, dashed line: the reference). (a) Evolution and reference of the state  $\psi_1$ ; (b) evolution and reference of the state  $\psi_{N/2}$ ; (c) evolution and reference of the state  $\psi_N$ ; (d) applied control signal  $u$ .

a reference change was applied. Fig. 3.2 shows the results: 3.2(a), (b) and (c) show the evolution of  $\psi_1$ ,  $\psi_{N/2}$  and  $\psi_N$  over time and their respective references.

It is interesting to note that the oscillations observed prior to the reference change are due to the fact that, when the controller is started, the "forgetting factor"  $\lambda(t)$  is set to zero and, for the unconstrained case, the regulator is started when the system has a state far away from the desired value (since it is not the product of a linearization around some reference position). This causes a large error to accumulate and, consequently, a large overshoot followed by oscillations is induced. Nevertheless, once the reference changes (and  $\lambda$  with it) the oscillations are greatly reduced and the system reaches the desired reference with a much better performance. Tweaking the values of the weighting matrices can also improve somewhat the transient response.

Fig. 3.2(d) shows the values of the unconstrained input during the simulation. This input does not respect the shape constraints imposed in subsection 3.1.2 and is not implementable.

### b. Controller with shape constraints

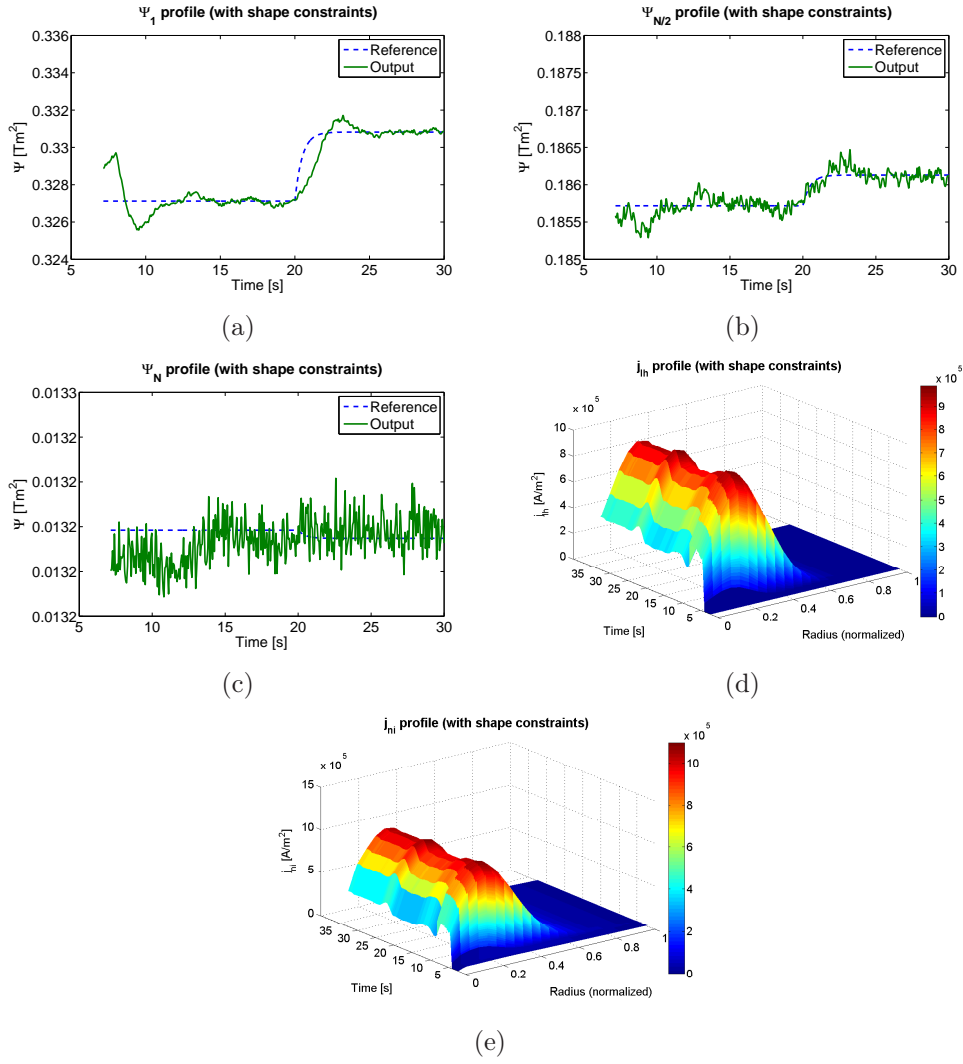


Figure 3.3: Regulation around  $\bar{\psi}$  with the shape-constrained controller (plain line: numerical simulation, dashed line: the reference). (a) Evolution and reference of the state  $\psi_1$ ; (b) evolution and reference of the state  $\psi_{N/2}$ ; (c) evolution and reference of the state  $\psi_N$ ; (d) applied control signal  $u$ ; (e) resulting  $j_{ni}$ .

The controller with shape constraints is tested by numerical simulation in this section. The system is allowed to almost reach the desired operating point by using an open-loop control (feeding the system with the actual parameters from the experimental run) before activating the controller at  $t = 8$  s. This initialization step is introduced since the constrained version of the controller is designed to work around a particular operating point. Again, Fig. 3.3(a), (b), and (c) show the evolution of  $\psi_1$ ,  $\psi_{N/2}$  and  $\psi_N$  with their respective references. The results of the regulation around  $\bar{\psi}$  are satisfactory, even when a small change in reference is introduced (the same one used in the unconstrained simulation, also at  $t = 20$  s).

The shape of  $j_{lh}$  shown in Fig. 3.3(d) is of particular interest. The input to the system is always a gaussian curve, calculated from the reference parameters plus the parameter variations given by the controller. In order to compare the current profile used with both approaches (constrained and unconstrained), Fig. 3.3(e) shows the resulting total  $j_{ni}$  current profile when using the controller under shape constraints.

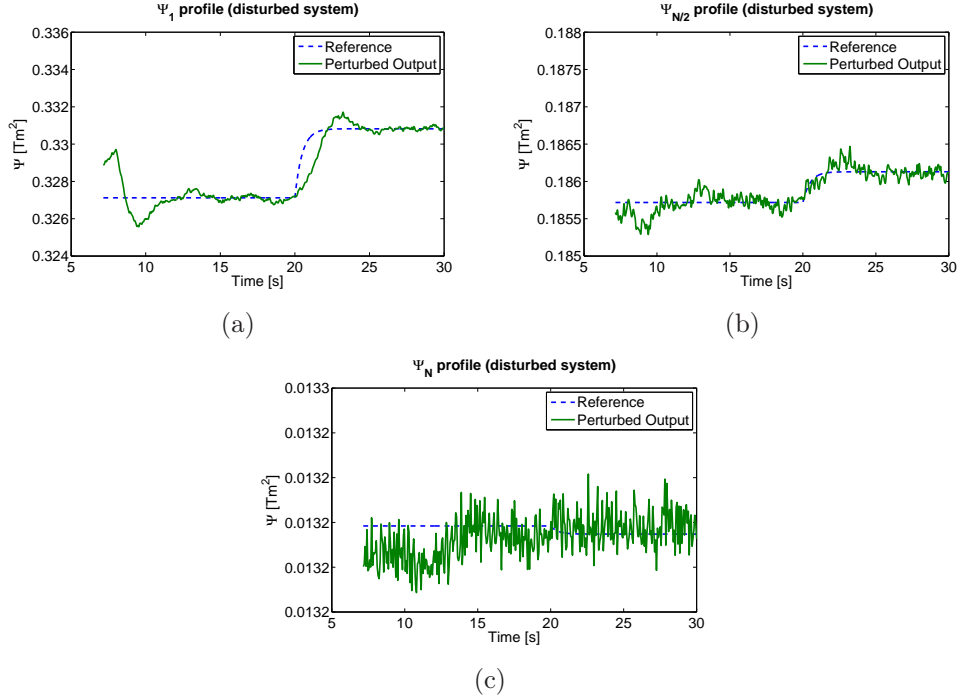


Figure 3.4: Reference and perturbed output caused by an error in the estimation of  $\eta_{||}$  (dashed line: reference, solid line: numerical simulation).

The robustness of the controller with respect to estimation errors was tested by using for the control calculations a value of  $\eta_{||}$  differing depending on  $x$  (linearly) by +10% at  $x = 0$  and -10% at  $x = 1$  from the one used to simulate the system evolution. The results can be appreciated in Fig. 3.4 (a), (b) and (c). In Fig. 3.4(a) negligible differences in the transient behavior of the perturbed system can be observed, while the stabilisation time remains unchanged.

### 3.1.4 Summary and Conclusions on LQR control

In this section, a controller was proposed for the stabilization of the poloidal magnetic flux profile  $\psi$  in a Tokamak plasma using the simplified distributed model of the system dynamics presented in the previous chapter. For this model, a pseudo-optimal feedback was constructed, based on the online solution of an ARE for the spatially discretized time-varying system. Furthermore, the introduction of a time-varying "forgetting factor"-like

term in the integration of the error allows for an improvement in the transient behavior of the system. In subsection 3.1.1 no shape constraints were considered on the current deposit of the non-inductive current sources and a global feedback-feedforward law was constructed. In subsection 3.1.2 a Gaussian distribution was imposed as a constraint for the  $j_{th}$  current profile linearizing the system dynamics around an equilibrium based on experimental data (Tore Supra shot TS-35109). It should be stressed that the time-varying nature of the system was preserved (a linear time-varying model was used as a reference). Finally, in the last subsection, simulation results for both the unconstrained and the constrained case are presented and discussed.

An important drawback of this approach is that the time-varying nature of the system does not allow for establishing stability guarantees (even though the closed-loop matrix is always Hurwitz). Furthermore, given the physical nature of the time-varying parameters, any hypothesis of "slow-enough" variation on these parameters is unrealistic (particularly since they vary according to the thermal confinement time, which is on a much faster timescale than the flux diffusion time). Furthermore, since the parameters do not stabilize unless the controlled input stops varying (due to internal couplings) a singular-perturbation analysis is not possible on these fast-varying parameters. Another drawback of the method is the computationally intensive solution of the ARE at each sampling time. This can become extremely cumbersome when the sampling time is small. In the next section we will focus on addressing the first drawback of this approach, namely, providing some stability guarantees for the closed-loop system.

## 3.2 Polytopic LPV

This section is based on results presented in [Bribiesca Argomedeo et al., 2011]. Our aim is now to develop a suitable control law for the regulation of the steady-state magnetic flux profile that allows an easier closed-loop stability analysis than the regulator developed in the last section (from [Bribiesca Argomedeo et al., 2010]). In particular, it is based on a polytopic approach similar to the one described in [Briat, 2008]. For some comprehensive surveys on Linear Parameter-Varying systems (LPV) control and gain scheduling controllers, see [Leith and Leithead, 2000] and [Rugh and Shamma, 2000]. For some applications of LPV/LMI gain-scheduling controls see [Wassink et al., 2005] and [Gilbert et al., 2010]. The actuation method under consideration is still restricted to the use of the non inductive Lower Hybrid Current Drive (LHCD) which acts as a current and heat source on the plasma.

### 3.2.1 LPV Model

Due to the characteristics of the distributed model, the time-varying components of equation (3.0.1) can be factorized as a positive definite, diagonal matrix  $M(t)$  as follows:

$$\dot{\psi}(t) = M(t) (A_{ct}\psi(t) + B_{ct}j_{ni}(t)) + W(t) \quad (3.2.1)$$

where  $A_{ct}$  and  $B_{ct}$  are constant matrices of appropriate dimensions. This specific architecture comes from the original non-homogeneous transport PDE model, where a single time and space-varying parameter (the resistivity) multiplies both the diffusive operator and the distributed exogeneous inputs.

As in the previous subsection, new variables are defined around an operating point:

$$\begin{aligned} \tilde{\psi} &\doteq \psi - \bar{\psi} \\ \tilde{j}_{ni} &\doteq j_{ni} - \bar{j}_{ni} \\ \tilde{W} &\doteq W - \bar{W} \end{aligned}$$

where  $(\bar{\psi}, \bar{j}_{ni}, \bar{W})$  is an equilibrium of the original system (that can be obtained from experimental data or numerical simulation). These variables have been defined in a slightly different way to the previous section since the variations from the equilibrium have been defined before extending the state with an integrator.

Using the same hypotheses as in the previous section, in particular concerning the fact that the plasma current is supposed to be almost constant during the steady-state operation of the tokamak, and considering the variations of the bootstrap current around the equilibrium as disturbances, the term  $\tilde{W}$  can be neglected. Furthermore,  $j_{ni}$  is reduced to the LHCD current deposit  $j_{lh}$  which can be represented as in (2.1.17).

Linearizing (2.1.17) with respect to a variation of the parameters around  $\bar{u}_p \doteq [\bar{\mu}_{lh}, \bar{\sigma}_{lh}, \bar{A}_{lh}]^T$  corresponding to the equilibrium condition  $\bar{j}_{lh}$ , and defining the variation of the parameters around the equilibrium as  $\tilde{u}_p \doteq u_p - \bar{u}_p$ , the resulting equation is:

$$\dot{\tilde{\psi}}(t) = M(t) \left( A_{ct}\tilde{\psi}(t) + B_{ct}\nabla_{u_p}j_{lh} \big|_{u_p=\bar{u}_p} \tilde{u}_p(t) \right) \quad (3.2.2)$$

Performing a change of variables  $\zeta \doteq M^{-1}(t)\tilde{\psi}$  and renaming the product  $B_{ct}\nabla_{u_p}j_{lh} \big|_{u_p=\bar{u}_p}$  as  $B_{lin}$ , the evolution of the new variable  $\zeta$  is given by:

$$\dot{\zeta}(t) = \left( A_{ct}M(t) - M^{-1}(t)\dot{M}(t) \right) \zeta(t) + B_{lin}\tilde{u}_p(t) \quad (3.2.3)$$

Since  $M(t)$  is diagonal and positive definite,  $M^{-1}(t)$  always exists and is bounded. Imposing boundedness and differentiability constraints on  $M(t)$ , we have that the matrix  $A_{\zeta}(t) \doteq A_{ct}M(t) - M^{-1}(t)\dot{M}(t)$  is also bounded. Choosing a nonempty basis



$\mathcal{A} = \{A_{\zeta_0}, A_{\zeta_1}, \dots, A_{\zeta_{n_p}}\}$ , subset of  $\mathbb{R}^{N \times N}$ , we write:

$$A_{\zeta}(t) = A_{\zeta_0} + \sum_{i=1}^{n_p} \lambda_i(t) A_{\zeta_i} \quad (3.2.4)$$

with  $n_p \leq N^2$ ,  $\lambda_i(t) \in [0, 1]$  for all  $i \leq n_p$  and all  $t \geq 0$ . Furthermore, it can be shown that, as a consequence of the diagonal structure of  $M(t)$ , an  $n_p \leq 2N$  is enough to exactly represent  $A_{\zeta}(t)$  (a basis of size  $N$  to represent the diagonal elements of  $M^{-1}(t)\dot{M}(t)$  and another of size  $N$  representing each of the columns of  $A_{ct}$ ).

Using (3.2.4) in (3.2.3), we get:

$$\dot{\zeta}(t) = \left( A_{\zeta_0} + \sum_{i=1}^{n_p} \lambda_i(t) A_{\zeta_i} \right) \zeta(t) + B_{lin} \tilde{u}_p(t) \quad (3.2.5)$$

In order to reject some disturbances, like the ones represented by the bootstrap current in the system, it is useful to extend the state to include an integrator of a virtual error  $\dot{E} = \varepsilon \doteq -C\zeta$ , with  $C$  in  $\mathbb{R}^{N_e \times N}$ , as follows:

$$z \doteq \begin{bmatrix} \zeta \\ E \end{bmatrix}, \quad A_0 \doteq \begin{bmatrix} A_{\zeta_0} & 0 \\ -C & 0 \end{bmatrix}$$

$$A_i \doteq \begin{bmatrix} A_{\zeta_i} & 0 \\ 0 & 0 \end{bmatrix}, \quad \forall i \geq 1, \quad B_e \doteq \begin{bmatrix} B_{lin} \\ 0 \end{bmatrix}$$

The extended system is:

$$\dot{z}(t) = \left( A_0 + \sum_{i=1}^{n_p} \lambda_i(t) A_i \right) z(t) + B_e \tilde{u}_p(t) \quad (3.2.6)$$

Notice that  $B_e$  is a constant matrix, unlike in the previous section. This equation represents the reference model used for the development of a control law in this section.  $N_e = N_c + N$  denotes the size of the vector  $z$ .

### 3.2.2 Controller Synthesis Results

Define the set of all partitions of  $\mathcal{N}_p \doteq \{1, 2, \dots, n_p\}$  as  $\Omega(\mathcal{N}_p) \doteq \{(\mathcal{C}_j, \mathcal{D}_j) \mid \mathcal{C}_j \cap \mathcal{D}_j = \emptyset, \mathcal{C}_j \cup \mathcal{D}_j = \mathcal{N}_p\}$ . It is clear that  $\text{card } \Omega(\mathcal{N}_p) = 2^{n_p}$ . Based on this set, consider a polytopic control law for a given set of vertex controllers  $K_1, \dots, K_{2^{n_p}} \in \mathbb{R}^{3 \times N}$  and time-varying parameters  $\lambda_1(t), \dots, \lambda_{n_p}(t) \in [0, 1]$  as:

$$\tilde{u}_p(t) = \sum_{j=1}^{2^{n_p}} \beta_j(t) K_j z(t) \quad (3.2.7)$$

where:

$$\beta_j(t) = \prod_{k \in \mathcal{C}_j} (1 - \lambda_k(t)) \prod_{l \in \mathcal{D}_j} \lambda_l(t)$$

and

$$(\mathcal{C}_j, \mathcal{D}_j) \in \Omega(\mathcal{N}_p), \forall j \in \mathcal{N}_p$$

**Remark 3.2.1.** For all  $j$  in  $\mathcal{N}_p$  and all  $t \geq 0$ :  $\beta_j(t) \in [0, 1]$ . It can also be shown, by induction on  $n_p$ , that  $\sum_{j=1}^{2^{n_p}} \beta_j(t) = 1$  for all  $t \geq 0$ .

**Theorem 3.2.2.** A polytopic control law, as defined in (3.2.7), that quadratically stabilizes system (3.2.6) can be constructed by setting  $K \doteq Q_j W^{-1}$ , with  $W \in \mathbb{R}^{N_e \times N_e}$  a positive definite symmetric matrix and  $Q_j \in \mathbb{R}^{3 \times N_e}$ ,  $j = 1, 2, 3, \dots, 2^{n_p}$ , full matrices such that the following LMIs are verified<sup>1</sup>:

$$\begin{bmatrix} \varepsilon^{-1} \mathbb{I}_{N_e} & W \\ W & -M_j \end{bmatrix} \succ 0, \forall j \in \{1, 2, 3, \dots, 2^{n_p}\} \quad (3.2.8)$$

where,  $\varepsilon$  is a positive constant and, for all  $j$ ,  $M_j$  is defined as:

$$M_j \doteq \left( A_0 + \sum_{i=1}^{n_p} s_{i,j} A_i \right) W + W \left( A_0 + \sum_{i=1}^{n_p} s_{i,j} A_i \right)^T + B_e Q_j + Q_j^T B_e^T$$

with, for all  $j$ ,  $s_{i,j} = 0$  if  $i \in \mathcal{C}_j$ , and  $s_{i,j} = 1$  otherwise.

*Proof.* Using the Schur complement, (3.2.8) is equivalent to:

$$\begin{aligned} \left( A_0 + \sum_{i=1}^{n_p} s_{i,j} A_i \right) W + W \left( A_0 + \sum_{i=1}^{n_p} s_{i,j} A_i \right)^T + B_e Q_j + Q_j^T B_e^T + \varepsilon W^2 \prec 0 \\ \forall j \in \{1, 2, 3, \dots, 2^{n_p}\} \end{aligned} \quad (3.2.9)$$

Set  $Q_j = K_j W$  and  $P = W^{-1}$ . Substituting these in equation (3.2.9) and pre- and post-multiplying by  $P$  we obtain:

$$\begin{aligned} P \left( A_0 + \sum_{i=1}^{n_p} s_{i,j} A_i + B_e K_j \right) + \left( A_0 + \sum_{i=1}^{n_p} s_{i,j} A_i + B_e K_j \right)^T P + \varepsilon \mathbb{I}_{N_e} \prec 0 \\ \forall j \in \{1, 2, 3, \dots, 2^{n_p}\} \end{aligned} \quad (3.2.10)$$

---

<sup>1</sup> Here  $\cdot \succ 0$  means that a matrix is positive definite.

Multiplying each inequality by the corresponding  $\beta_j$  and adding them up (remembering that  $\sum_{j=1}^{2^{np}} \beta_j(t) = 1$ ) we obtain:

$$\begin{aligned} & P \left( \sum_{j=1}^{2^{np}} \beta_j \left[ A_0 + \sum_{i=1}^{n_p} s_{i,j} A_i + B_e K_j \right] \right) \\ & + \left( \sum_{j=1}^{2^{np}} \beta_j \left[ A_0 + \sum_{i=1}^{n_p} s_{i,j} A_i + B_e K_j \right] \right)^T P + \varepsilon \mathbb{I}_{N_e} \prec 0 \end{aligned} \quad (3.2.11)$$

Rearranging the order of the sums, it is easy to see that:

$$\sum_{j=1}^{2^{np}} \beta_j \left[ \sum_{i=1}^{n_p} s_{i,j} A_i \right] = \sum_{i=1}^{n_p} A_i \left[ \sum_{j=1}^{2^{np}} \beta_j s_{i,j} \right] \quad (3.2.12)$$

And since  $\forall j \ s_{i,j} = 0$  if  $i \in \mathcal{C}_j$ , and  $s_{i,j} = 1$  otherwise, for any given  $j$ , we have:

$$\begin{aligned} \sum_{j=1}^{2^{np}} \beta_j(t) s_{i,j} &= \lambda_i(t) \prod_{k \in \mathcal{C}'_j} (1 - \lambda_k(t)) \prod_{l \in \mathcal{D}'_j} \lambda_l(t) \\ (\mathcal{C}'_j, \mathcal{D}'_j) &\in \Omega(\mathcal{N}_p \setminus \{i\}) \quad , \quad \forall j \in \mathcal{N}_p \setminus \{i\} \end{aligned} \quad (3.2.13)$$

Using a similar argument to the one required to prove that  $\sum_{j=1}^{2^{np}} \beta_j(t) = 1$ , it can be shown that  $\sum_{j=1}^{2^{np}} \beta_j s_{i,j} = \lambda_i$ . And using these two facts, equation (3.2.11) is equivalent to:

$$\begin{aligned} & P \left( A_0 + \sum_{i=1}^{n_p} \lambda_i A_i + B_e \sum_{j=1}^{2^{np}} \beta_j K_j \right) \\ & + \left( A_0 + \sum_{i=1}^{n_p} \lambda_i A_i + B_e \sum_{j=1}^{2^{np}} \beta_j K_j \right)^T P + \varepsilon \mathbb{I}_{N_e} \prec 0 \end{aligned} \quad (3.2.14)$$

which, if pre-multiplied by  $z^T$  and post-multiplied by  $z$  is actually the time derivative of  $V(z) = z^T P z$  for the system (3.2.6) under the control law (3.2.7). This implies that  $V$  is a Lyapunov function for the closed-loop system.  $\square$

It may also be desirable to constrain the gain of the controller (particularly since the application under consideration is based on a linearization around a given input value). Let us denote by  $\|\cdot\|_2$  the  $\mathcal{L}^2$ -norm of a vector or the respective induced norm of a matrix.

**Proposition 3.2.3.** *Let  $W \in \mathbb{R}^{N_e \times N_e}$  be a positive definite matrix,  $K \in \mathbb{R}^{3 \times N_e}$  a full matrix and  $Q \doteq KW$ . A sufficient condition to guarantee that  $\|K\|_2 < \sqrt{\gamma}$  is that the following LMIs are satisfied:*

$$\begin{aligned} \begin{bmatrix} -\mathbb{I}_3 & Q \\ Q^T & -\gamma\mathbb{I}_{N_e} \end{bmatrix} &\prec 0 \\ W &\succ \mathbb{I}_{N_e} \end{aligned} \quad (3.2.15)$$

where  $\mathbb{I}_l$  represents the  $l \times l$  identity matrix.

*Proof.* Using the Schur complement, the first inequality is clearly equivalent to  $Q^T Q - \gamma\mathbb{I}_{N_e} \prec 0$ , which in turn implies  $z^T Q^T Q z < \gamma z^T \mathbb{I}_{N_e} z, \forall z \in \mathbb{R}^{N_e}$ . That is,  $\|Q\|_2 < \sqrt{\gamma}$ . The second LMI implies  $\|W^{-1}\|_2 < 1$ . Since  $Q = KW$ , we have that  $\|K\|_2 < \sqrt{\gamma}$ .  $\square$

Combining Theorem 3.2.2 and Proposition 3.2.3, the following corollary is directly obtained:

**Corollary 3.2.4.** *Given  $\gamma > 0$ , a polytopic control law as defined in (3.2.7) that quadratically stabilizes system (3.2.6) and has an  $\mathcal{L}_2$  gain between the state and control input strictly less than  $\sqrt{\gamma}$  can be computed by setting  $K_j \doteq Q_j W^{-1}$ , with  $W \in \mathbb{R}^{N_e \times N_e}$  a positive definite symmetric matrix and  $Q_j \in \mathbb{R}^{3 \times N_e}, j = 1, 2, 3, \dots, 2^{n_p}$ , full matrices such that the following LMIs are verified:*

$$\begin{aligned} \begin{bmatrix} \varepsilon^{-1}\mathbb{I}_{N_e} & W \\ W & -M_j \end{bmatrix} &\succ 0 \\ \begin{bmatrix} -\mathbb{I}_3 & Q_j \\ Q_j^T & -\gamma\mathbb{I}_{N_e} \end{bmatrix} &\prec 0 \\ W &\succ \mathbb{I}_{N_e} \\ \forall j &\in \{1, 2, 3, \dots, 2^{n_p}\} \end{aligned} \quad (3.2.16)$$

where  $M_j$  is defined as in Theorem 3.2.2.

**Remark 3.2.5.** *It is interesting to note that the feasibility of the proposed control scheme clearly illustrates the compromise existing between accelerating the system (represented here by  $\varepsilon$ ) and limiting the gain (represented here by  $\gamma$ ). In general, it is not possible to arbitrarily accelerate the system while guaranteeing a small gain.*

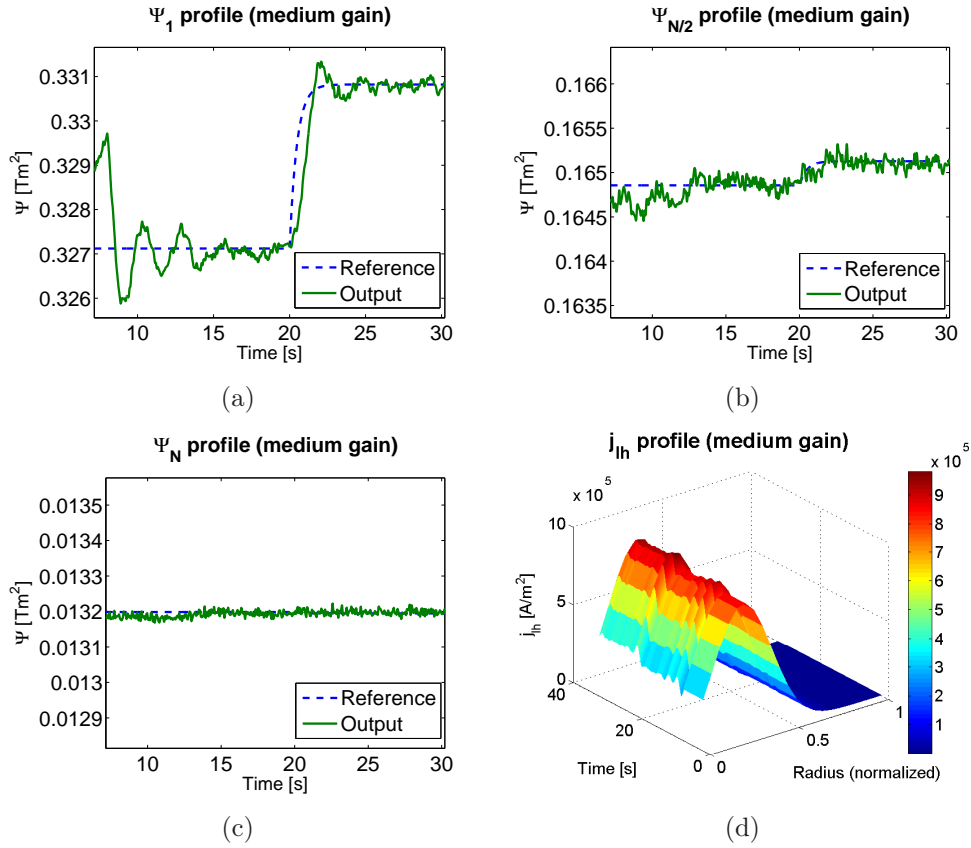


Figure 3.5: Regulation around  $\bar{\psi}$  with LMI controller with medium gain (plain line: numerical simulation, dashed line: the reference). (a) Evolution and reference of the state  $\psi_1$ ; (b) evolution and reference of the state  $\psi_{N/2}$ ; (c) evolution and reference of the state  $\psi_N$ ; (d) applied  $j_{lh}$  profile.

### 3.2.3 Validation

#### c. Implementation

In order to implement the proposed control scheme, a suitable approximation basis was determined for the time-varying components of the system. The basis used provides a sufficiently good approximation of the original function while reducing the computational cost by keeping the number of parameters  $n_p$  low. This is particularly important since the number of decision variables and the size of the LMIs grows exponentially with the number of parameters used. In this particular scenario the number of parameters chosen was 5, preserving a small approximation error: under 1% in average for the  $A_{ct}M(t)$  term and with a peak close to 10% for  $M^{-1}(t)\dot{M}(t)$  in a few points. The data was fitted using a least squares method with a positivity constraint on the coefficients, to prevent the existence of aberrant vertices corresponding to, for instance, a negative

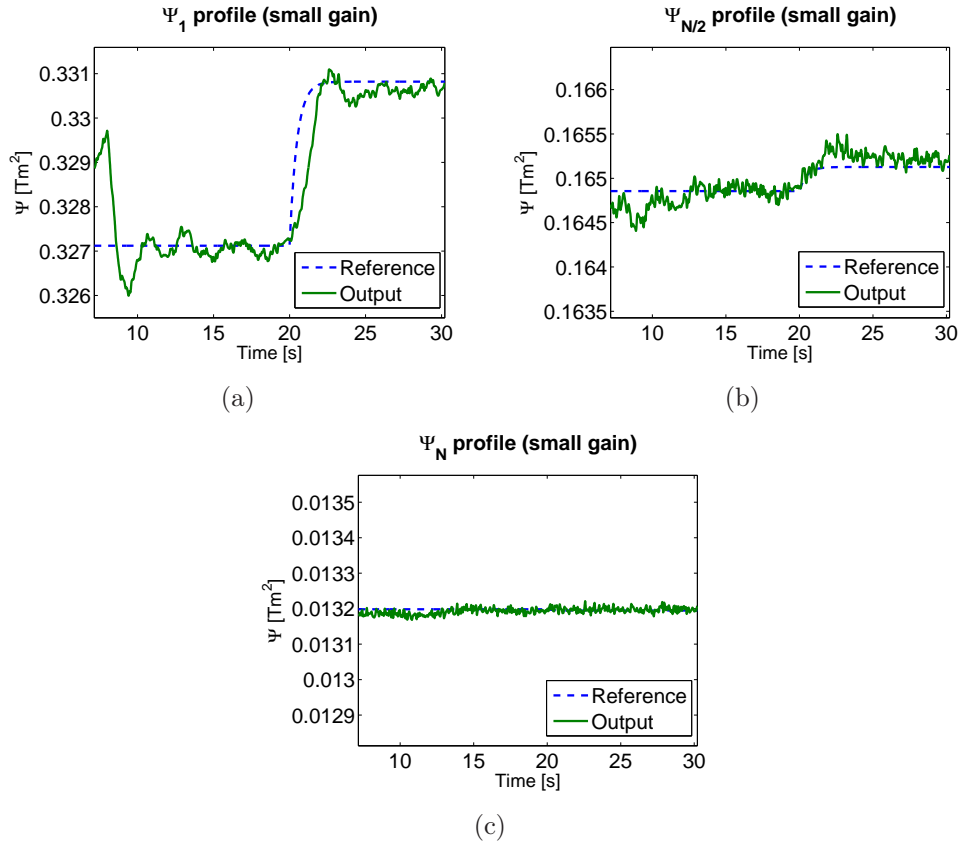


Figure 3.6: Regulation around  $\bar{\psi}$  with LMI controller with a more restricted gain than in Figure 3.5 (plain line: numerical simulation, dashed line: the reference). (a) Evolution and reference of the state  $\psi_1$ ; (b) evolution and reference of the state  $\psi_{N/2}$ ; (c) evolution and reference of the state  $\psi_N$ .

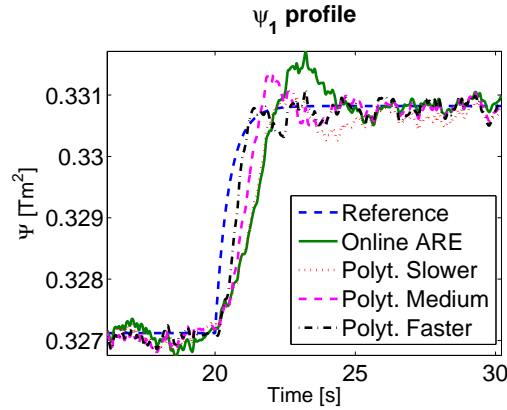


Figure 3.7: Regulation around  $\bar{\psi}$  for  $\psi_1$ . The thin dashed line is the reference, the solid line is the ARE-based simulation and the others are polytopic regulators with different  $\gamma$  values.

diffusion coefficient. As a further development a recursive least-squares algorithm could be implemented.

The parameter  $\varepsilon$  ensures that the real part of all closed-loop poles is less than  $-\varepsilon$ , indirectly allowing the controller to be more robust with respect to modeling errors due, for instance, to the use of only 5 parameters in the approximation of  $A_{ct}M(t)$  and  $M^{-1}(t)\dot{M}(t)$ . The systems of LMIs were solved using YALMIP, see [Löfberg, 2004], and SeDuMi, see [SeDuMi, 2011].

### d. Simulation Results

In order to test the proposed method using numerical simulation, a reference was chosen at three points of the  $\psi$  profile, taken from estimations based on Tore-Supra shot TS-35109 and equal to the one used in [Bribiesca Argomedo et al., 2010]. The global parameters of the simulation were also taken from shot TS-35109 ( $I_p = 0.6$  MA, power input around 1.8 MW). The system was discretized in 8 points for the controller calculation and in 22 for the simulation. In all the simulations, the system is taken close to the desired operating point by applying the open-loop control sequence of the actual shot TS-35109, and then, at  $t = 8$  s activating the controller. A change of reference is then applied at  $t = 20$  s.

In Figure 3.5, a controller with medium gain  $\gamma = 2.75 \times 10^{-6}$  was chosen with a settling time comparable to that presented in [Bribiesca Argomedo et al., 2010]. Figures 3.5(a), (b) and (c) show the evolution of the points  $\psi_1$ ,  $\psi_{N/2}$  and  $\psi_N$ , respectively; 3.5(d) shows the applied  $j_{lh}$  profile. It can be seen that  $j_{lh}$  is a gaussian curve, the parameters of which are calculated as  $u + \bar{u}_p$ .

To show the versatility of the proposed gain limit, another controller was calculated with stricter gain limitations by reducing the value of the  $\gamma$  parameter in the LMI system to  $2.5 \times 10^{-6}$ . The results are shown in Figure 3.6: (a), (b) and (c) show the evolution of the points  $\psi_1$ ,  $\psi_{N/2}$  and  $\psi_N$ , respectively. The settling time is greater than in the previous case, which is to be expected when restricting the gain.

To further illustrate the interest of the proposed scheme, Figure 3.7 shows a comparison of the behaviour of  $\psi_1$  for three different polytopic controllers with different values of  $\gamma$  and the online ARE approach used in the previous section (from [Bribiesca Argomedo et al., 2010]). It should be noted that the tuning of the LMI-based polytopic controllers is much easier than finding appropriate weighting matrices for the LQR computation used in [Bribiesca Argomedo et al., 2010]. It is also important to mention that the online computational cost of the polytopic controller is much less than the ARE-based one, since it only requires to estimate the current values of the parameters  $\lambda_i$  whereas the latter requires to solve an ARE at each sampling time. Nevertheless, the polytopic approach does require the prior solution of the system of LMIs (which can

be done offline and only needs to be done once).

### 3.2.4 Summary and Conclusions on the Polytopic Approach

In this section, a polytopic controller was developed for the regulation of the magnetic flux profile in a tokamak plasma based on the model presented in the previous chapter. After discretizing the model, a change of variables was performed that allowed for the simple construction of a polytopic control law. A sufficient condition for the stability of the closed-loop system with bounded time-varying parameters and bounded time derivatives of these parameters is established and then tested under simulation with a more complete model to test the robustness of the approach with respect to unmodeled dynamics, disturbances and approximation errors.

Although this approach adequately addresses the most important drawback of the previous section (i.e. the absence of stability guarantees for the closed-loop system with time-varying matrices) it still does not entirely satisfy the requirements of the physical system. First, small and slow variations of the operating point must be considered in order to limit the norm of the  $\dot{M}M^{-1}$  term. Second, the use of a linearized version of the actuator constraints limits the use of the control law far from the calculated operating point. Third, the use of three parameters in the gaussian as control inputs is unrealistic since only two engineering parameters are available in the LH antennas (the power  $P_{lh}$  and the refractive index  $N_{||}$ ). Fourth, the complexity of finding a suitable control law grows exponentially with the size of the base chosen to represent the time-varying matrices and the conservatism of the sufficient condition might make the problem unfeasible for large variations of some parameters (crucially including the time-derivative of the diffusivity coefficients). Finally, the algorithm remains computationally expensive, even if it is less so than the solution of the ARE proposed in the previous section.

## 3.3 Motivation for an Infinite-Dimensional Approach

In this chapter two control approaches have been proposed based on a discretized version of the model presented in Chapter 2. Both approaches presented here have some important drawbacks that leave several of the key challenges presented in Chapter 2 unsolved. Furthermore, the possibility to control a few points in the poloidal magnetic flux profile does not address the main objective of controlling the safety-factor profile. Since extending this results to the gradient of the magnetic flux is not straightforward and will require to impose some limits in the variation of the resistivity profile, a different, infinite-dimensional approach will be pursued in the rest of this thesis.





# Chapter 4

## Infinite-Dimensional Control

### Contents

---

<b>4.1</b>	<b>Some Possible Lyapunov Functions . . . . .</b>	<b>60</b>
4.1.1	First Candidate Lyapunov Function . . . . .	60
4.1.2	Second Candidate Lyapunov Function . . . . .	61
<b>4.2</b>	<b>Selected Control Lyapunov Function and Nominal Stability</b>	<b>63</b>
4.2.1	Candidate Control Lyapunov Function . . . . .	63
4.2.2	Some Implications . . . . .	66
<b>4.3</b>	<b>Input-to-State Stability and Robustness . . . . .</b>	<b>67</b>
4.3.1	Disturbed Model . . . . .	67
<b>4.4</b>	<b>D<sup>1</sup>-Input-to-State Stability . . . . .</b>	<b>71</b>
4.4.1	Strict Lyapunov Function and sufficient conditions for D <sup>1</sup> - Input-to-State Stability . . . . .	71
<b>4.5</b>	<b>Application to the Control of the Poloidal Magnetic Flux Profile in a Tokamak Plasma . . . . .</b>	<b>74</b>
4.5.1	Illustration of Stability: Numerical computation of the Lyapunov function . . . . .	74
4.5.2	Illustration of ISS property: Tokamak Simulation with Unconstrained Controller . . . . .	77
4.5.3	Exploiting the Lyapunov Approach: Tokamak Simulation with Constrained Control . . . . .	78

---

In this chapter, the concept of *input-to-state stability* (ISS) will be the chosen framework to study the stability and robustness of a diffusion equation in a circular domain under a revolution symmetry condition with symmetric initial conditions. The interest of studying such an equation is illustrated and motivated by the proposed application,

where a similar equation arises from the averaging of a 2-D physical equation (representing the evolution of the toroidal magnetic flux in a tokamak) over the angle at fixed radius (nested toroidal surfaces). A comprehensive survey of ISS concepts, in the finite-dimensional case, can be found in [Sontag, 2008]. ISS essentially implies guaranteeing some bounded gain between disturbances or errors and the states of the system. ISS-like properties in the infinite dimensional framework using a frequency-domain approach can be found for example in [Jayawardhana et al., 2008]. Nevertheless, we have favored the use of a Lyapunov-based approach to allow for an easier treatment of very general disturbances and errors in the system.

Although the use of Lyapunov functions in an infinite dimensional setting is not new, see for example [Baker and Bergen, 1969], it is still an active research topic. Some interesting results for parabolic PDEs can be mentioned: [Cazenave and Haraux, 1998], where a Lyapunov function is used to prove the existence of a global solution to the heat equation; [Krstic and Smyshlyaev, 2008], where a Lyapunov function is constructed for the heat equation with unknown destabilizing parameters (and subsequent control extensions [Smyshlyaev and Krstic, 2007a] and [Smyshlyaev and Krstic, 2007b]). Lyapunov based approaches are not limited to parabolic PDEs: Lyapunov functions are used in [Coron and d'Andréa Novel, 1998] for the stabilization of a rotating beam; in [Coron et al., 2008] for the stability analysis of quasilinear hyperbolic systems and in [Coron et al., 2007] for the construction of stabilizing boundary controls for a system of conservation laws. In particular, in [Mazenc and Prieur, 2011] and [Prieur and Mazenc, 2012] the interest of using a strict-Lyapunov function to obtain ISS-like properties is discussed in the parabolic and hyperbolic cases, respectively. The use of weighted  $L^2$  norms (or similar quadratic expressions with a weight) as Lyapunov functions is not new and a few examples can be found in [Peet et al., 2009] (for time delay systems) and [Gahlawat et al., 2011] (where a vanishing weight is also used for the control of the magnetic flux equation in a tokamak but not its gradient).

Some previous works on reaction-diffusion equations in cylindrical 2-D domains are, for instance, [Vazquez and Krstic, 2006] and [Vazquez and Krstic, 2010] in which boundary control laws are developed for the stabilization of thermal convection loops. However, in both of these articles the domain considered does not include the point  $r = 0$ , which implies that none of the coefficients in the equation are singular.

In this chapter, we develop a strict Lyapunov function for the diffusion equation for a certain set of diffusivity coefficient profiles. Our main contribution is that the coefficients are allowed to be space and time dependent without imposing any constraints on the rate of variation of the coefficients with respect to time. This is an improvement over other works that consider diffusivity coefficients as being space-dependent or time-varying but not both simultaneously. Examples of such approaches are provided by [Smyshlyaev and Krstic, 2004], where constant diffusion coefficients and distributed

convection coefficients are considered; [Smyshlyaev and Krstic, 2005], where the case of non-constant diffusion coefficients is treated (for continuous, time-invariant coefficients); or [Vazquez and Krstic, 2008], where distributed and time-varying convection coefficients are taken into account (with a constant diffusion coefficient). Also, stability and robustness of the system under a simple unconstrained feedback law (that includes the open-loop system as a limiting case) were derived from the Lyapunov function, with results addressing most sources of errors and uncertainties that may be present in a real system. In particular, the following sources of error were considered:

- *state disturbances*: accounting for example for unmodeled dynamics;
- *actuation errors*: accounting mainly for errors in the actuator models (similar to the concept of controller fragility);
- *estimation errors in the state and diffusivity coefficients*: accounting for instance for discretized measurements or uncertain models, as well as measurement noise.

In the first section, we consider two possible candidate Lyapunov functions based on an  $L^2(\Omega)$  norm, defined for functions on the domain  $\Omega$  defined for the Cartesian representation of (2.1.11)-(2.1.13), as:

$$\|\xi(\cdot)\|_{L^2(\Omega)}^2 = \int_{\Omega} \xi^2(y) dy \quad (4.0.1)$$

for some function  $\xi : \Omega \rightarrow \mathbb{R}$ . In the next sections we will consider a different  $L^2$  norm, defined for functions on an interval  $[0, 1]$  based on the spatial domain defined in (2.1.14)-(2.1.16), as:

$$\|\xi(\cdot)\|_{L^2([0,1])}^2 = \int_0^1 \xi^2(r) dr \quad (4.0.2)$$

for a function  $\xi$  now defined as  $\xi : [0, 1] \rightarrow \mathbb{R}$ .

It is important to note that the convergence in the topology induced by the  $L^2(\Omega)$  norm is not equivalent to that in the topology defined by the  $L^2([0, 1])$  norm proposed in the last sections (since the  $L^2(\Omega)$  norm is constructed with surface differentials which, when expressed in polar coordinates, are proportional to the radius). The choice of the  $L^2([0, 1])$  norm allows us to have a non-zero weight near the center, given that the central safety factor is an important quantity for the considered application. The results presented in this chapter are mostly based on [Bribiesca Argomedo et al., 2012a] and [Bribiesca Argomedo et al., 2012b].

## 4.1 Some Possible Lyapunov Functions

When considering the problem of guaranteeing the stability of the poloidal magnetic flux equation we may consider some Lyapunov functions that (at least in the case of constant diffusivity coefficients) simplify the analysis. We first consider the simple homogeneous case with a state  $v(x, t) \doteq \psi(x, t) - \bar{\psi}(x)$ . We choose to use in this section the notation  $v$  instead of the usual  $\tilde{\psi}$  to emphasize the fact that we will be using the alternate boundary condition (with  $V_{loop} = 0$ ). The dynamics of this state are given by:

$$v_t = \eta(x, t) \Delta v(x, t), \quad \forall (x, t) \in \Omega \times [0, T] \quad (4.1.1)$$

where  $\Omega$  is defined as in  $P_2$  in Chapter 2 (an open ball of radius 1 in  $\mathbb{R}^2$ ), with boundary condition:

$$v(x, t) = 0, \quad \forall (x, t) \in \partial\Omega \times [0, T] \quad (4.1.2)$$

Consider the  $L^2(\Omega)$  norm of this state, defined as:

$$\|v(\cdot, t)\|_{L^2(\Omega)}^2 = \int_{\Omega} v^2(y, t) dy \quad (4.1.3)$$

### 4.1.1 First Candidate Lyapunov Function

The first candidate Lyapunov function to be considered for system (4.1.1)-(4.1.2) is the following:

$$W(v, t) = \frac{1}{2} \int_{\Omega} \frac{1}{\eta(y, t)} v^2(y, t) dy \quad (4.1.4)$$

**Remark 4.1.1.** *It should be noted that Property  $P_1$  in Chapter 2 implies this norm is equivalent to (4.1.3).*

Differentiating (4.1.4) with respect to time along the solutions to (4.1.1)-(4.1.2) we obtain:

$$D_t W = \int_{\Omega} v(y, t) \Delta v(y, t) dy - \frac{1}{2} \int_{\Omega} \frac{\dot{\eta}(y, t)}{\eta^2(y, t)} v^2(y, t) dy$$

which, integrating by parts and using the boundary condition (4.1.2) implies:

$$D_t W = - \int_{\Omega} |\nabla v(y, t)|^2 dy - \frac{1}{2} \int_{\Omega} \frac{\dot{\eta}(y, t)}{\eta^2(y, t)} v^2(y, t) dy$$

Using Poincaré's inequality,

$$D_t W \leq -C_p \int_{\Omega} v^2(y, t) dy - \frac{1}{2} \int_{\Omega} \frac{\dot{\eta}(y, t)}{\eta^2(y, t)} v^2(y, t) dy$$

for some constant  $C_p > 0$  depending only on the domain  $\Omega$ .

Using the boundedness of  $\eta$  we obtain:

$$D_t W \leq -2\eta_{\min} C_p \left( \frac{1}{2} \int_{\Omega} \frac{1}{\eta(y, t)} v^2(y, t) dy \right) - \frac{1}{2} \int_{\Omega} \frac{\dot{\eta}(y, t)}{\eta^2(y, t)} v^2(y, t) dy$$

Defining  $\alpha \doteq 2\eta_{\min} C_p > 0$

$$D_t W \leq -\alpha W - \frac{1}{2} \int_{\Omega} \frac{\dot{\eta}(y, t)}{\eta^2(y, t)} v^2(y, t) dy$$

and

$$D_t W \leq -\alpha W - \inf_{x \in \Omega} \left( \frac{\dot{\eta}(x, t)}{\eta(x, t)} \right) W$$

We obtain therefore that, if:

$$\inf_{(x, t) \in \Omega \times [0, T]} \left( \frac{\dot{\eta}(x, t)}{\eta(x, t)} \right) \geq -(\alpha - \epsilon) \quad (4.1.5)$$

for some  $\epsilon > 0$ , then  $W$  is a Lyapunov function for the system (4.1.1)-(4.1.2), with:

$$D_t W \leq -\epsilon W \quad (4.1.6)$$

For the application under consideration, however, (4.1.5) is too restrictive, since it strongly limits the allowable rate of variation of the parameters at every point in time. In the next section, this Lyapunov function will be modified in order to relax this condition.

### 4.1.2 Second Candidate Lyapunov Function

In order to relax condition (4.1.5) using the same method presented in [Prieur and Mazenc, 2012] (for hyperbolic systems of conservation laws), let us consider the following candidate Lyapunov function:

$$U(v, t) = e^{s_k(t)} W(v, t) \doteq \frac{1}{2} e^{\frac{1}{T} \int_{t-T}^t \int_{\tau}^t q_k(\xi) d\xi d\tau} \int_{\Omega} \frac{1}{\eta(y, t)} v^2(y, t) dy \quad (4.1.7)$$

where  $q_k(t) = \inf_{x \in \Omega} (\dot{\eta}(x, t)/\eta(x, t))$  and  $s_k(t) \doteq \frac{1}{T} \int_{t-T}^t \int_{\tau}^t q_k(\xi) d\xi d\tau$ .

**Remark 4.1.2.** *It should be noted that, in order for  $U$  to be equivalent to norm (4.1.3),  $s_k(t)$  has to be uniformly bounded with respect to time.*

Calculating the time derivative of  $U$  along the solutions of (4.1.1)-(4.1.2) we obtain:

$$D_t U = \left( q_k(t) - \frac{1}{T} \int_{t-T}^t q_k(m) dm \right) e^{s_k(t)} W(v, t) + e^{s_k(t)} D_t W(v, t)$$

and therefore:

$$D_t U \leq e^{s_k(t)} \left[ -\frac{1}{T} \int_{t-T}^t \inf_{x \in \Omega} \left( \frac{\dot{\eta}(x, \tau)}{\eta(x, \tau)} \right) d\tau - \alpha \right] W(v, t)$$

$$D_t U \leq \left[ -\frac{1}{T} \int_{t-T}^t \inf_{x \in \Omega} \left( \frac{\dot{\eta}(x, \tau)}{\eta(x, \tau)} \right) d\tau - \alpha \right] U(v, t)$$

Hence, sufficient conditions for  $U$  to be a Lyapunov function are the existence of  $T, \epsilon > 0$  and  $\epsilon_1$  such that:

$$\int_{t-T}^t \inf_{x \in \Omega} \left( \frac{\dot{\eta}(x, \tau)}{\eta(x, \tau)} \right) d\tau \geq -T(\alpha - \epsilon), \forall t \in [0, T] \quad (4.1.8)$$

and:

$$\frac{1}{T} \int_{t-T}^t \int_{\tau}^t \inf_{x \in \Omega} \left( \frac{\dot{\eta}(x, \xi)}{\eta(x, \xi)} \right) d\xi d\tau \geq \epsilon_1, \forall t \in [0, T] \quad (4.1.9)$$

The first condition implies that:

$$D_t U \leq -\epsilon U, \forall t \in [0, T] \quad (4.1.10)$$

while the second guarantees that:

$$U \geq e^{\epsilon_1} W, \forall t \in [0, T] \quad (4.1.11)$$

which implies the convergence of the desired norm 4.1.3 due to the equivalence of norms stated in Remark 4.1.1.

Even though this condition is less strict than (4.1.5), it is still too conservative for the physical application due to the fast evolution of the diffusivity coefficients as a function of the inputs (including possible disturbances). Conditions (4.1.5) and (4.1.8) require, in order to guarantee the stability of the system to either limit the rate of variation of the diffusivity coefficients (incompatible with the physical evolution of the temperature equation) or to guarantee a control gain large enough to overcome the possible positive term in the time-derivative of the Lyapunov function (in general incompatible with the constraints imposed on the actuators).

## 4.2 Selected Control Lyapunov Function and Nominal Stability

In this section, the input  $u$  is considered to be perfectly controlled (without constraints) and a strict control Lyapunov function is developed, allowing us to construct a feedback law that ensures exponential convergence to the origin, at any desired rate, of the solutions of (2.1.14)-(2.1.16) in an  $L^2([0, 1])$  sense. The boundary condition at the edge is considered to be homogeneous in this section (equivalent to a perfect tracking of total plasma current). The extension to non-homogeneous boundary conditions will also be treated in this chapter to obtain a D<sup>1</sup>ISS condition and in the next chapter to obtain an ISS condition based on further physical properties of the system. For the remainder of this thesis, unless otherwise stated, one should understand the  $L^2$  norm as the  $L^2([0, 1])$  norm defined in (4.0.2).

The homogeneous (Dirichlet) boundary conditions considered in this section (and some other sections in this thesis) are:

$$z(0, t) = z(1, t) = 0, \quad \forall t \in [0, T] \quad (4.2.1)$$

### 4.2.1 Candidate Control Lyapunov Function

Given  $f : [0, 1] \rightarrow (0, \infty)$ , a (strictly) positive function with bounded second derivative, let us consider, as in [Bribiesca Argomedo et al., 2012a], a candidate control Lyapunov function for the system (2.1.14) with boundary condition (4.2.1) and initial condition (2.1.16) defined, for all  $z$  in  $L^2([0, 1])$ , by:

$$V(z(\cdot)) = \frac{1}{2} \int_0^1 f(r) z^2(r) dr \quad (4.2.2)$$

**Remark 4.2.1.** Since  $f(r)$  is positive and continuous on  $[0, 1]$ , the weighted norm  $\|z(\cdot)\|_f \doteq \sqrt{V(z(\cdot))}$  is equivalent to the usual  $L^2([0, 1])$  norm. In particular, it verifies:

$$\sqrt{\frac{f_{\min}}{2}} \|z(\cdot)\|_{L^2} \leq \|z(\cdot)\|_f \leq \sqrt{\frac{f_{\max}}{2}} \|z(\cdot)\|_{L^2} \quad (4.2.3)$$

where  $f_{\max} \doteq \max_{r \in [0, 1]} f(r)$  and  $f_{\min} \doteq \min_{r \in [0, 1]} f(r)$ .

**Remark 4.2.2.** We use the  $L^2([0, 1])$  norm to construct a candidate Lyapunov function since (in view of the physical application of this method) we can assume enough regularity in the solution of (2.1.14)-(2.1.16). Furthermore, we avoid infinite values of the weighting function since we need this approach to be implementable. Having zero values in the weighting function is not desirable since the equivalence to the classical  $L^2$  norm (widely used in the application) would be lost.



**Theorem 4.2.3.** *If there exist a positive function  $f : [0, 1] \rightarrow (0, \infty)$  with bounded second derivative, and a positive constant  $\alpha$  such that the following inequality is verified:*

$$f''(r)\eta + f'(r) \left[ \eta_r - \eta \frac{1}{r} \right] + f(r) \left[ \eta_r \frac{1}{r} - \eta \frac{1}{r^2} \right] \leq -\alpha f(r), \quad \forall (r, t) \in [0, 1] \times [0, T] \quad (4.2.4)$$

*then the time derivative  $\dot{V}$  of the function  $V$  defined by (4.2.2) verifies:*

$$\dot{V} \leq -\alpha V(z(\cdot, t)) + \int_0^1 f(r) [\eta u]_r z(r, t) dr, \quad \forall t \in [0, T] \quad (4.2.5)$$

*along the solutions of (2.1.14), (4.2.1), (2.1.16).*

*Proof.* Since Theorem 2.1.2 guarantees the existence of solutions to (2.1.14) such that  $V(z(\cdot, t))$  is differentiable with respect to time, the derivative of  $V$  along those trajectories is:

$$\begin{aligned} \dot{V} &= \int_0^1 f(r) z z_t dr \\ &= T_1 + T_2 + T_3 \end{aligned} \quad (4.2.6)$$

with:

$$\begin{aligned} T_1 &= \int_0^1 f(r) [\eta_r u + \eta u_r] z dr \\ T_2 &= \int_0^1 f(r) \left( \eta_r \left[ z_r + \frac{1}{r} z \right] z + \eta \left[ \frac{1}{r} z_r - \frac{1}{r^2} z \right] z \right) dr \\ T_3 &= \int_0^1 f(r) \eta z z_{rr} dr \end{aligned}$$

The term  $T_2$  can be rewritten as:

$$T_2 = \int_0^1 f(r) \left[ \frac{1}{r} \eta z \right]_r z dr + \int_0^1 f(r) \eta_r z z_r dr$$

Integrating by parts we get:

$$T_2 = \frac{1}{r} f(r) \eta z^2 \Big|_0^1 - \int_0^1 f'(r) \eta \frac{1}{r} z^2 dr - \int_0^1 f(r) \eta \frac{1}{r} z z_r dr + \int_0^1 f(r) \eta_r z z_r dr$$

and, using the boundary conditions (4.2.1), implies:

$$T_2 = - \int_0^1 f'(r) \eta \frac{1}{r} z^2 dr - \int_0^1 f(r) \eta \frac{1}{r} z z_r dr + \int_0^1 f(r) \eta_r z z_r dr \quad (4.2.7)$$

Integrating by parts  $T_3$ , the following equation is obtained:

$$T_3 = f(r) \eta z z_r \Big|_0^1 - \int_0^1 (f'(r) \eta + f(r) \eta_r) z z_r dr - \int_0^1 f(r) \eta z_r^2 dr$$

which, considering again the boundary conditions (4.2.1), becomes:

$$T_3 = - \int_0^1 (f'(r)\eta + f(r)\eta_r) z z_r dr - \int_0^1 f(r)\eta z_r^2 dr \quad (4.2.8)$$

From (4.2.7) and (4.2.8), (4.2.6) can thus be written as:

$$\dot{V} = T_1 + T_4 - \int_0^1 f'(r)\eta \frac{1}{r} z^2 dr - \int_0^1 f(r)\eta z_r^2 dr \quad (4.2.9)$$

with:

$$T_4 = \int_0^1 \left[ -f(r)\eta \frac{1}{r} - f'(r)\eta \right] z z_r dr$$

Integrating by parts  $T_4$ , the following equation is obtained:

$$\begin{aligned} T_4 &= \frac{1}{2} \left( -f(r)\eta \frac{1}{r} - f'(r)\eta \right) z^2 \Big|_0^1 \\ &\quad - \frac{1}{2} \int_0^1 \left( -f'(r)\eta \frac{1}{r} - f(r)\eta_r \frac{1}{r} + f(r)\eta \frac{1}{r^2} - f''(r)\eta - f'(r)\eta_r \right) z^2 dr \end{aligned}$$

and the boundary conditions (4.2.1) imply that:

$$T_4 = \frac{1}{2} \int_0^1 \left( f'(r)\eta \frac{1}{r} + f(r)\eta_r \frac{1}{r} - f(r)\eta \frac{1}{r^2} + f''(r)\eta + f'(r)\eta_r \right) z^2 dr \quad (4.2.10)$$

Using (4.2.10), (4.2.9) is equivalent to:

$$\begin{aligned} \dot{V} &= \int_0^1 f(r) [\eta_r u + \eta u_r] z dr - \int_0^1 f(r)\eta z_r^2 dr \\ &\quad + \frac{1}{2} \int_0^1 \left( -f'(r)\eta \frac{1}{r} + f(r)\eta_r \frac{1}{r} - f(r)\eta \frac{1}{r^2} + f''(r)\eta + f'(r)\eta_r \right) z^2 dr \end{aligned} \quad (4.2.11)$$

From (4.2.4) and the definition of the Lyapunov candidate function, (4.2.11) provides the inequality:

$$\dot{V} \leq -\alpha V(z(\cdot, t)) + \int_0^1 f(r) [\eta u]_r z dr - \int_0^1 f(r)\eta z_r^2 dr, \quad \forall t \in [0, T) \quad (4.2.12)$$

which implies the inequality (4.2.5), thus concluding the proof of Theorem 4.2.3.  $\square$

**Remark 4.2.4.** The last term in equation (4.2.12) can be bounded in order to obtain exponential stability of the system with a rate  $\alpha + \epsilon$ , where  $\epsilon$  is a positive constant given by the application of Poincaré's inequality, the lower bound of  $\eta$ , and some bounds on  $f$ . However, for the physical application described in Section 4.5, the rate of convergence obtained when adding this term is almost the same as the value of  $\alpha$  that can be obtained by adequately solving the differential inequality in Theorem 4.2.3.

**Remark 4.2.5.** For a large class of diffusivity profiles, the differential inequality in Theorem 4.2.3 has easily computable solutions: whenever  $\eta_r \frac{1}{r} - \eta_{r^2} \frac{1}{r^2} \leq -k$  for some  $k > 0$  and all  $(r, t) \in [0, 1] \times [0, T)$  (for example, if the spatial derivative of the diffusivity coefficient remains non-positive), a constant  $f$  satisfies (4.2.4). However, for our motivating application, this condition is not satisfied. Section 4.5 presents a suitable numerically computed weight satisfying (4.2.5) for the application. A heuristic method to compute such weights for the particular case of exponential diffusivity coefficient profiles is provided in Appendix B (from [Bribiesca Argomedeo et al., 2012b]).

## 4.2.2 Some Implications

**Corollary 4.2.6.** [Global Exponential Stability] If the conditions of Theorem 4.2.3 are verified, and if  $u(r, t) = 0$  for all  $(r, t)$  in  $[0, 1] \times [0, T)$ , then the origin of the system (2.1.14) with boundary conditions (4.2.1) and initial condition (2.1.16) is globally exponentially stable. The rate of convergence is  $-\alpha/2$  in the topology of the norm  $L^2$ , i.e.:  $\|z(\cdot, t)\|_{L^2} \leq ce^{-\frac{\alpha}{2}t} \|z_0\|_{L^2}$  for a positive constant  $c \doteq \sqrt{\frac{f_{\max}}{f_{\min}}}$ , where  $f_{\max}$  and  $f_{\min}$  are defined as in Remark 4.2.1, and for all  $t \in [0, T)$ .

*Proof.* From Theorem 4.2.3, and setting  $u(r, t) = 0$  for all  $(r, t)$  in  $[0, 1] \times [0, T)$ , the following inequality is obtained:

$$\dot{V} \leq -\alpha V(z(\cdot, t)), \quad \forall t \in [0, T)$$

Therefore, considering the function  $t \mapsto V(z(\cdot, t))$  and integrating the previous inequality over time implies that:

$$V(z(\cdot, t)) \leq e^{-\alpha t} V(z_0(r)), \quad \forall t \in [0, T)$$

and consequently:

$$\|z(\cdot, t)\|_f \leq e^{-\frac{\alpha}{2}t} \|z_0\|_f, \quad \forall t \in [0, T)$$

Since the norm  $\|\cdot\|_f$  is equivalent to the usual  $L^2$  norm<sup>1</sup> as shown in Remark 4.2.1, Corollary 4.2.6 follows.  $\square$

**Corollary 4.2.7.** [Convergence rate control] If the conditions of Theorem 4.2.3 are verified, and considering  $u \doteq u_{ctrl}$  where  $u_{ctrl}$  is chosen, for all  $(r, t) \in (0, 1) \times [0, T)$ , as:

$$u_{ctrl}(r, t) = -\frac{\gamma}{\eta} \int_0^r z(\rho, t) d\rho \quad (4.2.13)$$

with  $\gamma \geq 0$  a tuning parameter, then the system (2.1.14) with boundary conditions (4.2.1) and initial condition (2.1.16) is globally exponentially stable. Its convergence rate is  $-\beta/2 \doteq -(\alpha + \gamma)/2$ , in the topology of the norm  $L^2$ .

---

<sup>1</sup>For generality purposes, results in this chapter are stated in terms of usual norms. It should be noted, however, that the results stated in  $\|\cdot\|_f$  norm are less conservative.

The proof of this corollary is similar to that of Corollary 4.2.6, using Theorem 4.2.3 and the fact that  $[\eta u_{ctrl}]_r = -\gamma z$  for all  $(r, t) \in [0, 1] \times [0, T]$ .

## 4.3 Input-to-State Stability and Robustness

In this section, we consider the effect of disturbances, estimation and measurement errors on the system.

### 4.3.1 Disturbed Model

Let us first consider the effect of disturbing equation (2.1.14) by including a term  $w$  as follows:

$$z_t = \left[ \frac{\eta}{r} [rz]_r \right]_r + [\eta u]_r + w, \quad \forall (r, t) \in (0, 1) \times [0, T] \quad (4.3.1)$$

where  $w$  is a function of  $(r, t)$  and the following property is assumed to hold in addition to Properties  $P_1$ - $P_3$  in Chapter 2:

**P<sub>4</sub>:** The two-dimensional Cartesian representation of  $w$  belongs to  $C^{\alpha_c, \alpha_c/2}(\overline{\Omega} \times [0, T])$ ,  $0 < \alpha_c < 1$ .

**Proposition 4.3.1.** *[Disturbed version of Theorem 4.2.3] Let the conditions of Theorem 4.2.3 hold. Then, along the solution to (4.3.1), (4.2.1), (2.1.16), the following inequality holds:*

$$\dot{V} \leq -\alpha V(z(\cdot, t)) + \int_0^1 f(r) [\eta u]_r z dr + \int_0^1 f(r) w z dr, \quad \forall t \in [0, T] \quad (4.3.2)$$

This fact follows from Theorem 4.2.3, by using (4.2.2) and noting that  $\dot{V}|_{(4.3.1)} = \dot{V}|_{(2.1.14)} + \int_0^1 f(r) w z dr$  where  $\dot{V}|_{(4.3.1)}$  and  $\dot{V}|_{(2.1.14)}$  stand for the derivative of  $V$  along the solution of (4.3.1) and (2.1.14), respectively, with boundary conditions (4.2.1) and initial conditions (2.1.16).

**Theorem 4.3.2.** *[ISS] Let the conditions of Proposition 4.3.1 be verified and consider  $u \doteq u_{ctrl}$  as defined in Corollary 4.2.7. The following inequality holds for the evolution of the system (4.3.1) with boundary condition (4.2.1) and initial condition (2.1.16), for all  $t \in [0, T]$ :*

$$\|z(\cdot, t)\|_{L^2} \leq c e^{-\frac{\beta}{2}t} \|z_0\|_{L^2} + c \int_0^t e^{-\frac{\beta}{2}(t-\tau)} \|w(\cdot, \tau)\|_{L^2} d\tau \quad (4.3.3)$$

with  $c = \sqrt{\frac{f_{max}}{f_{min}}}$ ,  $f_{max} \doteq \max_{r \in [0,1]} f(r)$  and  $f_{min} \doteq \min_{r \in [0,1]} f(r)$ .

*Proof.* From Proposition 4.3.1 and Corollary 4.2.7 we have, along the solution of (4.3.1), (4.2.1), (2.1.16):

$$\dot{V} \leq -\beta V(z(\cdot, t)) + \int_0^1 |f(r)w(r, t)z(r, t)| dr, \quad \forall t \in [0, T]$$

The function  $f$  being positive and using the Cauchy-Schwarz inequality the following upper bound is obtained:

$$\begin{aligned} \dot{V} &\leq -\beta V(z(\cdot, t)) + \|\sqrt{f}z(\cdot, t)\|_{L^2} \|\sqrt{f}w(\cdot, t)\|_{L^2} \\ &= -\beta V(z(\cdot, t)) + 2\|z(\cdot, t)\|_f \|w(\cdot, t)\|_f, \quad \forall t \in [0, T] \end{aligned}$$

where the passage between  $\|\sqrt{f} \cdot\|_{L^2}$  and  $\|\cdot\|_f$  introduces a  $\sqrt{2}$  factor. Defining  $X(z(\cdot, t)) \doteq \sqrt{V(z(\cdot, t))} = \|z(\cdot, t)\|_f \geq 0$  this inequality implies:

$$2X(z(\cdot, t))\dot{X} \leq -\beta X^2(z(\cdot, t)) + 2X(z(\cdot, t))\|w(\cdot, t)\|_f, \quad \forall t \in [0, T]$$

where  $\dot{X} = \frac{d}{dt}X(z(\cdot, t))$ .

If  $X(z) = 0$ , then  $V(z) = 0$  and  $\dot{V} = 0$ . Otherwise we may divide both sides of the previous inequality by  $2X(z(\cdot, t))$  to get:

$$\dot{X} \leq -\frac{\beta}{2}X(z(\cdot, t)) + \|w(\cdot, t)\|_f, \quad \forall t \in [0, T]$$

From the last equation, by easy calculations, we get:

$$\|z(\cdot, t)\|_f \leq e^{-\frac{\beta}{2}t}\|z_0\|_f + \int_0^t e^{-\frac{\beta}{2}(t-\tau)}\|w(\cdot, \tau)\|_f d\tau \quad (4.3.4)$$

which in turn implies the desired result.  $\square$

**Corollary 4.3.3.** *[Actuation errors] In addition to the conditions in Theorem 4.2.3, we consider  $u \doteq u_{ctrl} - \varepsilon^u(r, t)$ , with  $u_{ctrl}$  as defined in Corollary 4.2.7 and  $\varepsilon^u(r, t)$  a distributed actuation error verifying the regularity conditions stated in  $P_2$ . Then, with  $w \doteq 0$ , the following inequality holds<sup>2</sup>:*

$$\|z(\cdot, t)\|_{L^2} \leq ce^{-\frac{\beta}{2}t}\|z_0\|_{L^2} + c \max\{\eta_{max}, \eta_{r, max}\} \int_0^t e^{-\frac{\beta}{2}(t-\tau)}\|\varepsilon^u(\cdot, \tau)\|_{H^1} d\tau, \quad \forall t \in [0, T] \quad (4.3.5)$$

with  $\eta_{max} \doteq \sup_{(r,t) \in [0,1] \times [0,T]} |\eta|$ ,  $\eta_{r, max} \doteq \sup_{(r,t) \in [0,1] \times [0,T]} |\eta_r|$ .

The proof of Corollary 4.3.3 is directly obtained by replacing  $w$  by  $[\eta\varepsilon^u]_r$  in Theorem 4.3.2.

---

<sup>2</sup>The  $H^1$  norm of  $\xi$  on  $[0, 1]$ , will be denoted as  $\|\xi\|_{H^1} \doteq \|\xi\|_{L^2} + \|\frac{\partial \xi}{\partial r}\|_{L^2}$

**Corollary 4.3.4.** *[Estimation errors in the  $z$  profile] Assume that the conditions of Theorem 4.2.3 are verified and consider the control defined in Corollary 4.2.7 but substituting  $z$  by an estimate,  $\hat{z}(r, t) \doteq z(r, t) - \varepsilon^z(r, t)$  for all  $(r, t) \in [0, 1] \times [0, T)$ , with  $\varepsilon^z(r, t)$  being a distributed estimation error verifying the regularity conditions stated in  $P_4$  (in the previous page). The following inequality is then verified:*

$$\|z(\cdot, t)\|_{L^2} \leq ce^{-\frac{\beta}{2}t} \|z_0\|_{L^2} + \gamma c \int_0^t e^{-\frac{\beta}{2}(t-\tau)} \|\varepsilon^z(\cdot, \tau)\|_{L^2} d\tau, \quad \forall t \in [0, T) \quad (4.3.6)$$

Corollary 4.3.4 follows readily by considering the error term  $(\gamma\varepsilon^z)$  that will appear in the system dynamics as a disturbance  $w$  in Theorem 4.3.2.

**Proposition 4.3.5.** *[Estimation errors in the  $\eta$  profile] Assume that the conditions of Theorem 4.2.3 are verified and consider the control defined in Corollary 4.2.7 but substituting  $\eta$  by an estimate,  $\hat{\eta}(r, t) \doteq \eta(r, t) - \varepsilon^\eta(r, t)$  for all  $(r, t) \in [0, 1] \times [0, T)$ , with  $\varepsilon^\eta(r, t)$  being a distributed estimation error verifying the regularity conditions stated in  $P_2$ . The following inequality is then verified:*

$$\|z(\cdot, t)\|_{L^2} \leq ce^{-\frac{\beta'}{2}t} \|z_0\|_{L^2}, \quad \forall t \in [0, T) \quad (4.3.7)$$

where  $\beta' \doteq \beta + \gamma \inf_{(r,t) \in [0,1] \times [0,T)} \left( \frac{\varepsilon^\eta}{\hat{\eta}} \right) - 2\gamma c \sup_{t \in [0,T)} \left\| \left[ \frac{\varepsilon^\eta}{\hat{\eta}} \right]_r \right\|_{L^2}$ .

*Proof.* Since the conditions of Theorem 4.2.3 are assumed to be verified to apply Corollary 4.2.7, inequality (4.2.5) holds. The control  $u$  in Corollary 4.2.7 with  $\hat{\eta}$  becomes:

$$u = -\frac{\gamma}{\hat{\eta}} \int_0^r z(\rho, t) d\rho$$

This implies:

$$\begin{aligned} \eta u &= -\gamma \frac{\eta}{\hat{\eta}} \int_0^r z(\rho, t) d\rho \\ &= -\gamma \frac{\hat{\eta} + \varepsilon^\eta}{\hat{\eta}} \int_0^r z(\rho, t) d\rho \\ &= -\gamma \int_0^r z(\rho, t) d\rho - \gamma \frac{\varepsilon^\eta}{\hat{\eta}} \int_0^r z(\rho, t) d\rho \end{aligned}$$

Differentiating with respect to the spatial variable:

$$[\eta u]_r = -\gamma z - \gamma \frac{\varepsilon^\eta}{\hat{\eta}} z - \gamma \left[ \frac{\varepsilon^\eta}{\hat{\eta}} \right]_r \int_0^r z(\rho, t) d\rho \quad (4.3.8)$$

Substituting (4.3.8) in (4.2.5) the following inequalities are obtained for all  $t \in [0, T)$ :

$$\dot{V} \leq -\alpha V(z) - \gamma \int_0^1 f(r) z^2 dr - \gamma \int_0^1 f(r) \frac{\varepsilon^\eta}{\hat{\eta}} z^2 dr$$

$$\begin{aligned}
 & -\gamma \int_0^1 f(r) \left[ \frac{\varepsilon^\eta}{\hat{\eta}} \right]_r \left( \int_0^r z(\rho, t) d\rho \right) z dr \\
 \leq & -(\alpha + \gamma) V(z) - \gamma \left[ \inf_{(r,t) \in [0,1] \times [0,T]} \left( \frac{\varepsilon^\eta}{\hat{\eta}} \right) \right] \int_0^1 f(r) z^2 dr \\
 & -\gamma \int_0^1 f(r) \left[ \frac{\varepsilon^\eta}{\hat{\eta}} \right]_r \left( \int_0^r z(\rho, t) d\rho \right) z dr \\
 \leq & -\left( \beta + \gamma \left[ \inf_{(r,t) \in [0,1] \times [0,T]} \left( \frac{\varepsilon^\eta}{\hat{\eta}} \right) \right] \right) V(z) \\
 & + \gamma \int_0^1 \left| f(r) \left[ \frac{\varepsilon^\eta}{\hat{\eta}} \right]_r \left( \int_0^r z(\rho, t) d\rho \right) z \right| dr \\
 \leq & -\left( \beta + \gamma \left[ \inf_{(r,t) \in [0,1] \times [0,T]} \left( \frac{\varepsilon^\eta}{\hat{\eta}} \right) \right] \right) V(z) \\
 & + \gamma \int_0^1 \left| f(r) \left[ \frac{\varepsilon^\eta}{\hat{\eta}} \right]_r \left( \int_0^1 |z(\rho, t)| d\rho \right) z \right| dr \\
 \leq & -\left( \beta + \gamma \left[ \inf_{(r,t) \in [0,1] \times [0,T]} \left( \frac{\varepsilon^\eta}{\hat{\eta}} \right) \right] \right) V(z) \\
 & + \gamma \|z\|_{L^1} \int_0^1 \left| f(r) \left[ \frac{\varepsilon^\eta}{\hat{\eta}} \right]_r z \right| dr
 \end{aligned}$$

Applying the Cauchy-Schwarz inequality on the integral term and on the  $L^1$  norm of  $z$  it implies that, for all  $t \in [0, T]$ :

$$\dot{V} \leq -\left( \beta + \gamma \left[ \inf_{(r,t) \in [0,1] \times [0,T]} \left( \frac{\varepsilon^\eta}{\hat{\eta}} \right) \right] \right) V(z(\cdot, t)) + 2\gamma \|z(\cdot, t)\|_{L^2} \left\| \left[ \frac{\varepsilon^\eta}{\hat{\eta}} \right]_r \right\|_f \|z(\cdot, t)\|_f$$

Using the equivalence between  $\|\cdot\|_f$  and the usual  $L^2$  norm, the previous inequality implies that:

$$\dot{V} \leq -\left( \beta + \gamma \left[ \inf_{(r,t) \in [0,1] \times [0,T]} \left( \frac{\varepsilon^\eta}{\hat{\eta}} \right) \right] \right) V(z(\cdot, t)) + \frac{2\sqrt{2}\gamma}{\sqrt{f_{\min}}} \|z(\cdot, t)\|_f^2 \left\| \left[ \frac{\varepsilon^\eta}{\hat{\eta}} \right]_r \right\|_f$$

which in turn implies:

$$\dot{V} \leq -\left( \beta + \gamma \left[ \inf_{(r,t) \in [0,1] \times [0,T]} \left( \frac{\varepsilon^\eta}{\hat{\eta}} \right) \right] \right) V(z(\cdot, t)) + 2\gamma c \|z(\cdot, t)\|_f^2 \left\| \left[ \frac{\varepsilon^\eta}{\hat{\eta}} \right]_r \right\|_{L^2}$$

with  $c$  as defined in Theorem 4.3.2. Consequently:

$$\begin{aligned}
 \dot{V} & \leq -\left( \beta + \gamma \left[ \inf_{(r,t) \in [0,1] \times [0,T]} \left( \frac{\varepsilon^\eta}{\hat{\eta}} \right) \right] - 2\gamma c \sup_{t \in [0,T]} \left\| \left[ \frac{\varepsilon^\eta}{\hat{\eta}} \right]_r \right\|_{L^2} \right) V(z(\cdot, t)), \quad \forall t \in [0, T] \\
 & \leq -\beta' V(z(\cdot, t)), \quad \forall t \in [0, T]
 \end{aligned}$$

and using the same arguments as in the proof of Corollary 4.2.6 it implies the desired result.  $\square$

**Remark 4.3.6.** *Although finding a stabilizing control law for system (2.1.14)-(2.1.16) considering unconstrained in-domain actuation is quite simple, the main interest of Sections 4.2 and 4.3 lies in the fact that the stability of the open-loop system is guaranteed while giving a precise characterization of the impact of the control action in the closed-loop behaviour of the system, both in terms of rate of convergence and ISS gains. Furthermore, the fact that ISS inequalities hold for the open-loop system is crucial for the application presented in Section 4.5, since it also implies that stabilizing control laws can be found despite strong shape constraints on the admissible control action imposed by the physical actuators (represented in Section 4.5.3 by a nonlinear function of the two available engineering parameters in the LH antennas that can only take values in bounded sets).*

## 4.4 D<sup>1</sup>-Input-to-State Stability

In this section, D<sup>1</sup>ISS properties of system (2.1.14)-(2.1.16), as defined in [Sontag, 2008], are obtained with respect to errors in the boundary condition (i.e.  $\tilde{I}_p \neq 0$ ). The conditions on the Lyapunov weight  $f$  will be reduced to having a piecewise-continuous second derivative. In order to keep the same notation, for any function  $g : r \mapsto g(r)$  that is twice-differentiable almost everywhere (a.e.) (i.e. a function having a second derivative equal to a piecewise continuous function except, perhaps, on a zero-measure set),  $g'(r)$  represents an absolutely continuous function equal a.e. to the first derivative of  $g$  with respect to  $r$ . Analogously,  $g''(r)$  represents a piecewise-continuous function equal a.e. to the second derivative of  $g$  with respect to  $r$ .

### 4.4.1 Strict Lyapunov Function and sufficient conditions for D<sup>1</sup>-Input-to-State Stability

Following [Sontag, 2008] and other references,  $V$  as defined in (4.2.2) is said to be a strict Lyapunov function for the undisturbed version of system (2.1.14)-(2.1.16) if, when setting  $\varepsilon(t) \doteq -R_0\mu_0\tilde{I}_p/(2\pi) = 0$  for all  $t \in [0, T]$ , there exists some positive constant  $\alpha$  such that, for every initial condition  $z_0$  as defined in (2.1.16):

$$\dot{V} \leq -\alpha V(z(\cdot, t)), \forall t \in [0, T] \quad (4.4.1)$$

where  $\dot{V}$  stands for the time derivative of  $V$  along the trajectory of the undisturbed system stemming from  $z_0$ .

Hereafter, we define for  $g \in L^2([0, 1])$  its weighted  $L^2$  norm as  $\|g\|_f \doteq (V(g))^{\frac{1}{2}}$ .

A useful technical assumption is introduced:



$A_1$ : There exists a weighting function  $f$  as defined in (4.2.2) such that  $V$  is a strict Lyapunov function for system (2.1.14)-(2.1.16) with  $u = 0$  if  $\varepsilon(t) \doteq -R_0\mu_0\tilde{I}_P(t)/(2\pi) = 0$  for all  $t \in [0, T)$ .

The next theorem constitutes the main contribution of this section:

**Theorem 4.4.1.** *[ $D^1$ -ISS] Under Assumption  $A_1$  and Properties  $P_1$ - $P_3$ , the following inequality is satisfied, for all  $t_0 \in [0, T)$ , by the state of the disturbed system (2.1.14)-(2.1.16) with  $u = 0$ :*

$$\begin{aligned} \|z(\cdot, t)\|_{L^2} &\leq ce^{-\frac{\alpha}{2}(t-t_0)} \left[ \|z(\cdot, t_0)\|_{L^2} + \frac{1}{\sqrt{3}}|\varepsilon(t_0)| \right] \\ &\quad + c \int_{t_0}^t e^{-\frac{\alpha}{2}(t-\tau)} \|\bar{\varepsilon}(\cdot, \tau)\|_{L^2} d\tau \\ &\quad + \frac{c}{\sqrt{3}}|\varepsilon(t)| \end{aligned} \quad (4.4.2)$$

where  $\bar{\varepsilon}(r, t) \doteq 2\eta_r(r, t)\varepsilon(t) - r\dot{\varepsilon}(t)$ , for all  $(r, t) \in [0, 1] \times [t_0, T)$ ,  $c \doteq \sqrt{\frac{f_{max}}{f_{min}}}$  and  $f_{min} \doteq \min_{r \in [0, 1]} \{f(r)\}$ ,  $f_{max} \doteq \max_{r \in [0, 1]} \{f(r)\}$ .

*Proof.* Consider an alternative definition of the state variable:

$$\hat{z}(r, t) \doteq z(r, t) - r\varepsilon(t), \forall (r, t) \in [0, 1] \times [t_0, T) \quad (4.4.3)$$

Using (4.4.3) and its time derivative in (2.1.14), the evolution of the new state variable  $\hat{z}$  is obtained as:

$$\hat{z}_t = \left[ \frac{\eta}{r} [r\hat{z}]_r \right] + 2\eta_r\varepsilon - r\dot{\varepsilon}, \forall (r, t) \in (0, 1) \times [t_0, T)$$

where  $\left[ \frac{\eta}{r} [r\hat{z}]_r \right] + 2\eta_r\varepsilon$  is equivalent to  $z_t(r, t)$ , with Dirichlet boundary conditions:

$$\hat{z}(0, t) = \hat{z}(1, t) = 0, \forall t \in [t_0, T) \quad (4.4.4)$$

and initial condition:

$$\hat{z}(r, t_0) = z(r, t_0) - r\varepsilon(t_0), \forall r \in (0, 1) \quad (4.4.5)$$

Consider the function  $V$  defined in (4.2.2) with a weighting function satisfying Assumption  $A_1$ , applied to the reformulated system (4.4.4)-(4.4.5):

$$V(\hat{z}) \doteq \frac{1}{2} \int_0^1 f(r) \hat{z}^2 dr$$

From the definition of  $\hat{z}$  in (4.4.3), we compute for all  $t \in [t_0, T)$ :

$$\dot{V} = \int_0^1 f(r) \hat{z} \left[ \frac{\eta}{r} [r\hat{z}]_r \right] dr + 2 \int_0^1 f(r) \hat{z} \eta_r \varepsilon dr - \int_0^1 f(r) \hat{z} r \dot{\varepsilon} dr$$

Using inequality (4.4.1) this implies:

$$\dot{V} \leq -\alpha V(\hat{z}) + 2 \int_0^1 f(r) \hat{z} \eta_r \varepsilon dr - \int_0^1 f(r) \hat{z} r \dot{\varepsilon} dr$$

The definition of  $\bar{\varepsilon}(r, t)$  in Theorem 4.4.1, provides the compact form:

$$\dot{V} \leq -\alpha V(\hat{z}) + \int_0^1 f(r) \hat{z} \bar{\varepsilon} dr, \quad \forall t \in [t_0, T]$$

where, by the boundedness of  $\varepsilon(t)$  and  $\dot{\varepsilon}(t)$ ,  $\bar{\varepsilon}(r, t)$  is uniformly bounded in  $[0, 1] \times [t_0, T]$ .

The last equation implies that:

$$\dot{V} \leq -\alpha V(\hat{z}) + \int_0^1 |f(r) \hat{z} \bar{\varepsilon}| dr, \quad \forall t \in [t_0, T] \quad (4.4.6)$$

Using the Cauchy-Schwarz inequality in (4.4.6), we have:

$$\dot{V} \leq -\alpha V(\hat{z}) + \|\sqrt{f(r)} \hat{z}\|_{L^2} \|\sqrt{f(r)} \bar{\varepsilon}\|_{L^2}$$

which implies:

$$\dot{V} \leq -\alpha V(\hat{z}) + 2 \|\hat{z}\|_f \|\bar{\varepsilon}\|_f$$

from which:

$$\frac{d}{dt} \|\hat{z}\|_f \leq -\frac{\alpha}{2} \|\hat{z}\|_f + \|\bar{\varepsilon}\|_f$$

We consequently get for all  $t \in [t_0, T]$ :

$$\|\hat{z}(\cdot, t)\|_f \leq e^{-\frac{\alpha}{2}(t-t_0)} \|\hat{z}(\cdot, t_0)\|_f + \int_{t_0}^t e^{-\frac{\alpha}{2}(t-\tau)} \|\bar{\varepsilon}(\cdot, \tau)\|_f d\tau$$

Recalling (4.4.3) and after some rearrangements, this implies:

$$\begin{aligned} \|z(\cdot, t)\|_f &\leq e^{-\frac{\alpha}{2}(t-t_0)} [\|z(\cdot, t_0)\|_f + |\varepsilon(t_0)| \|r\|_f] \\ &\quad + \int_{t_0}^t e^{-\frac{\alpha}{2}(t-\tau)} \|\bar{\varepsilon}(\cdot, \tau)\|_f d\tau \\ &\quad + |\varepsilon(t)| \|r\|_f, \quad \forall t \in [t_0, T] \end{aligned}$$

Using the equivalence between the  $L^2$  and  $\|\cdot\|_f$  norms, and simply majorating and minorating  $f$  by  $f_{max}$  and  $f_{min}$  respectively, the previous inequality implies (4.4.2) and completes the proof.  $\square$

A simple application of Theorem 4.4.1 yields the following corollary:

**Corollary 4.4.2.** *If there is a non-negative constant  $t_0$  such that for all  $t \geq t_0$ ,  $\varepsilon(t)$  is zero, the state of the system (2.1.14)-(2.1.16), with  $u = 0$ , converges exponentially fast to zero in the topology of the  $L^2$ -norm.*

Theorem 4.2.3 gives a sufficient condition for Assumption  $A_1$  to hold.

**Remark 4.4.3.** *Up to this point, no assumption on the shape or behaviour of  $\eta$  has been made other than some regularity requirements. In the next section a particular shape of  $\eta$ , motivated by a physical application, is used to illustrate our result.*

## 4.5 Application to the Control of the Poloidal Magnetic Flux Profile in a Tokamak Plasma

### 4.5.1 Illustration of Stability: Numerical computation of the Lyapunov function

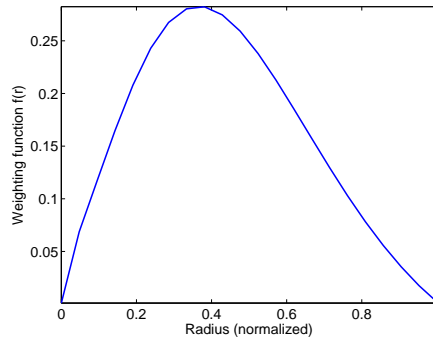
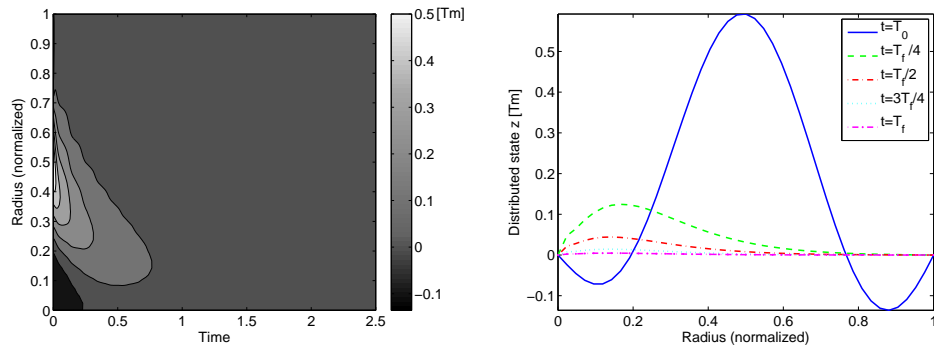
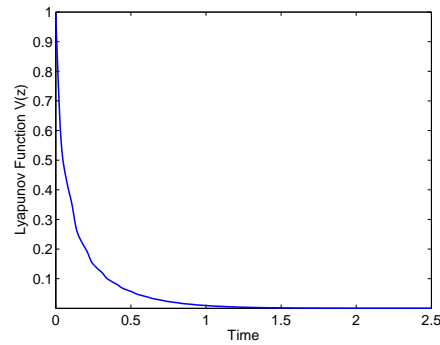


Figure 4.1: Function  $f$  verifying the conditions of Theorem 4.2.3 for an exponential  $\eta$  with time-varying parameters.  $f_{min} = 0.001$ ,  $f_{max} = 0.2823$ .

In order to test the proposed control law in Corollary 4.2.7 for the nominal system, we consider an identified estimate of the normalized plasma resistivity  $\eta(r, t) = A(t)e^{\lambda(t)r}$ , with  $A(t) \doteq 0.0107 - 0.0014 \cos 40\pi t$  and  $\lambda(t) \doteq 6.1 + 0.8 \sin 20\pi t$  for all  $t \in [0, T]$ . In particular  $0.0093 \leq A(t) \leq 0.0121$  and  $4.3 \leq \lambda(t) \leq 6.9$  for all  $t \in [0, T]$ . The limits for the variations were chosen from data extracted from Tore Supra shot 35109, described in [Witrant et al., 2007]. A function  $f$  satisfying the conditions of Theorem 4.2.3 for these values of  $\eta$  has been numerically computed using Mathematica. It is depicted in Fig. 4.1. It should be noted that, in practice, the knowledge of these coefficients does not need to be exact. It is enough to find a common weighting function  $f$  valid on a rich enough set of profiles (and thus on convex combinations of those profiles). Moreover, since  $\alpha$

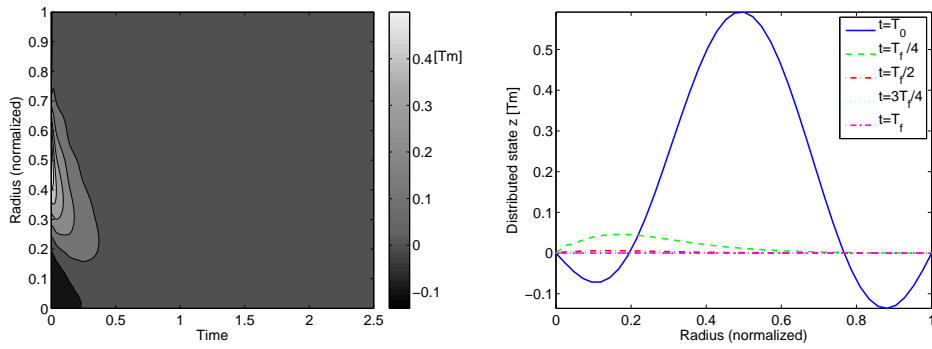


(a) Contour plot of the solution to the (b) Time-slices of the solution to the PDE. PDE.

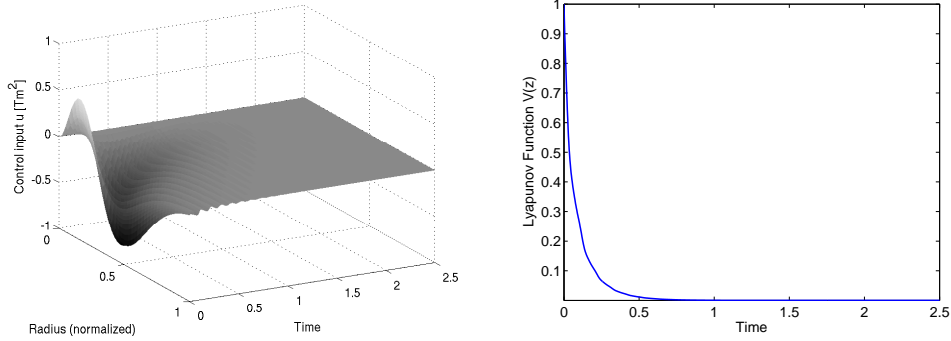


(c) Normalized evolution of the Lyapunov function.

Figure 4.2: Response of the nominal system without control action.



(a) Contour plot of the solution to the (b) Time-slices of the solution to the PDE.



(c) Evolution of the control  $u$ . (d) Normalized evolution of the Lyapunov function.

Figure 4.3: Response of the nominal system with unconstrained control action ( $\gamma = 1.6$ ).

in (4.2.4) is positive, it provides a robustness margin with respect to small numerical errors.

Using this  $f$ , the time-evolution of equation (2.1.14) with boundary conditions (4.2.1), initial condition (2.1.16) and of the associated Lyapunov function  $V$  without control action ( $u_{ctrl} = 0$ ), for an arbitrary numerical value of the initial condition, is shown in Fig. 4.2. The guaranteed convergence rate  $\alpha$  is indeed respected but is conservative. This is not unexpected, since inequality (4.2.4) holds for all values of  $r$  and the central and edge diffusivities vary considerably (almost by a factor 1000).

**Remark 4.5.1.** *For a detailed discussion on how to compute adequate Lyapunov weights, as well as an example computed for a more general shape of diffusivity coefficients, we refer to Appendix B.*

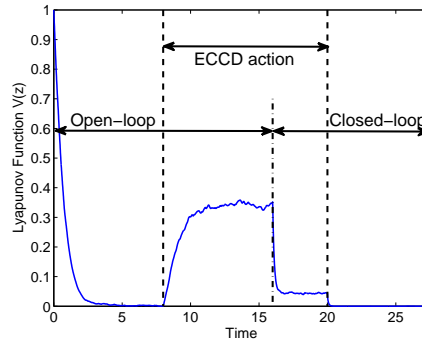
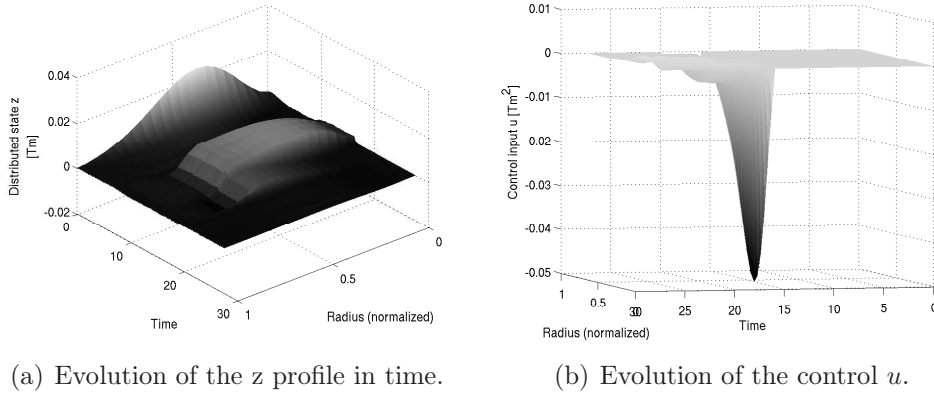
Finally, the response of the system using the control defined in Corollary 4.2.7, with  $\gamma = 1.6$  is shown in Fig. 4.3. Comparing Fig. 4.2 (c) and Fig. 4.3 (d) we can verify that the exponential decrease of  $V$  with the control defined in Corollary 4.2.7 is indeed increased by at least  $e^{-\gamma t}$ , in agreement with the theoretical results.

### 4.5.2 Illustration of ISS property: Tokamak Simulation with Unconstrained Controller

In order to test the controller defined in Corollary 4.2.7 in a more realistic setting, not only considering the evolution of the diffusion equation but also the dynamics of the diffusivity coefficients and other system parameters, the simulator presented in [Witrant et al., 2007] was used to test the behaviour of the system under the effect of disturbances and neglected inputs. In particular, the effect of the variation of the so-called bootstrap current (a plasma self-generated current source proportional to the inverse of the magnetic flux and pressure gradients that introduces a nonlinearity in the system dynamics) around the equilibrium and the Electron Cyclotron Current Drive (ECCD) input, turned on for  $8 \text{ s} \leq t \leq 20 \text{ s}$ , act as unknown exogeneous current sources in the evolution equation. For a rigorous treatment, they can be considered as disturbances both in the state and input (as in Theorem 4.3.2 and Corollary 4.3.3). The variation of the resistivity coefficients is caused mainly by variations in the temperature profile, which is affected by the LH antenna.

The original equilibrium was chosen from experimental data drawn from Tore Supra shot 35109. The effect of the ECCD antennas was overemphasized in order to better illustrate its action on the state and the Lyapunov function (the power in the simulation was chosen as three times the actual capacity of these actuators). A controller parameter  $\gamma = 0.75$  was found to yield acceptable results (both in terms of the amplitude of the control and the effect of the noisy measurements in the system). The results are shown

in Fig. 4.4, with control action starting at  $t = 16$  s and the corresponding values of the physical variables (in absolute terms) can be seen in Fig. 4.5. While a steady-state error remains when the ECCD is turned on, it is significantly reduced by the feedback action. The convergence speed is also noticeably improved.

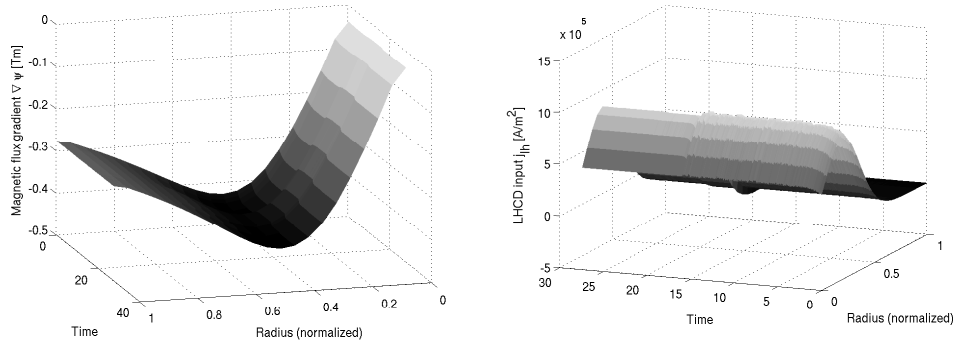


(c) Normalized evolution of the Lyapunov function.

Figure 4.4: Response of the disturbed system, disturbance applied at  $t = 8$  s and removed at  $t = 20$  s with unconstrained control action beginning at  $t = 16$  s ( $\gamma = 0.75$ ).

### 4.5.3 Exploiting the Lyapunov Approach: Tokamak Simulation with Constrained Control

In view of a possible implementation of the control law in a real tokamak experiment, strict constraints have to be imposed on the control action. For this application, the actuator considered is the current density generated by the lower hybrid radiofrequency waves. This current deposit profile  $j_{lh}(r, t)$  depends on two main physical parameters: the power delivered by the antennas  $P_{lh}(t)$  and the parallel refractive index  $N_{\parallel}(t)$ . In Tore Supra two LH antennas exist and their parameters may vary in the following manner:  $P_{lh,1} \leq 1.5$  MW,  $P_{lh,2} \leq 3$  MW,  $N_{\parallel,1} \in [1.43, 2.37]$  and  $N_{\parallel,2} \in [1.67, 2.33]$ . However, in this section only one set of parameters ( $P_{lh}, N_{\parallel}$ ) is used to derive a controller



(a) Evolution of the physical  $\nabla\psi$  profile. (b)  $j_{lh}$  input equivalent to the control  $u$ .

Figure 4.5: Response of the disturbed system, disturbance applied at  $t = 8$  s and removed at  $t = 20$  s with unconstrained control action beginning at  $t = 16$  s ( $\gamma = 0.75$ ).

that illustrates the usefulness of the control Lyapunov function, as defined in Proposition 4.3.1, from a practical standpoint.

Based on Proposition 4.3.1, we propose to choose, at each time step, a couple  $(P_{lh}^*, N_{\parallel}^*)$  as follows:

$$(P_{lh}^*, N_{\parallel}^*) = \arg \min_{(P_{lh}, N_{\parallel}) \in \mathcal{U}} \int_0^1 f(r) [\eta u(P_{lh}, N_{\parallel})]_r z dr \quad (4.5.1)$$

subject to the constraints:

$$0 \geq \int_0^1 f(r) [\eta u(P_{lh}^*, N_{\parallel}^*)]_r z dr \geq -\gamma V(z) \quad (4.5.2)$$

where  $\mathcal{U} \doteq [P_{lh, \min}, P_{lh, \max}] \times [N_{\parallel, \min}, N_{\parallel, \max}]$  and  $u : \mathcal{U} \rightarrow C^\infty([0, 1])$  is a nonlinear function representing the relation between the engineering parameters and the variations in the  $j_{lh}$  profile as presented in [Witrant et al., 2007].

**Remark 4.5.2.** The inequality in the left-hand side of (4.5.2) guarantees that the worst case of the optimization scheme is  $\int_0^1 f(r) [\eta u(P_{lh}^*, N_{\parallel}^*)]_r z dr = 0$ . In other words, the closed-loop system verifies the ISS inequalities of Theorem 4.3.2 and Corollary 4.3.3 for a value of  $\beta \geq \alpha$ . The inequality in the right-hand side of (4.5.2) is not necessary for the stability of system (2.1.14)-(2.1.16), but aims to limit the contribution of the controller on the rate of convergence of the closed-loop system. If, for all time, there exist  $(P_{lh}, N_{\parallel}) \in \mathcal{U}$  such that the control proposed in Corollary 4.2.7 is exactly  $u(P_{lh}, N_{\parallel})$ , then it is a solution to the constrained optimization problem.

Since solving this optimization problem analytically is quite difficult, a numerical method using a gradient-descent algorithm on the discretized parameter space was implemented in practice. As the state dynamics describe the system deviation from an equilibrium, choosing  $u = 0$  (i.e.  $(P_{lh}, N_{\parallel}) = (\bar{P}_{lh}, \bar{N}_{\parallel})$ ) always gives a feasible starting



point. In general, we might not find a solution of the proposed problem (4.5.1), and we could have problems facing local-minima, but under simulation with data taken from Tore Supra shots 35109 and 31463 (the first generated by modulating the LH power, the second including also ECCD action) the results are satisfying.

The values of  $u$  and  $u_r$  for the different vertices of the parameter grid were calculated off-line to allow real-time control. In this case, the mean time taken by the algorithm to determine the control values was  $432 \mu\text{s}$  using a Matlab<sup>©</sup> function running on a processor at 2.54 GHz.

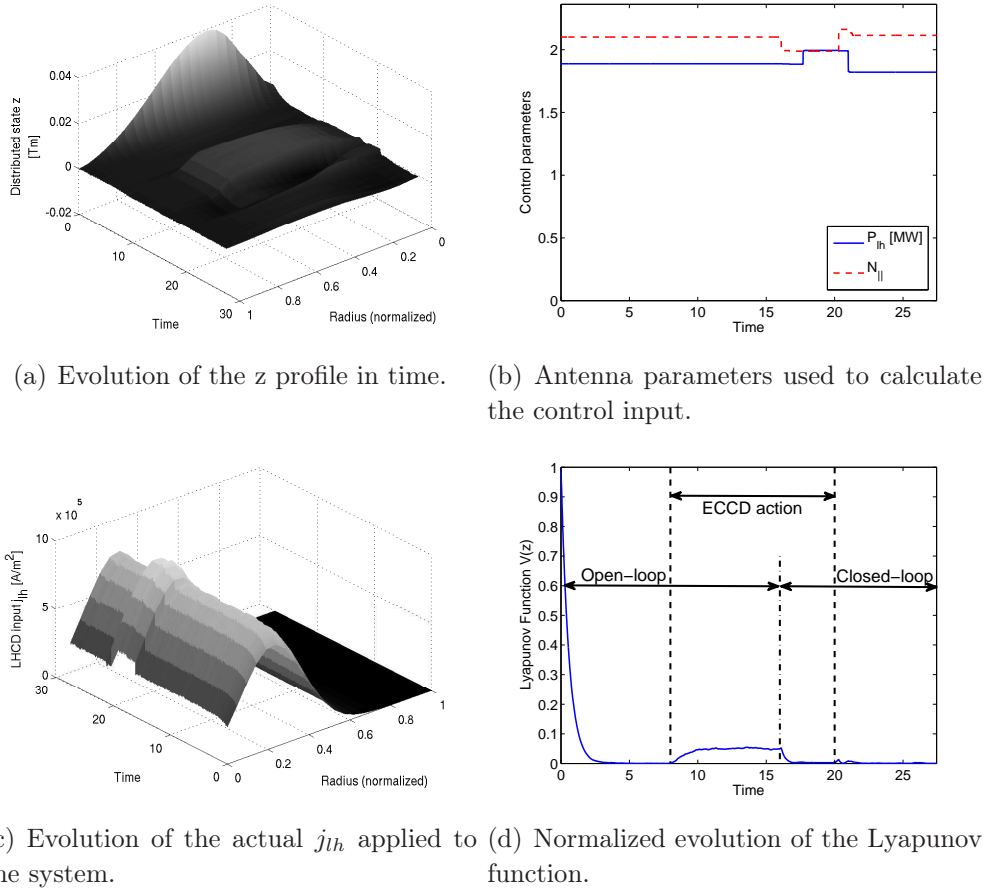


Figure 4.6: Response of the disturbed system, disturbance applied at  $t = 8$  s and removed at  $t = 20$  s with constrained control action beginning at  $t = 16$  s ( $\gamma = 0.6$ ).

For the first simulation, using an equilibrium point taken from Tore Supra shot 35109, we introduce a disturbance as in the previous section, corresponding to three times the maximum ECCD power for  $8 \text{ s} \leq t \leq 20 \text{ s}$  and then activate the control at  $t = 16$  s to attenuate its effect. Results are shown in Fig. 4.6. It can be seen that, despite the constraints, the attenuation of the disturbance is very effective, with the value of the Lyapunov function rapidly reduced once the feedback control is activated. The control value was updated every 0.1 s, which is much greater than the required computing time.

The second proposed scenario is a change of operating point, where both equilibria were drawn from Tore Supra shot 35109. Control action starts at  $t = 4$  s and the change of reference is applied at  $t = 17$  s. The results can be seen in Fig. 4.7. It is interesting to see the behaviour of the Lyapunov function under the constrained control: even though an exponentially decreasing upper bound exists, the actual shape is more irregular than in the unconstrained case (similar to a time-varying gain guaranteeing at all times a negative derivative for the Lyapunov function).

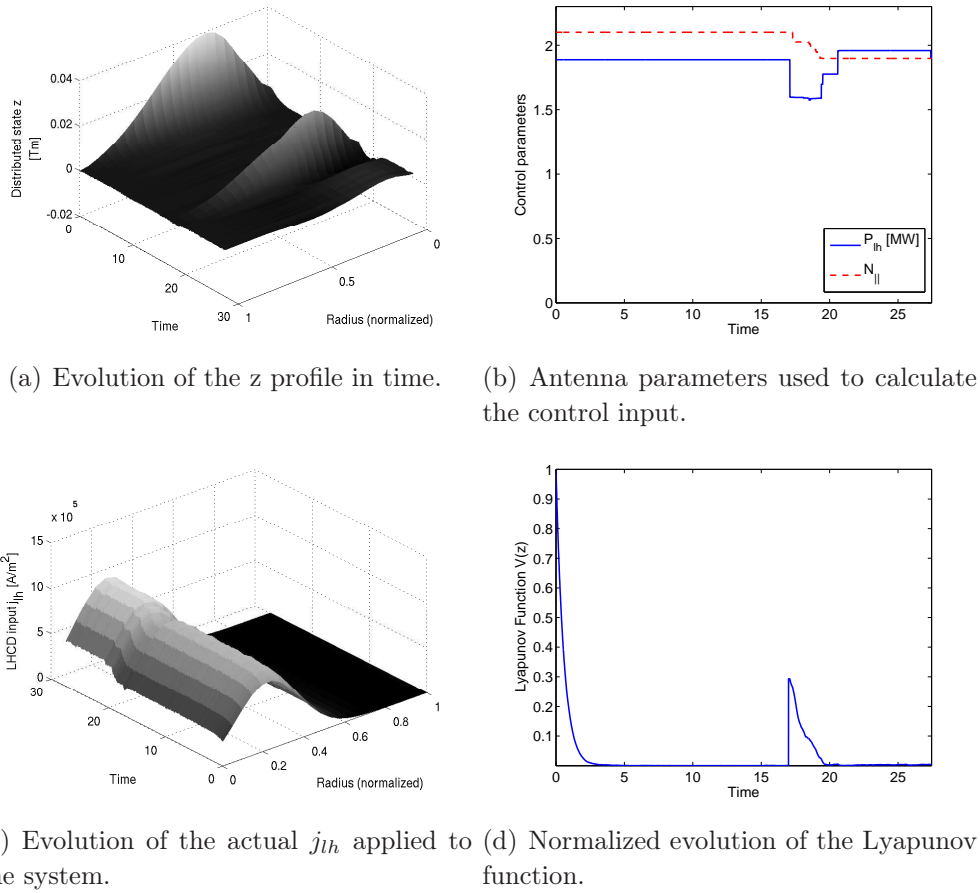
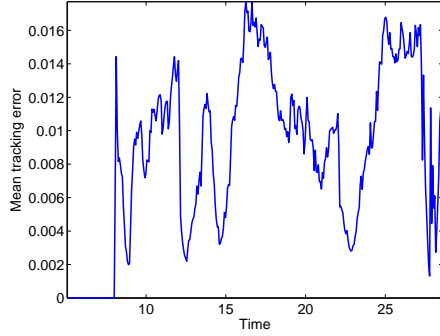


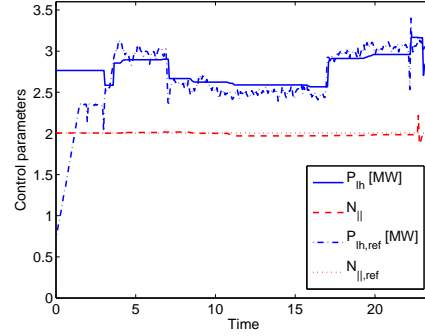
Figure 4.7: Response of the system, change of reference applied at  $t = 17$  s with constrained control action beginning at  $t = 4$  s ( $\gamma = 0.6$ ).

Finally, a more complicated tracking scenario is proposed, where a time-varying reference is generated from Tore Supra shot 31463 (which involves both LH and ECCD action). Furthermore, only one equilibrium point is calculated, corresponding to the mean value of the parameters applied during the shot instead of one for each point of the trajectory. Fig. 4.8 represents (a) the mean tracking error, (b) the values for the engineering parameters of the LH antenna, (c) the LH current deposit profile, (d) the safety factor profile and the current profiles at two different times (e) and (f). This result illustrates the robustness of the controller with respect to deviations from the calculated

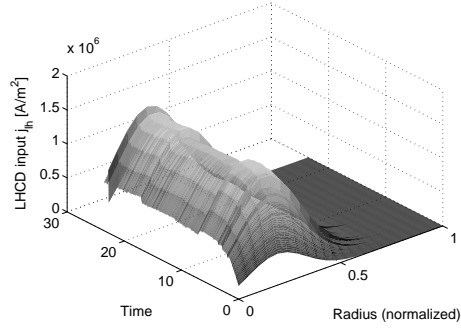
equilibrium (used in the computation of the feedback).



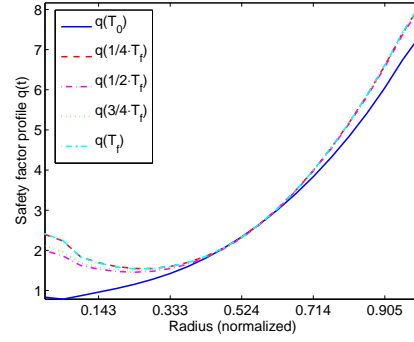
(a) Evolution of the normalized mean error in time.



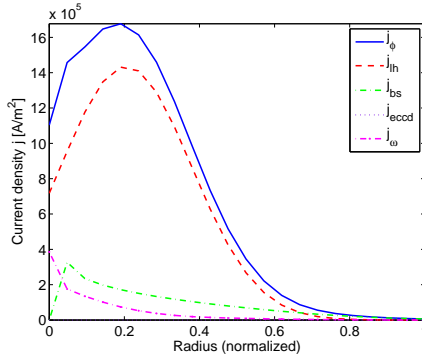
(b) Antenna parameters used to calculate the control input.



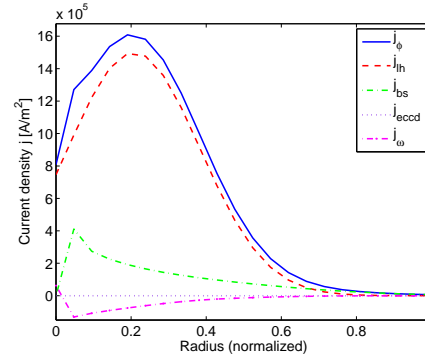
(c) Evolution of the actual  $j_{||h}$  applied to the system.



(d) Evolution of the safety factor profile.



(e) Effective current profile  $j_\phi$  and composition at  $t = 14$  s.



(f) Effective current profile  $j_\phi$  and composition at  $t = 19$  s.

Figure 4.8: Response of the system, with constrained control action beginning at  $t = 3.1$  s ( $\gamma = 2.5$ ).



# Chapter 5

## Controller Implementation

### Contents

---

<b>5.1</b>	<b>Total Plasma Current Dynamic Model . . . . .</b>	<b>86</b>
5.1.1	Perfect Decoupling and Cascade Interconnection of ISS Systems	87
5.1.2	Interconnection Without Perfect Decoupling . . . . .	88
<b>5.2</b>	<b>Modified Lyapunov Function . . . . .</b>	<b>89</b>
<b>5.3</b>	<b>Simulation Results of Closed-loop Tracking with Approximated Equilibrium using METIS . . . . .</b>	<b>92</b>
5.3.1	General Description . . . . .	93
5.3.2	First case: Independent $I_p$ control, large variations of $P_{lh}$ , temperature profile disturbed by ICRH heating. . . . .	94
5.3.3	Second case: Independent $I_p$ control, large variations of $N_{  }$ , temperature profile disturbed by ICRH heating. . . . .	97
<b>5.4</b>	<b>Some Preliminary Extensions . . . . .</b>	<b>97</b>
5.4.1	Profile Reconstruction Delays . . . . .	99
5.4.2	Extension for TCV . . . . .	99
<b>5.5</b>	<b>Summary and Conclusions . . . . .</b>	<b>105</b>

---

The main objectives of this chapter are:

- to introduce a simplified model for the evolution of the boundary condition (2.1.15) involving the coupling between the LH power injected into the system and the total plasma current;
- to use this simplified model to explore the possible impact of these couplings on the stability of the interconnected system (see Figure 5.1);

- to implement the control law, developed in Chapter 4, in simulation using the METIS code, part of the CRONOS suite of codes [Artaud et al., 2010];
- to simulate the effect of profile-reconstruction delays of 100ms (based on the sampling time in [Blum et al., 2012]);
- to extend the control law developed in Chapter 4 in simulation using the RAPTOR code [Felici et al., 2011] for TCV scenarios.

In the first section of this chapter, we present an extended model for the system, taking into account not only the resistive diffusion equation governing the poloidal magnetic flux (infinite-dimensional system), but also the couplings that exist between the the LH power injected into the system and the boundary conditions given by the total plasma current (finite-dimensional dynamical system). The dynamic behaviour of the finite-dimensional subsystem is approximated using a transformer model as proposed, for instance, in [Kazarian-Vibert et al., 1996].

Since the parameters of the LH antennas are considered as control inputs for the infinite-dimensional subsystem and are calculated considering only their impact on this system, it is important to study their impact in the full interconnected system. This could be particularly challenging since in Chapter 4 we did not obtain ISS inequalities for the gradient of the magnetic flux with respect to boundary disturbances (only D<sup>1</sup>ISS). However, with the introduction of a useful physical hypothesis (related to the total current density at the last closed magnetic surface), we are able to develop stronger (ISS) inequalities. The resulting interconnected system is illustrated in Figure 5.1.

Two main approaches for guaranteeing the stability of the coupled system are explored in this chapter: a perfect decoupling controller for the total plasma current and a stabilizing (not decoupling) controller (both using the ohmic voltage as actuator). The idea behind these controllers is to be able to use the constrained control law proposed in Chapter 4, with as little modifications as possible, in a more realistic (coupled) scenario while preserving some interesting theoretical properties (ISS, for instance).

For the perfect decoupling controller, a trajectory that perfectly decouples the total plasma current and the LH power and a stabilizing controller for the subsystem are required. Since constructing a stabilizing controller for this subsystem (assumed here to be LTI and verified to be controllable) is quite simple, we focus on calculating the decoupling trajectory. Eliminating the coupling (dashed line in Figure 5.1) the entire system becomes nothing more than a cascade interconnection of two ISS systems. Since the output operators of both systems are bounded, this directly implies that the full system is ISS (in particular, all properties presented in Chapter 4 hold). Nevertheless, this trajectory turns out to be physically unrealistic and cannot be used for safety factor profile regulation. In particular, the presence of an integrator in the transfer between the variations of LH current ( $\tilde{P}_{lh}$ ) and the ohmic voltage ( $\tilde{V}_\Omega$ ) is undesirable.

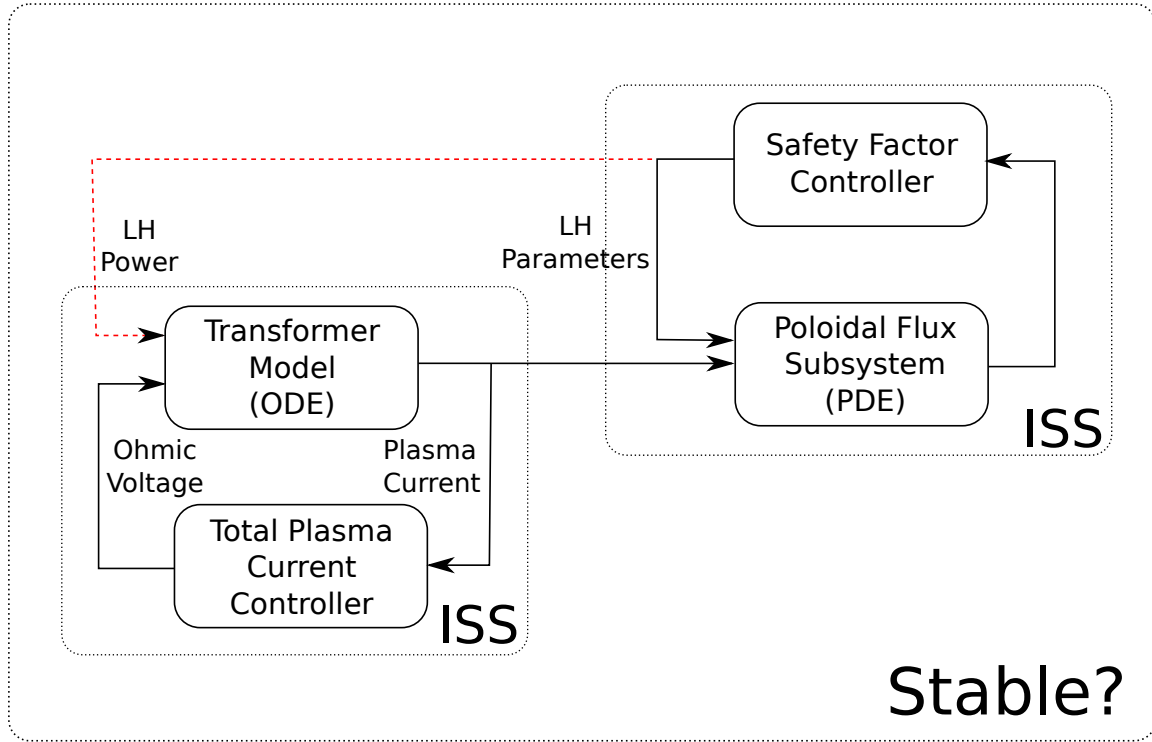


Figure 5.1: Diagram representing the coupling between the finite-dimensional and infinite-dimensional subsystems.

Next, we turn to a stabilizing (but not perfectly decoupling) controller. Instead of calculating a perfectly decoupling trajectory, we extend the system to include an output integrator (integrating the error in the total plasma current tracking) and we assume that there exists a controller gain such that the closed-loop matrix of the system has all its eigenvalues in the left-hand side of the complex plane (with negative real parts). For an LTI system, this implies the existence of a quadratic Lyapunov function (and also the desired ISS properties of the subsystem). We then use this Lyapunov function to build a global Lyapunov candidate function (encompassing both subsystems) and find sufficient conditions for the stability of the interconnected system. Simulation results of this approach, using the METIS code, are presented and discussed in the last section.

## 5.1 Total Plasma Current Dynamic Model

In order to present the transformer model, let us assume the total current deposited by the LH antennas can be expressed as  $I_{lh} = \eta_{lh} P_{lh} / (R_0 \bar{n})$  (where  $R_0$  is the location of the magnetic center,  $\eta_{lh}$  is the efficiency of the LH current drive,  $P_{lh}$  is the power delivered by the LH antennas and  $\bar{n}$  is the electron line average density). The current drive efficiency of the antennas can be approximated using scaling laws, such as those

presented in [Goniche et al., 2005].

Considering the plasma as being the secondary circuit in a transformer (with the poloidal magnetic field coils being the primary), as in [Kazarian-Vibert et al., 1996], the evolution of  $\tilde{I}_p \doteq I_p - \bar{I}_p$  around an equilibrium  $(\bar{I}_p, \bar{P}_{lh}, \bar{N}_{||}, \bar{V}_\Omega, \bar{I}_\Omega)$  can be considered, neglecting the variations of bootstrap current, as given by:

$$\begin{bmatrix} L_p & M \\ M & L_\Omega \end{bmatrix} \begin{bmatrix} \dot{\tilde{I}}_p \\ \dot{\tilde{I}}_\Omega \end{bmatrix} = \begin{bmatrix} -R_p & 0 \\ 0 & -R_\Omega \end{bmatrix} \begin{bmatrix} \tilde{I}_p \\ \tilde{I}_\Omega \end{bmatrix} + \begin{bmatrix} \frac{\eta_{lh} R_p}{\bar{n} R_0} & 0 \\ 0 & 1 \end{bmatrix} \begin{bmatrix} \tilde{P}_{lh} \\ \tilde{V}_\Omega \end{bmatrix} \quad (5.1.1)$$

where, for all variables, a tilde represents the difference between the actual value and the equilibrium (i.e.  $\tilde{\xi} \doteq \xi - \bar{\xi}$ ), and with initial condition  $\tilde{I}_p(0) = \tilde{I}_\Omega(0) = 0$ . Here,  $L_p$  and  $L_\Omega$  represent the plasma and coil inductances, respectively,  $M$  represents the mutual inductance, and  $R_p$  and  $R_\Omega$  represent the plasma and coil electrical resistances.  $I_\Omega$  and  $V_\Omega$  represent the ohmic current and voltage, respectively.

### 5.1.1 Perfect Decoupling and Cascade Interconnection of ISS Systems

The first idea that we explore is the construction of a decoupling feedback (in this section referred to as a decoupling trajectory since, due to the linearity of the system, it defines a trajectory for the state variables in the finite-dimensional subsystem that can be superposed to that of an independent controller for the same subsystem). The purpose behind this decoupling trajectory is to simplify the stability analysis of the system and to be able to use the control algorithm already developed in the previous chapter with few, if any, modifications.

If this perfect decoupling can be achieved, the stability analysis of the overall system is reduced to showing that the cascade interconnection of two ISS systems is asymptotically stable (and in particular ISS). This result is straightforward, since the ISS property is equivalent to a bounded gain between the input and state of the system. The first system being linear and finite-dimensional, ISS implies BIBO stability (the output operator is clearly bounded by the norm of the state). The bounded output of the first system becomes a bounded input to the infinite dimensional system (via the boundary condition) and, introducing a further physical hypothesis (on the total current density at the last closed magnetic surface), the D<sup>1</sup>ISS inequality presented on the previous chapter for boundary disturbances can be replaced by a stronger ISS one.

Consider then a *decoupling* trajectory  $(\bar{\bar{V}}_\Omega, \bar{\bar{I}}_\Omega)$  calculated as:

$$\begin{bmatrix} \dot{\bar{\bar{I}}}_\Omega \\ \dot{U} \end{bmatrix} = \begin{bmatrix} -\frac{L_p R_\Omega}{L_p L_\Omega - M^2} & \frac{L_p}{L_p L_\Omega - M^2} \\ 0 & 0 \end{bmatrix} \begin{bmatrix} \bar{\bar{I}}_\Omega \\ U \end{bmatrix} + \begin{bmatrix} \frac{\eta_{lh} R_p}{\bar{n} M R_0} \\ \frac{R_\Omega \eta_{lh} R_p}{M \bar{n} R_0} \end{bmatrix} \tilde{P}_{lh}$$



$$\begin{bmatrix} \bar{\bar{V}}_\Omega \\ \bar{\bar{I}}_\Omega \end{bmatrix} = \begin{bmatrix} 0 & 1 \\ 1 & 0 \end{bmatrix} \begin{bmatrix} \bar{\bar{I}}_\Omega \\ U \end{bmatrix} + \begin{bmatrix} \frac{\eta_{lh} L_\Omega R_p}{\bar{n} M R_0} \\ 0 \end{bmatrix} \tilde{P}_{lh} \quad (5.1.2)$$

with initial conditions  $\bar{\bar{I}}_\Omega(0) = U(0) = 0$ . Here,  $U$  is merely an internal variable used to generate the required trajectory (i.e. it does not necessarily have a physical meaning). Adding this trajectory to the original equilibrium (using equation (5.1.1)) effectively decouples the variables  $\tilde{P}_{lh}$  and  $\tilde{I}_p$ , i.e. after some computations we obtain:

$$\begin{bmatrix} L_p & M \\ M & L_\Omega \end{bmatrix} \begin{bmatrix} \dot{\tilde{I}}_p \\ \dot{\tilde{I}}_\Omega - \dot{\bar{\bar{I}}}_\Omega \end{bmatrix} = \begin{bmatrix} -R_p & 0 \\ 0 & -R_\Omega \end{bmatrix} \begin{bmatrix} \tilde{I}_p \\ \tilde{I}_\Omega - \bar{\bar{I}}_\Omega \end{bmatrix} + \begin{bmatrix} 0 \\ 1 \end{bmatrix} (\tilde{V}_\Omega - \bar{\bar{V}}_\Omega) \quad (5.1.3)$$

and therefore, the evolution of  $\tilde{I}_p$  does not depend on  $\tilde{P}_{lh}$ .

Since (5.1.2) describes an LTI system, the transfer function between  $\tilde{P}_{lh}$  and  $\bar{\bar{V}}_\Omega$  can be easily calculated and it is actually a PI gain. Therefore, in order to perfectly decouple (at all frequencies) the total plasma current from the variations of the LH power, the ohmic voltage has to integrate the deviation from the equilibrium total LH current deposit. As mentioned in the chapter introduction, this decoupling feedback poses two main problems: first, small variations on the LH power will eventually result in actuator saturation ( $V_\Omega$  is limited, as is the total flux that can be produced using the inductive actuators); and second, it requires a very aggressive control action that, as discussed in the next subsection, is not really required by the application. Furthermore, the total plasma current controllers currently employed are not designed to achieve perfect decoupling. Based on these observations, although this approach may be appealing from a theoretical standpoint, it is not pursued in the next sections. Instead, a second approach (with less stringent conditions on the total plasma current tracking) will be presented and we will show that, under certain conditions, we do not require such a decoupling to ensure the stability of the interconnected system.

### 5.1.2 Interconnection Without Perfect Decoupling

In order to deal with the shortcomings of the previous approach (thus obtaining something more easily implementable) we consider an imperfect decoupling and establish some sufficient conditions for the interconnected system to remain stable (and, under certain circumstances, with a similar rate of convergence as that obtained in the previous section). This will be assumed to be the case for the remainder of this thesis.

Let us define the matrices  $A$ ,  $B$  and  $D$  as follows:

$$A \doteq \begin{bmatrix} -\frac{L_\Omega R_p}{L_p L_\Omega - M^2} & \frac{M R_\Omega}{L_p L_\Omega - M^2} & 0 \\ \frac{M R_p}{L_p L_\Omega - M^2} & -\frac{L_p R_\Omega}{L_p L_\Omega - M^2} & 0 \\ -1 & 0 & 0 \end{bmatrix},$$

$$B \doteq \begin{bmatrix} -\frac{M}{L_p L_\Omega - M^2} \\ \frac{L_p}{L_p L_\Omega - M^2} \\ 0 \end{bmatrix},$$

$$D \doteq \begin{bmatrix} \frac{L_\Omega \eta_{lh} R_p}{(L_p L_\Omega - M^2) \bar{n} R_0} \\ -\frac{M \eta_{lh} R_p}{(L_p L_\Omega - M^2) \bar{n} R_0} \\ 0 \end{bmatrix}$$

Equation (5.1.1) can be expressed, around the equilibrium and adding an integrator to reject constant disturbances, as:

$$\dot{\zeta} = A\zeta + B\tilde{V}_\Omega + D\tilde{P}_{lh} \quad (5.1.4)$$

where  $\zeta \doteq \begin{bmatrix} \tilde{I}_p & \tilde{I}_\Omega & E \end{bmatrix}^T$ , and  $E$  is the integral of the tracking error of  $I_p$ .

For simplicity in the calculations and proofs, this chapter considers constant matrices  $A$ ,  $B$  and  $D$ . Applying other methods to the total plasma current subsystem, like the polytopic LPV approach shown in Chapter 3 (from [Bribiesca Argomedo et al., 2011]), it is possible to extend these results to some time-varying cases.

Since (from the physics of the system)  $L_p L_\Omega - M^2 > 0$ , the matrix  $A$  has two eigenvalues with negative real parts (corresponding to the physical system) and one zero eigenvalue (corresponding to the integrator).

The second boundary condition in (2.1.15) writes as:

$$z(1, t) = C\zeta \quad (5.1.5)$$

where  $C \doteq \begin{bmatrix} -\frac{R_0 \mu_0}{2\pi} & 0 & 0 \end{bmatrix}$ .

## 5.2 Modified Lyapunov Function

Consider the following candidate Lyapunov function:

$$\begin{aligned} V(z, \zeta) &= V_1(z) + \kappa V_2(\zeta) \\ V_1(z) &= \frac{1}{2} \int_0^1 f(r) z^2(r, t) dr \\ V_2(\zeta) &= \frac{1}{2} \zeta^T P \zeta \end{aligned} \quad (5.2.1)$$

with  $f : [0, 1] \rightarrow [\varepsilon, \infty)$  a twice continuously differentiable positive function,  $P = P^T \in \mathbb{R}^{2 \times 2}$  a symmetric positive definite matrix, and  $\kappa$  a positive constant.

**Theorem 5.2.1.** *If the following two conditions are satisfied:*

- (i) *there exists a twice continuously differentiable positive weight  $f : [0, 1] \rightarrow [\varepsilon, \infty)$  as defined in (4.2.2) such that the function  $V_1$  in (5.2.1) is a strict Lyapunov function for system (2.1.14)-(2.1.16) with homogeneous boundary conditions (i.e. verifying for some positive constant  $\alpha_1$ ,  $\dot{V}_1 \leq -\alpha_1 V_1$ );*
- (ii) *an independent control loop (i.e. a local controller that does not take into account the infinite-dimensional dynamics when computing the control action) regulates the total plasma current while ensuring, for some symmetric positive definite matrix  $P \in \mathbb{R}^{3 \times 3}$ , some matrix  $K \in \mathbb{R}^{1 \times 3}$  and some positive constant  $\alpha_2$ :*

$$P[A + BK + \alpha_2 \mathbb{I}_3] \prec 0 \quad (5.2.2)$$

where  $\cdot \prec 0$  denotes the negative definiteness of a square matrix,  $\mathbb{I}_3$  is the  $3 \times 3$  identity matrix;

then there exists  $\kappa$  large enough such that the function  $V(z, \zeta)$  is a strict Lyapunov function for the interconnected system whose derivative along the solutions of (2.1.14)-(2.1.16) and (5.1.4) satisfies, for some positive constants  $c_1, c_2$ :

$$\dot{V}(t) \leq -c_1 V(z, \zeta) + c_2 \tilde{P}_{lh}^2(t), \forall t \in [0, T] \quad (5.2.3)$$

*Proof.* Choosing an adequate function  $f(r)$ , for example the one proposed in [Bribiesca Argomedo et al., 2012b], satisfying condition (i) of Theorem 3.2.8 we have that, along the solution of (2.1.14)-(2.1.16):

$$\dot{V}_1(t) \leq -\alpha_1 V_1(z) - \frac{1}{2} (f(1) + f'(1)) \eta(1, t) z^2(1, t) \quad (5.2.4)$$

where  $\alpha_1 > 0$ . This equation is obtained by keeping the terms that depend on the boundary condition in the proof of Theorem 4.2.3 and assuming that the total current density, defined as in [Blum, 1989]:

$$j_T = -\frac{1}{\mu_0 R_0 a^2 r} (r \psi_{rr} + \psi_r)$$

is zero on the last closed magnetic surface. If avoiding this hypothesis were desirable, uniform boundedness and uniform Lipschitz-continuity in time could be assumed with some modifications, based on the results presented in [Bribiesca Argomedo et al., 2012b], albeit at the expense of more conservative bounds (D<sup>1</sup>ISS instead of ISS).

Differentiating  $V_2$  along the solution of (5.1.4), we get:

$$\dot{V}_2 = \frac{1}{2} \zeta^T P \left[ A\zeta + B\tilde{V}_\Omega + D\tilde{P}_{lh} \right] + \frac{1}{2} \left[ \zeta^T A^T + \tilde{V}_\Omega^T B^T + \tilde{P}_{lh}^T D^T \right] P \zeta \quad (5.2.5)$$

Considering a control  $\tilde{V}_\Omega$  of the form  $K\zeta$ , with  $K$  a row vector with three elements, the previous equation is equivalent to:

$$\dot{V}_2 = \zeta^T P [A + BK] \zeta + \zeta^T P \left[ D \tilde{P}_{lh} \right] \quad (5.2.6)$$

Applying Young's inequality, for any positive constant  $\epsilon$ :

$$\dot{V}_2 \leq \zeta^T P [A + BK] \zeta + \frac{\epsilon}{2} \zeta^T P D D^T P \zeta + \frac{1}{2\epsilon} \tilde{P}_{lh}^2 \quad (5.2.7)$$

Let us choose  $\epsilon$  small enough so that:

$$-\alpha_2 P + \frac{\epsilon}{2} P D D^T P \prec -\alpha_3 P \quad (5.2.8)$$

with  $0 < \alpha_3 < \alpha_2$ . Then:

$$\dot{V}_2 \leq -\alpha_3 \zeta^T P \zeta + \frac{1}{2\epsilon} \tilde{P}_{lh}^2 \quad (5.2.9)$$

Recalling the definition of the boundary condition (5.1.5), and from the definition of  $C$ , the derivative of  $V$  along the solution of the coupled system is bounded by:

$$\begin{aligned} \dot{V}(t) \leq & -\alpha_1 V_1(z) - \frac{R_0^2 \mu_0^2}{8\pi^2} (f(1) + f'(1)) \eta(1, t) \zeta^T \zeta \\ & - 2\kappa \alpha_3 V_2(\zeta) + \frac{\kappa}{2\epsilon} \tilde{P}_{lh}^2(t) \end{aligned} \quad (5.2.10)$$

We now consider two cases: depending on the sign of  $f(1) + f'(1)$ . We will focus first on the case where  $f(1) + f'(1) < 0$ . In this case, we can choose  $\kappa$  large enough so that:

$$-\kappa \alpha_3 P - \frac{R_0^2 \mu_0^2}{8\pi^2} (f(1) + f'(1)) \eta(1, t) \mathbb{I}_3 \prec -\frac{\alpha_4}{2} P$$

for some  $0 < \alpha_4 < \alpha_3$  uniform in time (by using  $P_1$ ).

The case where  $f(1) + f'(1) \geq 0$  is even simpler, since we can choose  $\kappa = 1$  and get the same inequality with  $\alpha_4 \geq \alpha_3$ .

This implies that, in both cases:

$$\dot{V} \leq -\alpha_1 V_1 - \alpha_4 V_2 + \frac{\kappa}{2\epsilon} \tilde{P}_{lh}^2 \quad (5.2.11)$$

and therefore:

$$\dot{V} \leq -\min\{\alpha_1, \alpha_4\} V + \frac{\kappa}{2\epsilon} \tilde{P}_{lh}^2 \quad (5.2.12)$$

thus completing the proof.

□

**Remark 5.2.2.** Based on equation (5.2.12) and the boundedness of  $\tilde{P}_{lh}$  ( $\tilde{P}_{lh}$  is bounded since both  $P_{lh}$  and  $\bar{P}_{lh}$  belong to the same bounded interval in  $\mathbb{R}_+^+$ ), for any bounded initial state, the state of the system will remain bounded at all times. Furthermore, the ISS gain of the system can be bounded by a function of the rates of convergence of both subsystems and the constants  $\kappa$  and  $\epsilon$  used in the proof. In order to obtain as small an ISS gain as possible, it would be desirable to have a big value for  $\epsilon$  and a small value for  $\kappa$ , together with as big as possible convergence rate (given by  $\min\{\alpha_1, \alpha_4\}$ ). To obtain this, an  $\alpha_2$  as large as possible is desirable (which is quite logical, the faster the finite dimensional system converges, the less impact the coupling will have). The limiting case would, of course, be the case of perfect decoupling mentioned in the previous section.

**Remark 5.2.3.** From equation (5.2.12), we conclude that if, in addition to the constraints already included in the control law, see (4.5.2), an additional constraint is imposed as:

$$\tilde{P}_{lh}^2 \leq (-\alpha_5 + \min\{\alpha_1, \alpha_4\}) \frac{2\epsilon}{\kappa} V(z, \zeta), \quad \forall t \in [0, T] \quad (5.2.13)$$

for some  $0 < \alpha_5 < \min\{\alpha_1, \alpha_4\}$ , then the interconnected system is exponentially stable.

This condition is indeed a small-gain condition involving the ISS gain of the cascade interconnection of both subsystems, represented by  $\kappa/(2\epsilon \min\{\alpha_1, \alpha_4\})$  (see equation (5.2.12)), and the gain of the controller (given by the previous inequality).

**Remark 5.2.4.** We may also remark that if  $\tilde{I}_p$  ever converges to zero, the infinite-dimensional state will converge to zero as well (this will happen, for instance when  $\tilde{P}_{lh}$  is constant, due to the added integrator in the system).

### 5.3 Simulation Results of Closed-loop Tracking with Approximated Equilibrium using METIS

Although rapid simulations using the simplified model described in [Witrant et al., 2007] were used in the early stages of controller development for tuning purposes, the proposed scheme is validated on a more complex simulation scheme. The Matlab/Simulink interface of the METIS code developed by the french CEA [Artaud, 2008] was included in a flexible platform, developed to easily simulate the Tokamak evolution under different assumptions (e.g.: prescribed total plasma current vs. independent control loop using  $V_\Omega$ ) and different actuator models (such as the LH current deposit profile). This platform includes a controller subsystem, a local plasma current control loop and the METIS interface.

### 5.3.1 General Description

The presented simulation results are based on general parameters of Tore Supra shot TS-31463, but with a much larger variation range for  $P_{lh}$  and  $N_{||}$  (in order to better illustrate the robustness of the controller when the equilibrium is poorly known or when large variations around the known equilibrium are needed). The shot was simulated with METIS in the previously discussed platform. The evaluated control law is given by (4.5.1), as in Section 4.5.3. The gradient descent optimization algorithm parameters were modified to obtain a response with less noise and limiting the rate of variation (for implementation purposes).

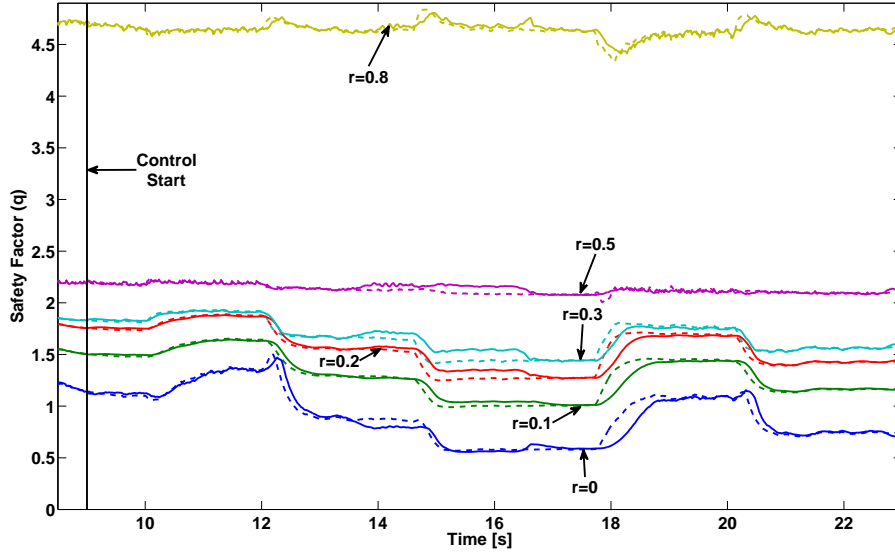
The chosen inputs to the controller were the spatial derivative of the poloidal magnetic flux profile, as well as a reference profile (which could be generated from a reference safety factor profile), and an estimate of the parallel resistivity profile. Although the poloidal magnetic flux profile (considered available in Tore Supra from Equinox reconstructions in real time [Blum et al., 2012]) and parallel resistivity may not be perfectly known, the robustness of our Lyapunov-based controllers with respect to estimation errors in both profiles is ensured as described in Section 4.3. Plasma parameter estimation could also be done using other methods, such as those found in [Felici et al., 2011]. The controller outputs were chosen to be  $N_{||}$  and  $P_{lh}$ .

Since, in practical applications, the full set of available or desired equilibria might not be easily known (in particular due to nonlinearities such as the bootstrap current and couplings with the temperature equation), a single approximated equilibrium point was estimated, simulating in METIS the Open-Loop behaviour of the system for fixed values of the  $N_{||}$  and  $P_{lh}$  inputs. The ability of the controller to reach or approach other desired profiles and stabilize the system around the corresponding equilibrium was tested.

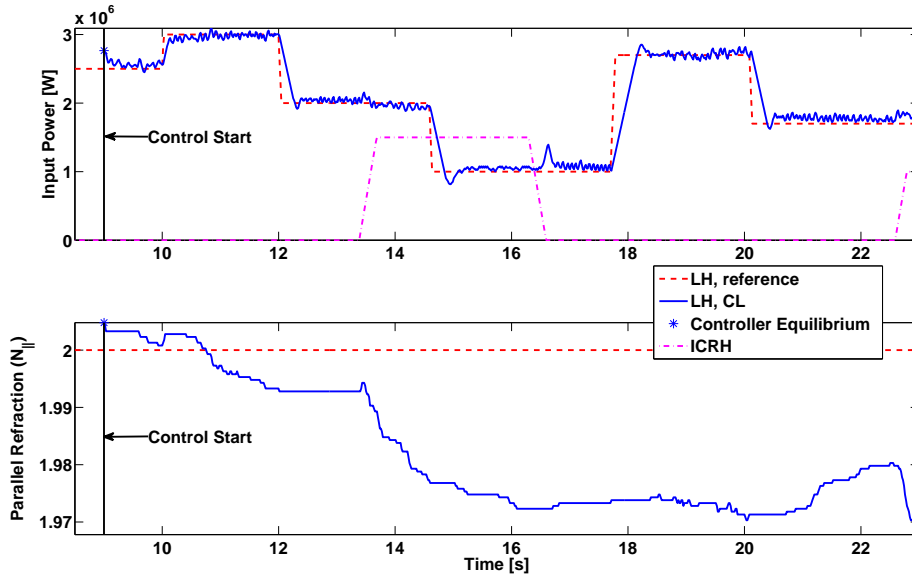
The ramp-up phase of the simulated shot was done in open-loop (as far as  $N_{||}$  and  $P_{lh}$  are concerned, using only an independent control loop for  $I_p$ ) based on TS-31463. The controller was activated at  $t = 9$  s. Since Real-Time implementation is desired, an offline computation was done to construct a table with profiles of  $LH$  current deposit as a function of the input parameters to the controller using scaling laws as in [Witrant et al., 2007]. The real-time optimization algorithm can then perform a constrained gradient-descent, using the estimated values of the resistivity profile and the state, and find a suitable control action in less than two hundred microseconds (using MATLAB functions and an Intel processor running at 2.43 GHz).

The global parameters during the flat-top phase are: constant total plasma current of 580 kA; constant line-average electron density of  $14.5 \times 10^{18} \text{ m}^{-2}$ ; non-inductive heating and current drive using LHCD with  $P_{lh} \in [0.17, 3.5] \text{ MW}$  and  $N_{||} \in [1.70, 2.30]$ ; and constant toroidal magnetic field at the center of the plasma of 3.69 T.

### 5.3.2 First case: Independent $I_p$ control, large variations of $P_{lh}$ , temperature profile disturbed by ICRH heating.



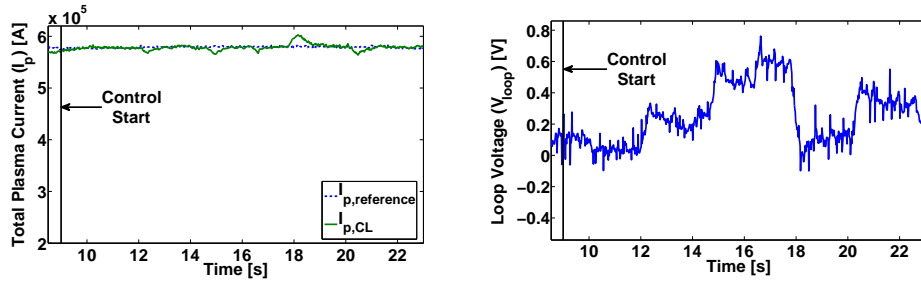
(a) Tracking of the safety factor profile. Dashed line: reference q value; full line: obtained q value.



(b) Controller action and ICRH disturbance.

Figure 5.2: Safety factor profile tracking and radio-frequency antenna control parameter evolution.

This test case was chosen in order to illustrate the robustness of the controller under non-ideal circumstances:



(a) Tracking of the total plasma current. (b) Resulting  $V_{loop}$  due to  $I_p$  tracking.

Figure 5.3: Total plasma current evolution and corresponding loop voltage.

- The total plasma current  $I_p$  is independently controlled using the poloidal field coils. Since it is no longer considered to be perfectly followed, it becomes a source of disturbances in the plasma edge (boundary condition of the partial differential equation);
- during the shot, reference profiles are chosen far from the equilibrium used for the controller design (corresponding to values of  $P_{lh}$  and  $N_{||}$  of 2.76 MW and 2, respectively). This is done in order to highlight the contribution of non-linear terms in the equations that were neglected near the equilibrium;
- a disturbance in the temperature profile is introduced in the form of 1.5 MW of power from ion-cyclotron radio heating (ICRH) antennas, which cannot be compensated with the LH actuator, thus rendering the target q-profile inaccessible to the controller;
- the model given to the controller for the LH current deposit is based on a gaussian profile approximation with parameters determined by scaling laws, as described in [Witrant et al., 2007]. This does not correspond to the internal METIS model (where, even though the LH efficiency is calculated using scaling laws depending on plasma and wave parameters [Goniche et al., 2005], the shape is based on Landau absorption, accessibility and caustics [Artaud, 2008]);
- the general parameters were taken from experimental measurements of shot TS-31463 and therefore introduce measurement noise to all the variables used to compute the control action.

The tracking of the desired safety factor profiles and the engineering parameters prescribed by the controller for the LH antenna are presented in Figure 5.2. First, Figure 5.2 (a) depicts the evolution of the safety factor at five points (corresponding to  $r = 0, 0.1, 0.2, 0.3, 0.5$  and  $0.8$ ) during the control window ( $9 \text{ s} \leq t \leq 23 \text{ s}$ ). The solid lines represent the simulated evolution of the closed-loop system while the dashed



lines represent the reference values given to the controller (calculated from an open-loop simulation without disturbances). It can be seen that the tracking is satisfactory regardless of the radial position. For  $t$  between 13.4 s and 16.6 s (and again after 22.6 s) the tracking error does not converge to zero, which corresponds to the introduction of a disturbance caused by ICRH. Nevertheless, the system remains stable and the error small, even though the reference profile is no longer achievable. As soon as the disturbance is removed, the tracking errors are promptly reduced. Neither undershoot nor overshoot is appreciable in the tracking of the reference profile (in order to avoid triggering unwanted magnetohydrodynamic modes). There is a time-lag between the reference profile and the response of the system, which is to be expected since: (a) an error between both signals has to appear before the feedback controller can act, and (b) the rate at which the gradient-descent optimization algorithm is allowed to modify the controlled inputs is limited to filter out noise and to prevent sudden changes to the engineering parameters of the LH antennas. Figure 5.2 (b) presents the evolution of the engineering parameters used to track the safety factor profile. In solid lines, the parameters  $N_{\parallel}$  and  $P_{lh}$  set by the controller are shown. The parameters used to construct the reference profile are depicted with dashed lines. These figures show that the controller is able to properly reconstruct the engineering parameters required to obtain the desired safety factor (with the saturation on the rate of change of the parameters reflected by the constant slope during big changes in reference). A mark at the beginning of the control action shows the approximated equilibrium around which the controller was designed. The dashed-dotted line shows the ICRH power injected into the system (only applied to the closed-loop system and not taken into account for the reference generation, as would be the case with unexpected disturbances encountered during actual tokamak operation). These results show the robustness of the proposed Lyapunov-based approach to changes in operating conditions. Although the value of  $N_{\parallel}$  is modified during closed-loop operation, the changes are very small. Finally, even though there is some overshoot in the control parameters chosen by the controller, as mentioned before, these do not cause overshoots in the tracked safety factor profiles. The effect of measurement noise on the control action can be appreciated in the small high-frequency variations of  $P_{lh}$  which, if desired, can be reduced by decreasing the gain of the controller.

The tracking of the total plasma current and the resulting loop voltage are depicted in Figure 5.3. Figure 5.3 (a) shows the plasma current tracking efficiency of a well-tuned proportional-integral (PI) controller despite constant disturbances (in this case, induced by changes in LH current). During the shot, the current driven by the LH antenna varies considerably (since the LH power is driven between 3 and 1 MW), yet the tracking error in the plasma current remains small and goes to zero once the safety factor profile stabilizes (which acts as a small disturbance in the boundary condition of the partial differential equation that eventually vanishes). The resulting loop voltage can be seen in Figure 5.3 (b). This figure shows the capability of the controller to handle both the non-inductive

current drives and the addition of inductive current.

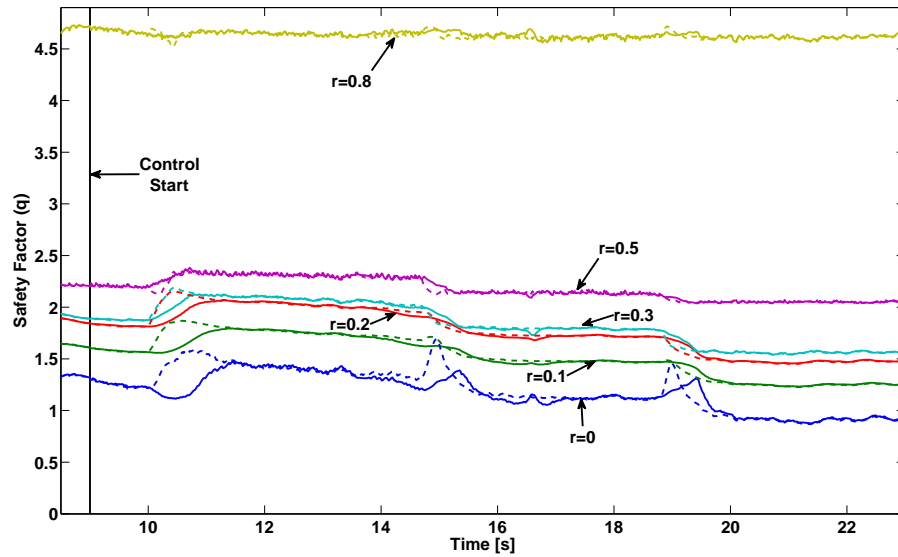
### 5.3.3 Second case: Independent $I_p$ control, large variations of $N_{||}$ , temperature profile disturbed by ICRH heating.

The purpose of this second test case is to show the versatility of the controller with respect to different available control parameters. The general shot conditions are the same as those chosen for the previous example. Nevertheless, the safety factor reference profile is generated by changing the  $N_{||}$  parameter between 1.75 and 2.25 while  $P_{lh}$  is held constant at 2.7 MW. The results of the simulation can be seen in Figures 5.4 and 5.5. Although the safety factor reference is different from that used in the previous example (for instance, the variations of the safety factor at  $r = 0.5$  are much more important in the second simulation, while the central safety factor varies less), the tracking remains satisfactory, as seen in Figure 5.4 (a). As in the previous example, the tracking error does not converge to zero when the ICRH disturbance is introduced (between 13.4 s and 16.6 s, and after 22.6 s), yet the system remains stable and the error small. Figure 5.4 (b) shows a good reconstruction of the original engineering parameters used to generate the reference, except when the ICRH disturbance is present. The effect of the disturbance is attenuated by an offset in the equilibrium  $N_{||}$  values. As in the previous example, the overshoot present at some points in the control profile does not translate into overshoot for the safety-factor tracking.

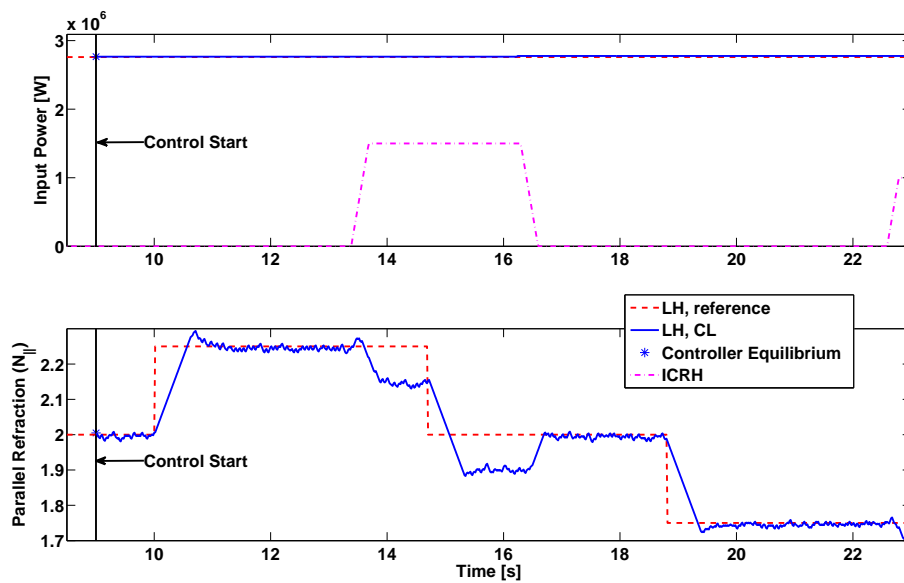
Figure 5.5 shows that the total plasma current tracking (boundary condition) is better than in the previous case, which is to be expected since the variations of LH power are much smaller. This has a direct impact in the tracking of the safety factor profile near the edge ( $r = 0.8$  in Figure 5.4 (a)). Finally, Figure 5.5 (b) shows that the non-inductive control effort to maintain the prescribed total plasma current is smaller than in the previous case.

## 5.4 Some Preliminary Extensions

In this section, we present simulation results illustrating some possible extensions of the methods discussed in this thesis. All simulation results for TCV, using ECCD (Electron Cyclotron Current Drive) actuation, were computed with the RAPTOR code [Felici et al., 2011]. Tore Supra results were obtained using the METIS code as discussed in the previous section.

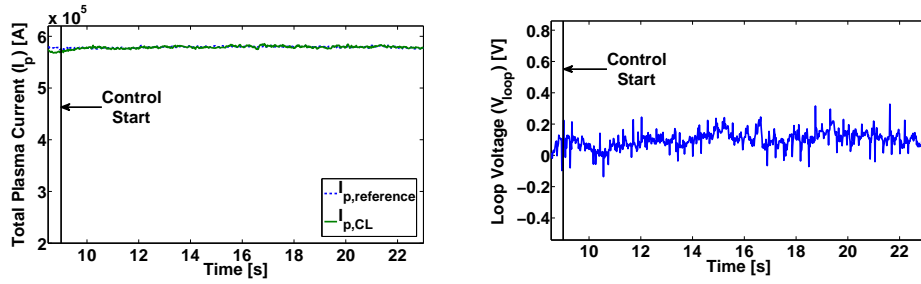


(a) Tracking of the safety factor profile. Dashed line: reference  $q$  value; full line: obtained  $q$  value.



(b) Controller action and ICRH disturbance.

Figure 5.4: Safety factor profile tracking and radio-frequency antenna parameter evolution.



(a) Tracking of the total plasma current. (b) Resulting  $V_{loop}$  due to  $I_p$  tracking.

Figure 5.5: Total plasma current evolution and corresponding loop voltage.

### 5.4.1 Profile Reconstruction Delays

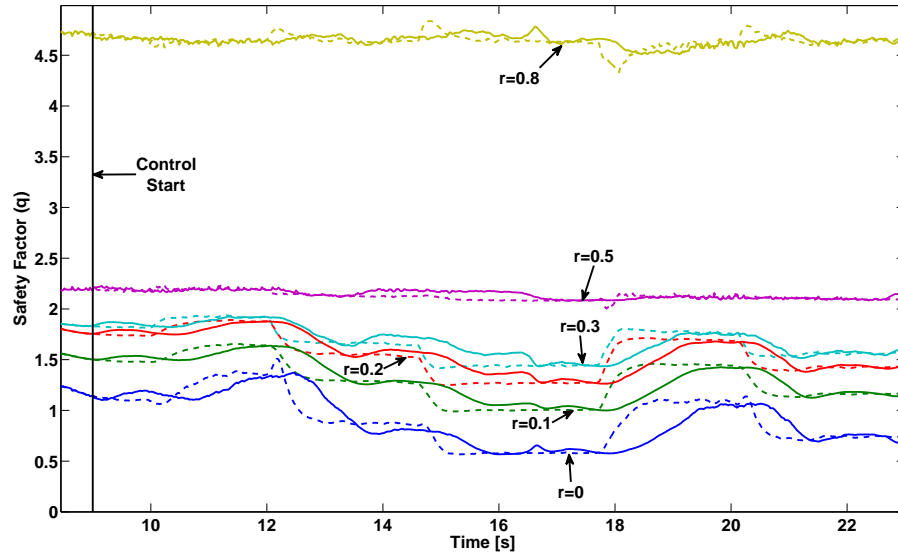
Based on the sampling time set for the profile reconstruction in [Blum et al., 2012], the proposed control scheme was tested under simulation adding a 100 ms delay in the control action. The test case is otherwise exactly as described in Section 5.3.2. The results are presented in Figure 5.6. Some tuning was required to avoid overshoots or oscillations and the resulting response is expectedly slower than that shown in Figure 5.2. However, good convergence is maintained even for references far from the equilibrium value and in the presence of ICRH disturbances. If some overshoots are tolerated, a bigger gain can be used to decrease the settling time. However, since the delay is not negligible compared to the response time obtained in Figure 5.2, some performance degradation is unavoidable without explicitly addressing the delay (with some predictive structure, for example).

### 5.4.2 Extension for TCV

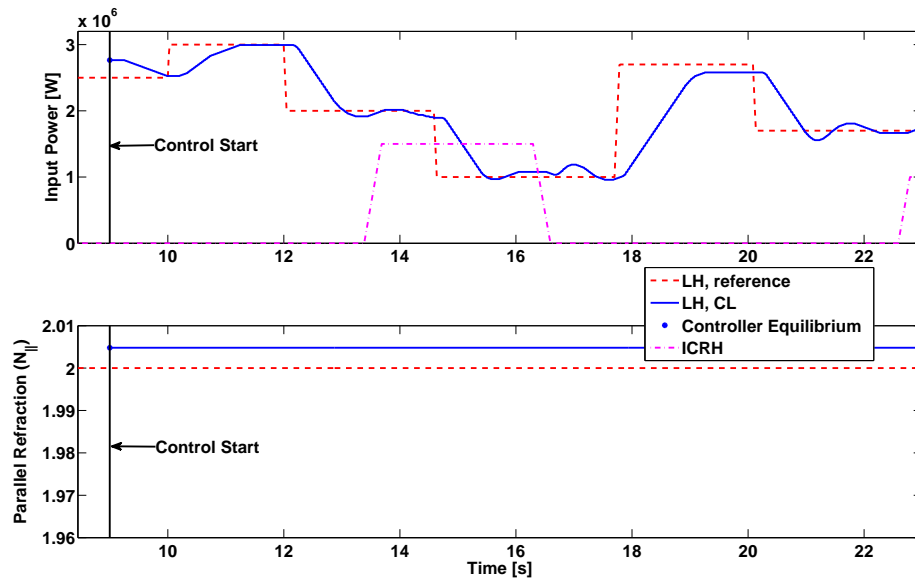
In this subsection we present simulation results using ECCD actuation in a simulated shot for the TCV tokamak. A typical shape for the different coefficients and functions in equation (2.1.1) can be found in [Felici et al., 2011]. These coefficients can be adequately represented by defining the diffusivity coefficients as in (B.1.1) and slightly modifying the definition of the control  $u$  to reflect the small deviations caused by the actual coefficients. Furthermore, the proposed approach is not exclusive to LH actuation. By changing the function  $u$  in the optimization problem used to calculate the control action, the same methods previously discussed can be implemented. The reference ECCD model is the one proposed in [Felici et al., 2011]:

$$j_{ECCD}(\rho, t) = c_{cd} e^{-\rho^2/0.5^2} \frac{T_e}{n_e} e^{-(\rho - \rho_{dep})^2/w_{cd}^2} P_{ECCD}(t) \quad (5.4.1)$$

where  $c_{cd}$  is an experimentally determined coefficient,  $\rho_{dep}$  and  $w_{cd}$  define the position and width of the current deposit and  $P_{ECCD}$  represents the power used by the actuator. All



(a) Tracking of the safety factor profile. Dashed line: reference  $q$  value; full line: obtained  $q$  value.



(b) Controller action and ICRH disturbance.

Figure 5.6: Safety factor profile tracking and radio-frequency antenna control parameter evolution.

other variables are defined as in Chapter 2. Furthermore, the controller is used around a precomputed open-loop trajectory for the actuators that could be obtained using the methods described in [Felici and Sauter, 2012] or, possibly, that presented in [Ou et al., 2008]. For this application, we consider two ECCD actuators with deposits located at  $r = 0$  and  $r = 0.4$ . The two normalized control profiles considered available are shown in Figure 5.7. The following simulations aim to illustrate the flexibility of the proposed method when considering different non-inductive actuators and a different plasma shape.

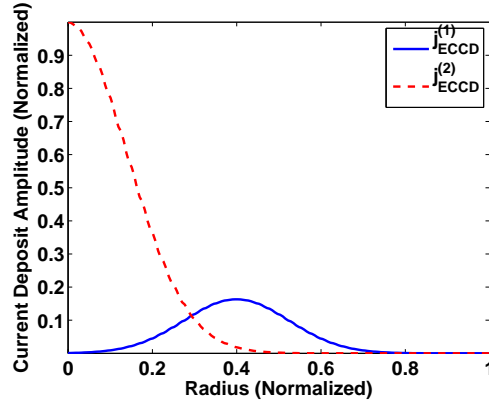
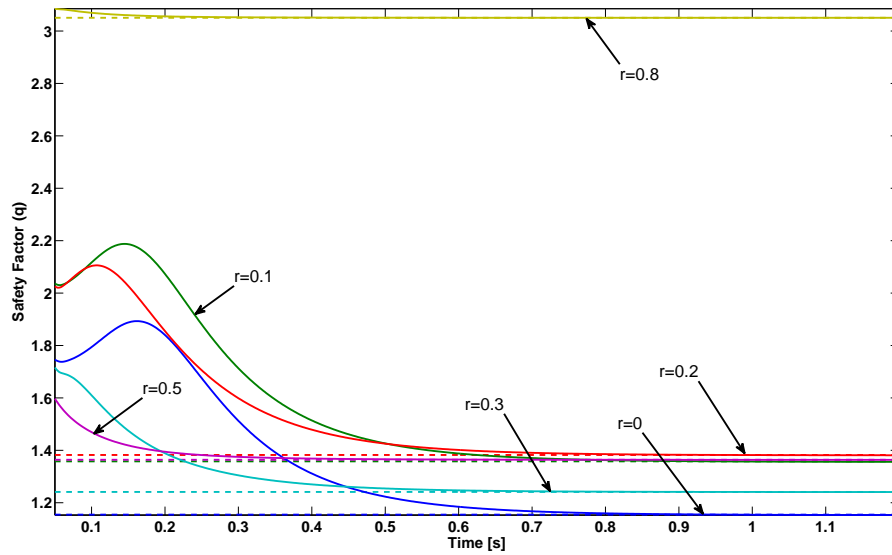


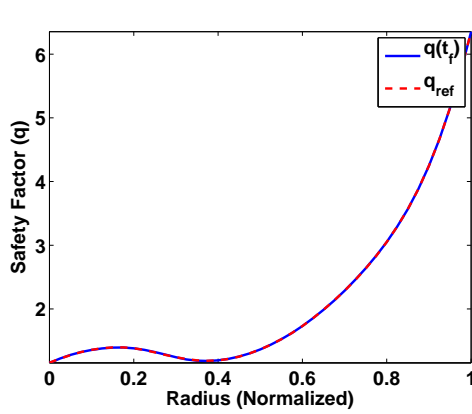
Figure 5.7: Available ECCD control profiles.

The first set of simulations presents the behaviour of the undisturbed system in open-loop and closed-loop, see Figures 5.8 and 5.9, respectively. In both cases the initial power ramp-up is done with an open-loop profile. For the closed-loop simulation, after the ECCD power of the first actuator reaches 2 MW, the controller is activated to accelerate the convergence of the system. Since no disturbances are present, both the open-loop and the closed-loop case reach the desired safety-factor reference at the end of the simulation time. The closed-loop system converges faster than the open-loop system ( $\sim 0.5$  s vs  $\sim 0.8$  s), the acceleration being most noticeable for small values of  $r$ . Some undershoot is present in the closed-loop behaviour, but the control algorithm is tuned so that the safety factor does not reach values under 1. At the end of the simulation time, the values of the ECCD power in both antennas are the same in the open-loop and closed-loop cases.

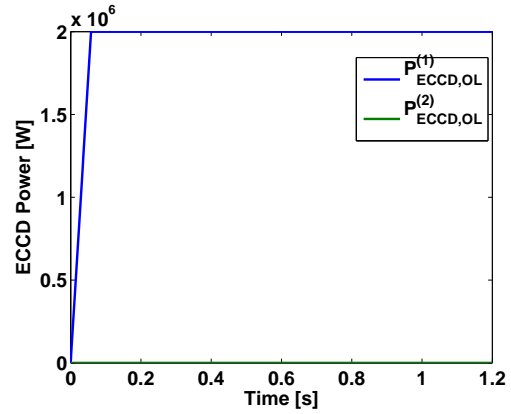
The second set of simulations includes a disturbance induced by extra ECCD current that peaks at  $r = 0.4$ . Since one of our available actuators is placed at this particular position, we may expect the controller to be able to greatly attenuate the effect of such a disturbance. The open-loop behaviour of the system is shown in Figure 5.10, while the closed-loop behaviour is presented in Figure 5.11. Figures 5.10 and 5.11 (b) illustrate the main interest of the closed-loop action: at the end of the simulation time only the closed-loop system is able to reach the desired q-profile. The final value of the ECCD power in the closed-loop system presents a negative offset that corresponds to the value of the applied disturbance. The power of the central actuator is used only to accelerate the convergence of the system and, at the end of the simulation time, returns to its



(a) Tracking of the safety factor profile. Dashed line: reference  $q$  value; full line: obtained  $q$  value.

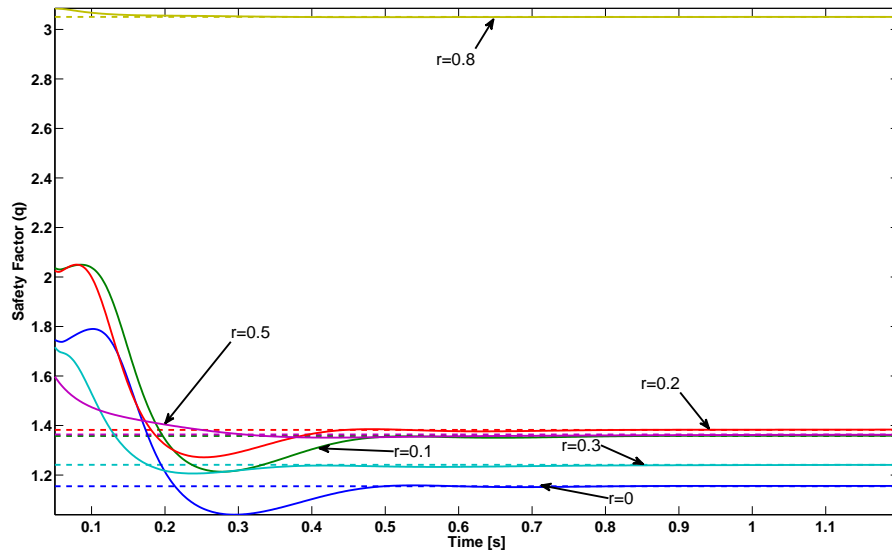


(b) Final safety factor profile and reference.

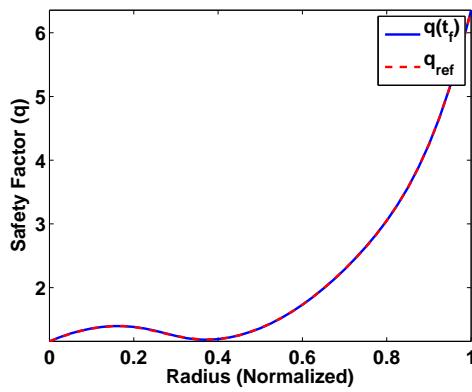


(c) Applied ECCD power.

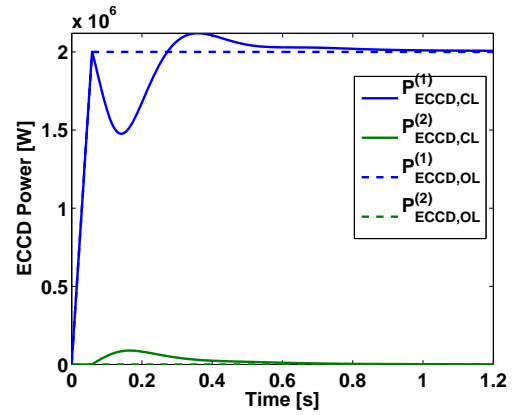
Figure 5.8: Safety factor profile and open-loop ECCD power evolution.



(a) Tracking of the safety factor profile. Dashed line: reference  $q$  value; full line: obtained  $q$  value.



(b) Final safety factor profile and reference.

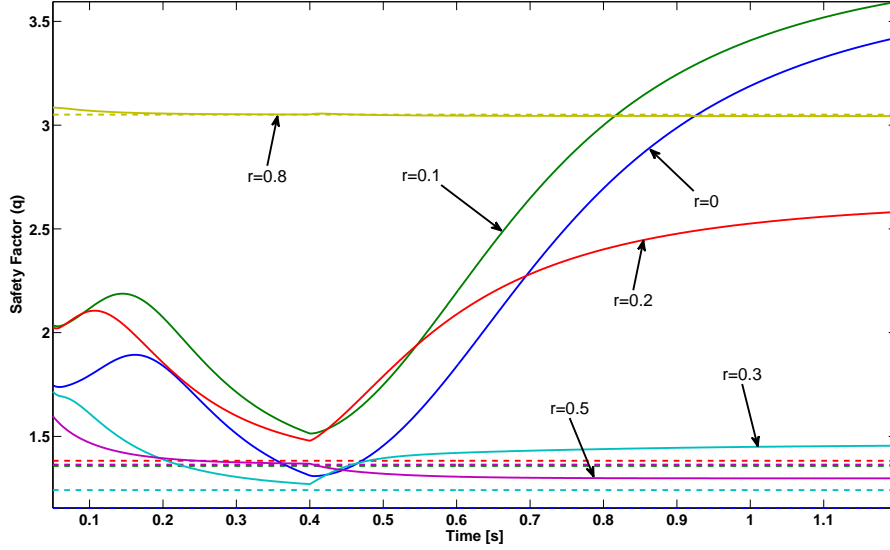


(c) Applied ECCD power and open-loop reference value.

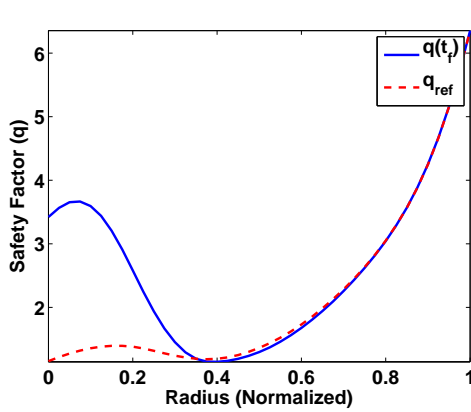
Figure 5.9: Safety factor profile tracking and closed-loop ECCD power evolution.



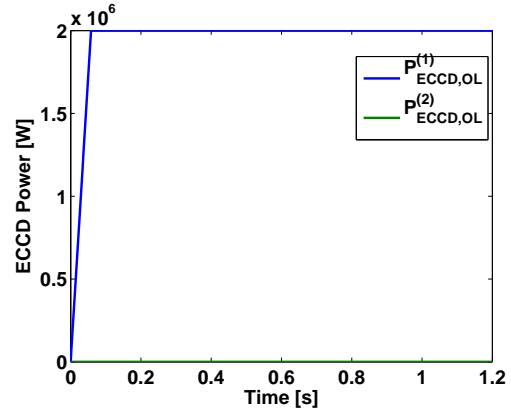
open-loop value.



(a) Tracking of the safety factor profile. Dashed line: reference  $q$  value; full line: obtained  $q$  value.



(b) Final safety factor profile and reference.



(c) Applied ECCD power.

Figure 5.10: Safety factor profile and open-loop ECCD power evolution with ECCD disturbance applied at  $r = 0.4$  for  $t \geq 0.4$  s.

The third set of simulations presents a more realistic scenario: a disturbance that cannot be entirely offset by the available actuators will be introduced in the system. In this case, we chose a combination of a heating input (ECRH), located at  $r = 0.2$ , and a current drive input (ECCD), located at  $r = 0.4$ . The combination of these two inputs cannot be exactly offset by the two available actuators. Nevertheless, comparing the open-loop response (Figure 5.12) and the closed-loop one (Figure 5.13), the closed-loop action is clearly beneficial. At the end of the simulation time, the reduction of the error between the reference and the safety factor profile in Figure 5.13 (b) with respect to

Figure 5.12 (b) is quite apparent.

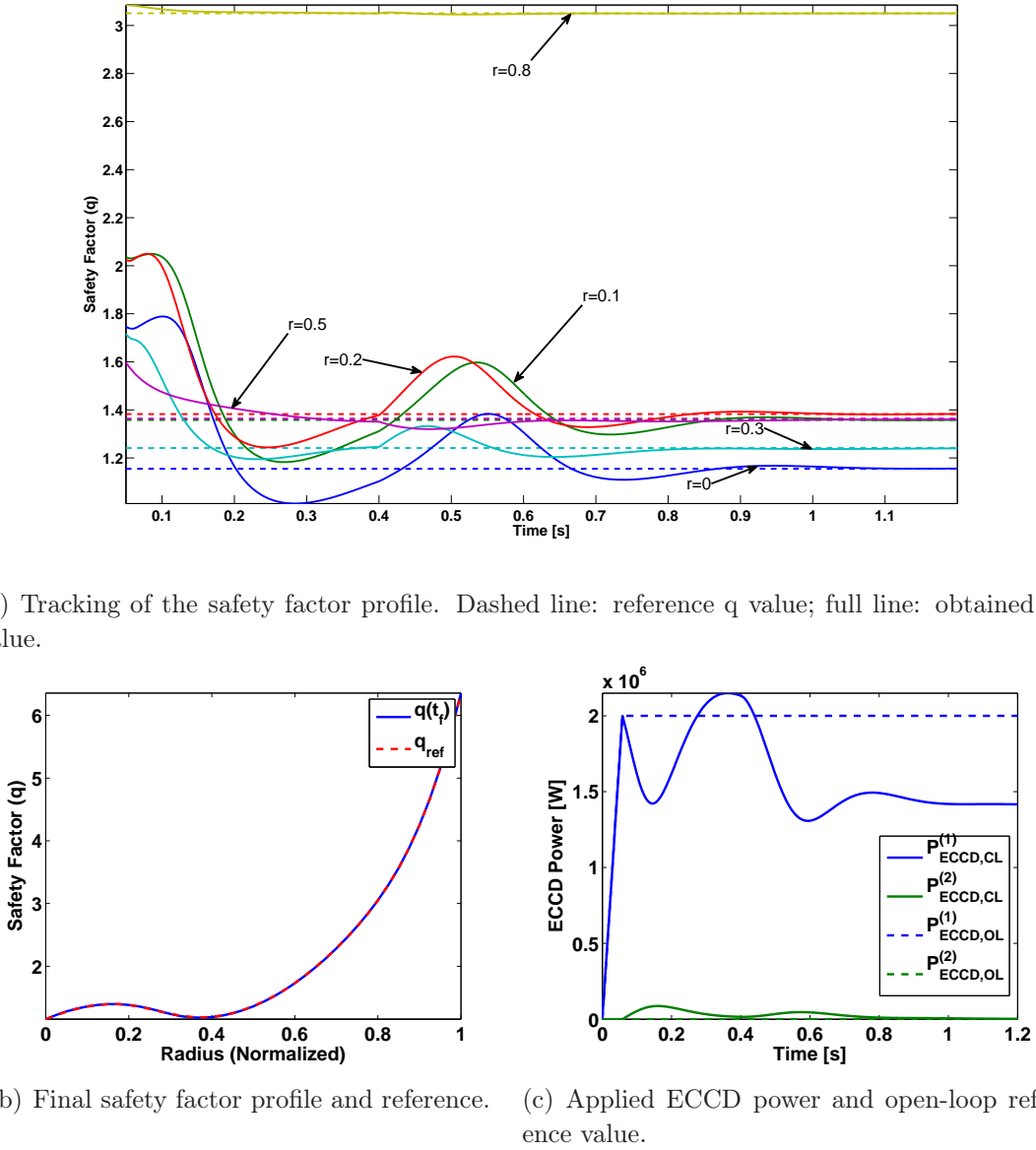
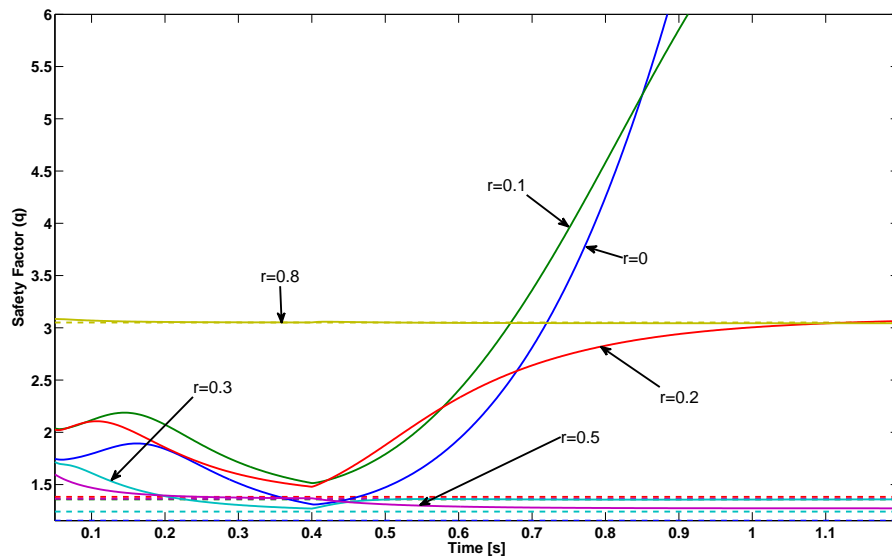


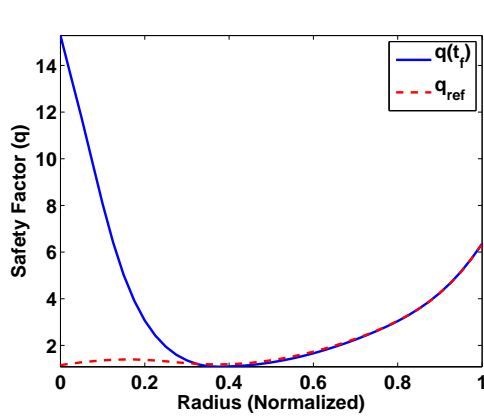
Figure 5.11: Safety factor profile tracking and closed-loop ECCD power evolution with ECCD disturbance applied at  $r = 0.4$  for  $t \geq 0.4$  s.

## 5.5 Summary and Conclusions

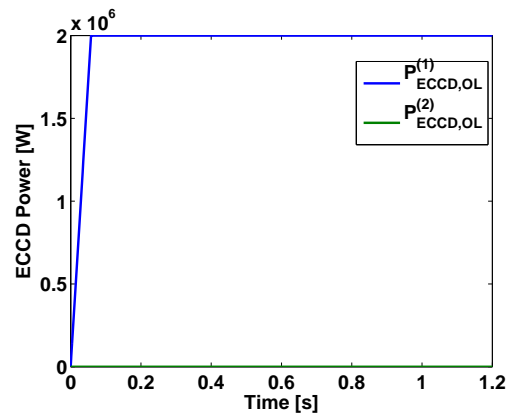
In this chapter, the strict Lyapunov function (4.2.2) for the poloidal magnetic flux resistive diffusion equation in 1D was modified to consider the couplings that exist between the flux diffusion and the total plasma current circuit (assumed to behave like a transformer, as in [Kazarian-Vibert et al., 1996]). By adding a component representing the



(a) Tracking of the safety factor profile. Dashed line: reference  $q$  value; full line: obtained  $q$  value.

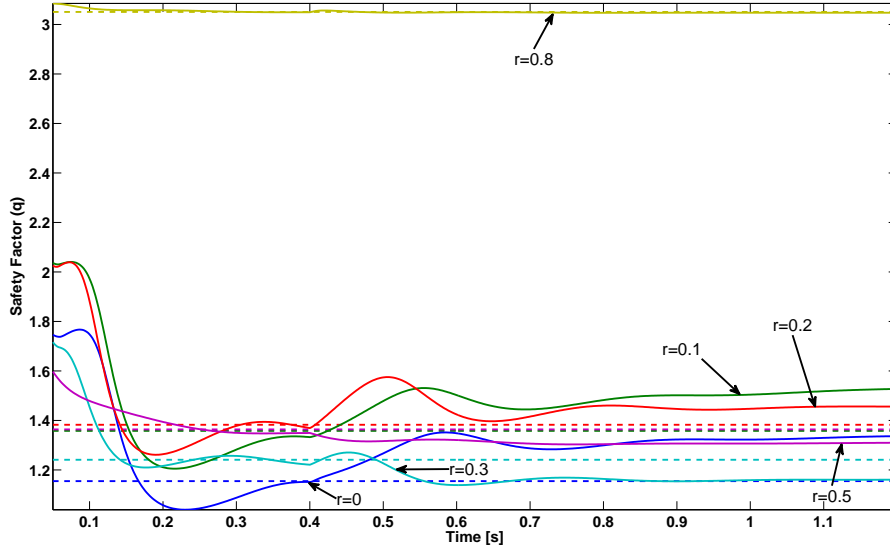


(b) Final safety factor profile and reference.

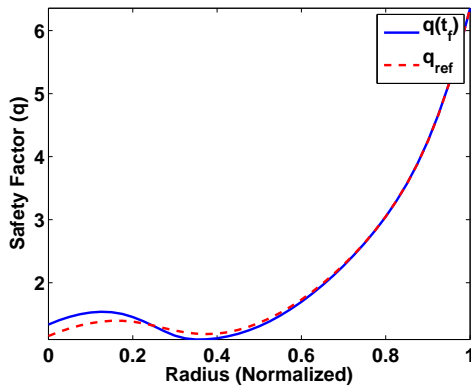


(c) Applied ECCD power.

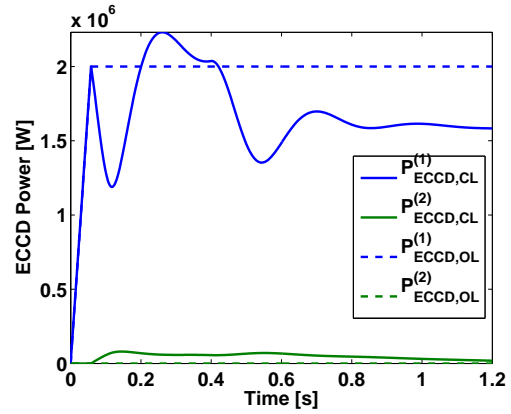
Figure 5.12: Safety factor profile and open-loop ECCD power evolution with ECCD and ECRH disturbances applied at  $r = 0.4$  and  $r = 0.2$ , respectively, for  $t \geq 0.4$  s.



(a) Tracking of the safety factor profile. Dashed line: reference  $q$  value; full line: obtained  $q$  value.



(b) Final safety factor profile and reference.



(c) Applied ECCD power.

Figure 5.13: Safety factor profile tracking and closed-loop ECCD power evolution with ECCD and ECRH disturbances applied at  $r = 0.4$  and  $r = 0.2$ , respectively, for  $t \geq 0.4$  s.

energy of the finite-dimensional subsystem, ISS properties similar to those established in the previous chapter can be obtained. A particularly interesting conclusion of this section is that we can always find a controller gain small enough (in terms of the variations of LH power) to guarantee the exponential stability of the interconnected system and that, as we approach a perfectly decoupled system (when the rate of convergence of the finite-dimensional system is much faster than that of the infinite-dimensional one), this constraint becomes less strict.

At this point, most of the difficulties outlined in Chapter 2 have been tackled:

- the time-varying distributed nature of the diffusion coefficients is taken into account (for more details see Appendix B);
- the strong nonlinear shape constraints imposed on the actuators are considered in the control algorithm;
- the robustness of any proposed control scheme with respect to different sources of error and disturbances has been analyzed;
- the coupling between the controller for the infinite-dimensional system and the boundary condition is taken into account;
- the control algorithms considered are implementable in real-time.

Some preliminary extensions of the proposed approach have also been presented. Namely, the addition of a profile-reconstruction delay in the closed-loop simulations and the use of ECCD actuation with TCV parameters.



# Chapter 6

## Conclusion and Perspectives

In this thesis, the problem of controlling the poloidal magnetic flux profile in a tokamak plasma has been studied. The motivation for this problem is the possibility of controlling the safety factor profile necessary to attain and maintain advanced operating modes in a tokamak with enhanced confinement and MHD stability.

The first two control approaches illustrate classical methods consisting on a spatial discretization of the distributed parameter system before applying established techniques for finite-dimensional systems. In Chapter 3 we illustrate an updating LQR controller (that requires the online solution of an Algebraic Riccati Equation) and does not guarantee the stability of the time-varying system. This approach is not too different from some existing approaches in the tokamak control field in the sense that the time-varying nature is overlooked to simplify the problem. Knowing that the diffusivity coefficients can vary much faster than the flux diffusion time and that some concurrent actuation may be in use (to control other plasma parameters), neglecting the variations of the diffusivity profiles is unsatisfactory. In order to take into account these variations, a Polytopic LPV formulation is developed for the discretized system. While it allows us to consider some variations, this approach can be too conservative and fail to provide usable results when a large operating range is considered. Furthermore, the extension of this approach to the gradient of the poloidal flux profile (a more significant physical variable) is far from straightforward and the proposed change of variables (leading to a constant  $B$  matrix) cannot be applied.

In order to address the weaknesses discovered in the first proposed approaches, in Chapter 4 we present a new approach based on a strict Lyapunov function developed for the open-loop system. Since the physical flux diffusion system is known to be stable, this allows us to construct strongly constrained control laws that guarantee the closed-loop stability of the system while accelerating the rate of convergence and attenuating disturbances. A detailed analysis of robustness properties of control laws based on the

constructed ISS Lyapunov function is developed to illustrate the impact of different design parameters in the controller. This approaches are tested under simulation using both a simple simulation of only the diffusion equation and a more complete model based on [Witrant et al., 2007] that corresponds to the model presented in Chapter 2.

Finally, in Chapter 5, the interconnection of the poloidal magnetic flux diffusion equation with the peripheral dynamics controlling the boundary conditions of the model is explored. An extended Lyapunov function is constructed to show the stability of the interconnected system and the control scheme is tested using METIS. Some extensions are presented, taking into account other important aspects that directly add to the relevance of the proposed approach, mainly the effect of profile-reconstructuon delays and the possibility of extending the results to other tokamaks (done here using the RAPTOR code [Felici et al., 2011] and TCV parameters) and other non-inductive actuators (in this case ECCD).

The main contributions of this thesis are:

- the explicit consideration of the time-varying nature of the diffusivity profiles (not limiting their variation to a scalar quantity multiplying a static shape);
- the explicit consideration of the nonlinear dependency of the current deposit on the antenna parameters;
- allowing for actuator saturation;
- the explicit consideration of the couplings existing between the control action and the boundary condition in the stability analysis;
- a thorough characterization of the gains between different sources of error and disturbances and the state;
- the lack of imposed limits on the rate of time variation of the diffusivity profiles to maintain the stability;
- particular provisions for the real-time implementation of the proposed approach for safety factor control on a real tokamak.

The main remaining challenges are:

- extending the stability results to incorporate performance guarantees (to limit overshoots, for instance);
- considering the coupled problem of temperature and current profile control (necessary for burn-control);



- considering the nonlinear impact of the bootstrap current, first to guarantee the stability of the system and then to maximize the bootstrap current fraction;
- finding conditions to guarantee the stability of the system in the presence of delays;
- experimental validation of the proposed approaches.



# Appendix A

## Proof of Theorem 2.1.2

*Proof of Theorem 2.1.2:* This proof is organized as follows:

- (a) First, an auxiliary problem in two-dimensional Cartesian coordinates under symmetry conditions is formulated.
- (b) Next, the existence and uniqueness of solutions to the auxiliary problem is shown using Theorem 5.1.21 and Corollary 5.1.22 in [Lunardi, 1995] (pages 206-208). Which in turn imply the existence and uniqueness of solutions to the problem (2.1.14)-(2.1.16).

(a): Consider the following two-dimensional Cartesian auxiliary system:

$$\zeta_t(x_1, x_2, t) = \eta(x_1, x_2, t)\Delta\zeta(x_1, x_2, t) + F(x_1, x_2, t), \quad \forall (x_1, x_2, t) \in \Omega \times [0, T] \quad (\text{A.0.1})$$

with symmetric boundary condition:

$$\zeta_\nu(x_1, x_2, t) = -\frac{R_0\mu_0\tilde{I}_p(t)}{2\pi}, \quad \forall (x_1, x_2, t) \in \partial\Omega \times [0, T] \quad (\text{A.0.2})$$

where  $\zeta_\nu$  is the derivative of  $\zeta$  in the outward normal direction to  $\partial\Omega$ , and with symmetric initial condition  $\zeta_0 \in \mathcal{C}^{3+\alpha_c}(\overline{\Omega})$ ,  $0 < \alpha_c < 1$ :

$$\zeta(x_1, x_2, 0) = \zeta_0(x_1, x_2), \quad \forall (x_1, x_2) \in \Omega \quad (\text{A.0.3})$$

where  $\Delta$  is the Laplacian,  $F(x_1, x_2, t) \doteq \eta(x_1, x_2, t)u(x_1, x_2, t)$ . This system is equivalent, when imposing a central symmetry condition and sufficient regularity of the initial condition, to (2.1.11)-(2.1.13).

(b): To apply Theorem 5.1.21 and Corollary 5.1.22 in [Lunardi, 1995] (pages 206-208) it must be shown first that the diffusive operators verify a uniform ellipticity condition in  $\overline{\Omega}$ . This is trivially verified as a direct consequence of  $P_1$  and therefore Theorem

5.1.21 gives the existence and uniqueness of solutions and Corollary 5.1.22 establishes the desired regularity (such that the gradient is in  $C^{2+\alpha_c, 1+\alpha_c/2}(\overline{\Omega} \times [0, T])$ ). This degree of regularity is sufficient to ensure that all the integrals used for the definition of the Lyapunov function and its time derivative are well defined. This concludes the proof of Theorem 2.1.2. ■

Existence, uniqueness and regularity results are also valid when the control input is of the form proposed in Corollary 4.2.7 (which amounts to a feedback in the variable  $\zeta$ ). and can extend to certain forms of non-homogeneous boundary conditions thanks to the structure of the operators considered in [Lunardi, 1995].

# Appendix B

## Finding a Lyapunov Function

### Contents

---

<b>B.1 Finding a Weighting Function . . . . .</b>	<b>116</b>
B.1.1 Considered Set of Diffusivity Profiles . . . . .	116
B.1.2 Sufficient Conditions and Algorithm . . . . .	117
<b>B.2 Numerical Application . . . . .</b>	<b>119</b>
B.2.1 Weighting Function . . . . .	119
B.2.2 Simulations . . . . .	120

---

### B.1 Finding a Weighting Function

#### B.1.1 Considered Set of Diffusivity Profiles

The objective of this Appendix is to propose a heuristic for numerically computing an adequate weighting function such that Assumption  $A_1$  in Section 4.4 holds. This is done by verifying the conditions of Theorem 4.2.3 for a particular set of diffusivity coefficients. In the rest of this section, the  $\eta$  profile is assumed to be of the form:

$$\eta(r, t) = a(t)e^{\int_0^r \phi(\xi, t) d\xi}, \forall (r, t) \in [0, 1] \times [0, T) \quad (\text{B.1.1})$$

where  $0 < \underline{a} \leq a(t) \leq \bar{a}$ ,

$$\phi(r, t) \in \Phi = \{\phi(r, t) \in \mathcal{C}^\infty([0, 1] \times [0, T]) \mid \forall t \in [0, T], \phi(\cdot, t) \in \Lambda\}$$

and

$$\Lambda = \{\lambda(r) \in \mathcal{C}^\infty([0, 1]) \mid \forall r \in [0, 1], \underline{\lambda} \leq \lambda(r) \leq \bar{\lambda}\}$$

This choice of profiles is physically motivated by the application of magnetic flux profile control in Tokamak plasmas, see Section V of [Bribiesca Argomedo et al., 2012a] for a more detailed discussion.

### B.1.2 Sufficient Conditions and Algorithm

**Proposition B.1.1.** *With  $\eta$  defined as in (B.1.1), a sufficient condition to apply Theorem 4.2.3 is the existence of an a.e. twice-differentiable positive function  $f : [0, 1] \rightarrow \mathbb{R}^+$  with piecewise-continuous second derivative such that the following inequality is verified:*

$$f''(r) + f'(r) \left[ \lambda(r) - \frac{1}{r} \right] + f(r) \left[ \frac{\lambda(r)}{r} - \frac{1}{r^2} + \epsilon \right] \leq 0 \quad (\text{B.1.2})$$

for every  $(r, \lambda) \in (0, 1] \times \Lambda$  and some positive constant  $\epsilon$ .

*Proof.* This proposition results from multiplying (B.1.2) by  $e^{\int_0^r \lambda(\xi) d\xi}$  and setting  $\alpha \doteq \epsilon \inf_{(r, \lambda) \in [0, 1] \times \Lambda} \{ \underline{a} e^{\int_0^r \lambda(\xi) d\xi} \} > 0$  (keeping  $a(t)$  in front of the exponential is not necessary since we are using  $\underline{a}$  in the definition of  $\alpha$ ).  $\square$

An a.e. twice-differentiable positive function with piecewise-continuous second derivative  $f : [0, 1] \rightarrow \mathbb{R}^+$  satisfies (B.1.2) if there exists  $w(r, \lambda) \leq 0$  such that, for all  $(r, \lambda) \in (0, 1] \times \Lambda$  the following equation is verified:

$$\begin{bmatrix} f \\ f' \end{bmatrix}' = \begin{bmatrix} 0 & 1 \\ \frac{1}{r^2} - \frac{\lambda(r)}{r} - \epsilon & \frac{1}{r} - \lambda(r) \end{bmatrix} \begin{bmatrix} f \\ f' \end{bmatrix} + \begin{bmatrix} 0 \\ 1 \end{bmatrix} w(r, \lambda) \quad (\text{B.1.3})$$

In order to avoid testing the condition for all  $\lambda \in \Lambda$ , the following result is used:

**Proposition B.1.2.** *Given an a.e. twice-differentiable positive function with piecewise-continuous second derivative  $f : [0, 1] \rightarrow \mathbb{R}^+$ , the following two conditions are equivalent:*

- i: *there exists  $w(r, \lambda) \leq 0$  such that (B.1.3) is verified for all  $(r, \lambda) \in (0, 1] \times \Lambda$ ;*
- ii: *there exists  $w_2(r) \leq 0$  such that the following equation is verified for all  $r \in (0, 1]$ :*

$$\begin{bmatrix} f \\ f' \end{bmatrix}' = A(f, r) \begin{bmatrix} f \\ f' \end{bmatrix} + \begin{bmatrix} 0 \\ 1 \end{bmatrix} w_2(r) \quad (\text{B.1.4})$$

where:

$$A(f, r) = \begin{cases} \begin{bmatrix} 0 & 1 \\ \frac{1}{r^2} - \frac{\lambda}{r} - \epsilon & \frac{1}{r} - \lambda \end{bmatrix} & \text{if } \frac{f(r)}{r} + f'(r) \leq 0 \\ \begin{bmatrix} 0 & 1 \\ \frac{1}{r^2} - \frac{\bar{\lambda}}{r} - \epsilon & \frac{1}{r} - \bar{\lambda} \end{bmatrix} & \text{if } \frac{f(r)}{r} + f'(r) > 0 \end{cases}$$

## Appendix B. Finding a Lyapunov Function

---

*Proof.* The proof stems from the fact that the left-hand side of (B.1.2), which is equivalent to the right-hand side of (B.1.3), is linear in  $\lambda(r)$  and  $\lambda$  (and therefore is bounded by  $\bar{\lambda}$  or  $\underline{\lambda}$ ). It is easy to verify that the switching condition in matrix  $A(f, r)$  corresponds to the sign of the coefficient of  $\lambda(r)$  (at any given point  $r$ ) in (B.1.2). Therefore,  $w_2(r) = \sup_{\lambda \in \Lambda} \{w(r, \lambda)\}$  for all  $r \in [0, 1]$  (i.e. we are verifying the inequality at the critical point).  $\square$

**Remark B.1.3.** *The easiest way to find a function  $f$  that satisfies condition (B.1.4) is to fix some boundary conditions for  $f$  and  $f'$ , set  $w_2(r) = 0$  for all  $r \in [0, 1]$ , and solve the resulting equation backwards from the values  $f(1)$  and  $f'(1)$ . Nevertheless, it yields solutions with a singularity at the origin, as can be seen in Figure B.1 for  $\underline{\lambda} = \bar{\lambda} = 4$ .*

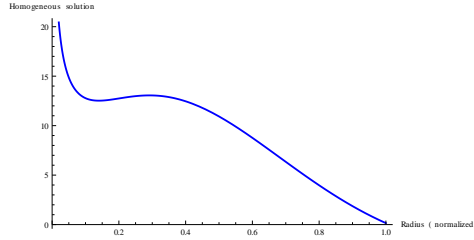


Figure B.1: Function  $f$  obtained by numerically solving the homogeneous equation (B.1.3) for a single value of  $\lambda = 4$ .

Since setting  $w_2(r) = 0$  does not suffice to find adequate weighting functions, a more structured approach is developed to tackle this problem. In order to compute a weight verifying condition ii of Proposition B.1.2, boundary conditions are set at  $r = 1$  and the equation is solved backwards up to  $r = 0$  using Algorithm B.1.4.

### Algorithm B.1.4.

- 1: Set numerical values for the boundary conditions at  $r = 1$ ,  $f(1)$  and  $f'(1)$ , and for  $\epsilon$ .
- 2: Evaluate  $\frac{f(r)}{r} + f'(r)$  and fix the value of the dynamic matrix  $A(f, r)$  accordingly, using (B.1.4).
- 3: Find a numerical solution going backwards until hitting a zero-crossing of  $\frac{f(r)}{r} + f'(r)$ , setting  $w_2(r) = 0$ , and verifying that  $f(r)$  remains positive. Otherwise, change the boundary conditions or the value of  $\epsilon$ .
- 4: Use the values of  $f(r)$  and  $f'(r)$  at the zero-crossings of  $\frac{f(r)}{r} + f'(r)$  as initial values for the next step in solving the equation, switching the dynamic matrix but keeping  $w_2(r) = 0$ , always verifying that  $f(r)$  remains positive and bounded.

- 5: Repeat 3-4 until either reaching  $r = 0$  or finding a point such that both elements in the lower row of the  $A$  matrix are positive, as well as  $f$  and  $f'$ , with  $f(r) - rf'(r) > 0$ . If no such point exists before  $r = 0$ , change the boundary conditions or the value of  $\epsilon$  and start over.
- 6: If  $r = 0$  has not been reached yet, complete the solution by setting  $w_2(r)$  to have  $f''(r) = 0$  for the remaining interval, in order to avoid singularities in the solution near zero.

**Remark B.1.5.** *Although this heuristic does not guarantee finding an adequate weighting function, it does provide a methodic framework to solve the nonlinear boundary value problem (B.1.4) and yields good results in practice, as shown in the next section.*

The conclusion of this section is that Algorithm B.1.4 gives a practical way for numerically testing condition ii in Proposition B.1.2, which in turn, by Proposition B.1.1 implies that the conditions of Theorem 4.2.3 are verified for  $\eta$  defined as in (B.1.1). It should be noted that the results also hold for any convex combination of functions  $\eta$  satisfying (B.1.1).

## B.2 Numerical Application

### B.2.1 Weighting Function

We aim at finding an adequate weighting function for  $a(t) \in [0.0093, 0.0121]$ ,  $\underline{\lambda} = 4$  and  $\bar{\lambda} = 7.3$  (see (B.1.1)). This would imply a 55% increase in the allowable range for  $\eta(1, t)$  with respect to the objective set in [Bribiesca Argomedeo et al., 2012a] if we considered  $\lambda$  constant in  $r$ . However, it should be noted that a much more general form of  $\lambda(r)$  is being considered in this section.

The boundary conditions at  $r = 1$  were chosen as  $f(1) = 0.15$ ,  $f'(1) = -15$ , and a suitable weighting function was found for a maximum value of  $\epsilon = 5.3$ . Given the values of the boundary conditions, the solution was obtained first using the dynamic matrix with  $\underline{\lambda}$  and then switching dynamics at  $r \approx 0.52$ . For  $r \in [0, 0.015]$ ,  $f''$  was set to 0 using  $w(r)$ . The resulting weighting function, numerically computed using Mathematica®, can be seen in Figure B.2. The piecewise continuous and bounded second derivative of the weighting function is also shown in Figure B.3. The maximum value of  $f$  is  $\sim 12.40$  and its minimum is 0.15, which means that the constant  $c$  used for the norm equivalence and in (4.4.2) has a value of  $\sim 9.09$ . Other functions with a much lower value of  $c$  can be found, but usually there is a compromise between this constant and the guaranteed value for  $\epsilon$ .



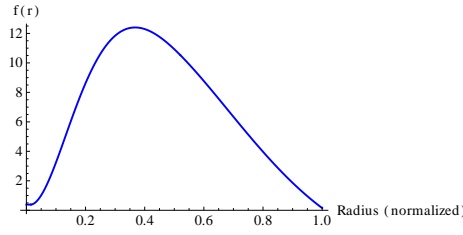


Figure B.2: Function  $f$  obtained using the heuristic.

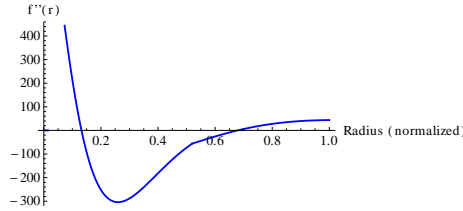


Figure B.3: Piecewise continuous second derivative of function  $f$  obtained using the heuristic.

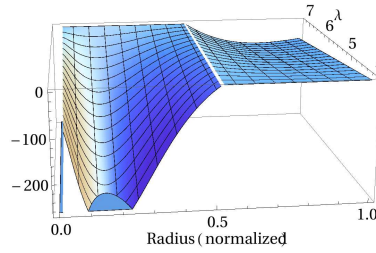


Figure B.4: Numerical test of the conditions of Proposition [B.1.1](#).

In order to illustrate the fact that this function verifies the conditions of Proposition [B.1.1](#), the value of the left-hand side of inequality [\(B.1.2\)](#) was plotted for values of  $(r, \lambda) \in [0, 1] \times [4, 7.3]$  (with constant  $\lambda$  throughout  $r$ ). The result can be seen in Figure [B.4](#). It is interesting to note that for each value of  $r$ , the critical value of  $\lambda$  in the inequality is the one used to compute the weighting function. For values of  $r$  close to zero however, the slack variable  $w$  is different from zero for all values of  $\lambda$ , thus avoiding the singularity in  $f(r)$  as desired.

### B.2.2 Simulations

The evolution of the diffusion equation was simulated using Matlab<sup>®</sup> and the weighting function found in the previous subsection. The numerical scheme used for the simulations is an explicit finite-difference method with space and time steps chosen such that the CFL condition,  $\max_{(r,t) \in [0,1] \times [0,T)} \{\eta\} \frac{\Delta t}{(\Delta x)^2} \leq 0.5$ , is verified.

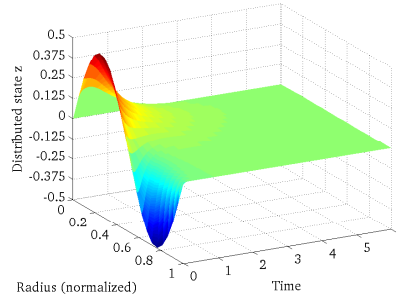


Figure B.5: Evolution of the state without disturbances and with the minimum diffusivity.

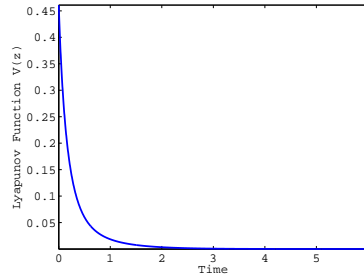


Figure B.6: Evolution of the Lyapunov function without disturbances and with the minimum diffusivity.

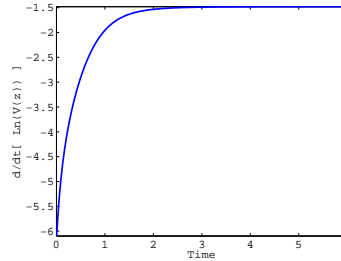


Figure B.7: Exponential convergence rate for  $V(z)$  without disturbances and with the minimum diffusivity.

First, choosing the minimum values for the diffusion coefficients and without disturbances, the evolution of the distributed state can be seen in Figure B.5. With this simulation, the evolution of the Lyapunov function and the equivalent rate of convergence are shown in Figures B.6 and B.7, respectively. For this initial condition, the guaranteed rate of convergence is  $\sim 23$  times smaller than the obtained one. This results can be explained by considering that the condition imposed in Theorem 4.2.3 was verified at every point and that the diffusivity at the right boundary is  $\sim 55$  times the one at the center, this level of conservatism is therefore not unexpected.

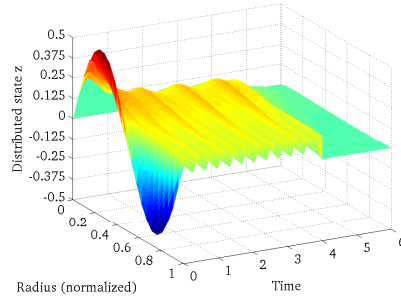


Figure B.8: Evolution of the state with disturbance acting until  $t = 4$ s and time-varying diffusivity.

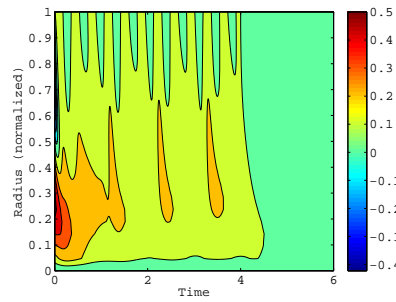


Figure B.9: Contour plot of the evolution of the state with disturbance acting until  $t = 4$ s and time-varying diffusivity.

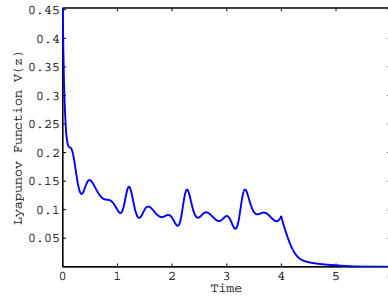


Figure B.10: Evolution of the Lyapunov function with disturbance acting until  $t = 4$ s and time-varying diffusivity.

Next, introducing a boundary disturbance  $\varepsilon(t) = 0.1 + 0.05 \sin(4.56\pi t)$  and letting the diffusivity coefficient vary with  $a(t) = 0.0107 - 0.0014 \cos(4\pi t)$  and  $\phi(r, t) = 5.65 + 1.65 \sin(2\pi t)$  (independent of  $r$  in this case). The resulting evolution can be seen in Figures B.8 and B.9. The behaviour of the Lyapunov function is shown in Figure B.10. The Lyapunov function remains bounded when the disturbance is present and, once the disturbance is removed at  $t = 4$ s the exponential convergence to zero is observed.



# Bibliography

- Amato, F., Celentano, G., and Garofalo, F. (1993). New sufficient conditions for the stability of slowly varying linear systems. *IEEE Transactions on Automatic Control*, 38:1409–1411.
- Ariola, M. and Pironti, A. (2008). *Magnetic Control of Tokamak Plasmas*. Advances in Industrial Control. Springer-Verlag.
- Artaud, J. F. (2008). *METIS user’s guide*. CEA/IRFM/PHY/NTT-2008.001.
- Artaud, J. F. et al. (2010). The CRONOS suite of codes for integrated tokamak modelling. *Nucl. Fusion*, 50, 043001.
- Baker, R. A. and Bergen, A. R. (1969). Lyapunov stability and Lyapunov functions of infinite dimensional systems. *IEEE Transactions on Automatic Control*, 14(4):325–334.
- Barana, O., Mazon, D., Caulier, G., Garnier, D., Jouve, M., Laborde, L., and Peyson, Y. (2006). Real-time determination of supratermal electron local emission profile from hard x-ray measurements on Tore Supra. *IEEE Transaction on Nuclear Science*, 53:1051–1055.
- Barana, O., Mazon, D., Laborde, L., and Turco, F. (2007). Feedback control of the lower hybrid power deposition profile on Tore Supra. *Plasma Phys. Control. Fusion*, 49:947–967.
- Blum, J. (1989). *Numerical Simulation and Optimal Control in Plasma Physics*. Wiley/Gauthier-Villars Series in Modern Applied Mathematics. Gauthier-Villars, John Wiley & Sons.
- Blum, J., Boulbe, C., and Faugeras, B. (2012). Reconstruction of the equilibrium of the plasma in a Tokamak and identification of the current density profile in real time. *Journal of Computational Physics*, 231(3):960–980.
- Briat, C. (2008). *Robust Control and Observation of LPV Time-Delay systems*. PhD thesis, Grenoble INP, France.

- Bribiesca Argomedo, F., Prieur, C., Witrant, E., and Brémond, S. (2011). Polytopic control of the magnetic flux profile in a tokamak plasma. In *Proceedings of the 18th IFAC World Congress. Milan, Italy*.
- Bribiesca Argomedo, F., Prieur, C., Witrant, E., and Brémond, S. (2012a). A strict control Lyapunov function for a diffusion equation with time-varying distributed coefficients. *To appear, IEEE Transactions on Automatic Control*.
- Bribiesca Argomedo, F., Witrant, E., and Prieur, C. (2012b). D1-Input-to-State stability of a time-varying nonhomogeneous diffusive equation subject to boundary disturbances. In *Proceedings of the American Control Conference, Montréal, Canada*.
- Bribiesca Argomedo, F., Witrant, E., Prieur, C., Georges, D., and Brémond, S. (2010). Model-based control of the magnetic flux profile in a tokamak plasma. In *Proceedings of the 49th IEEE Conference on Decision and Control*, pages 6926–6931, Atlanta, GA.
- Cazenave, T. and Haraux, A. (1998). *An introduction to semilinear evolution equations*. Oxford University Press.
- Coron, J.-M., Bastin, G., and d’Andréa Novel, B. (2008). Dissipative boundary conditions for one-dimensional nonlinear hyperbolic systems. *SIAM Journal on Control and Optimization*, 47(3):1460–1498.
- Coron, J.-M. and d’Andréa Novel, B. (1998). Stabilization of a rotating body beam without damping. *IEEE Transactions on Automatic Control*, 43(5):608–618.
- Coron, J.-M., d’Andréa Novel, B., and Bastin, G. (2007). A strict Lyapunov function for boundary control of hyperbolic systems of conservation laws. *IEEE Transactions on Automatic Control*, 52(1):2–11.
- Desoer, C. A. (1969). Slowly varying system  $\dot{x} = a(t)x$ . *IEEE Transactions on Automatic Control*, 14:780–781.
- Felici, F. and Sauter, O. (2012). Non-linear model-based optimization of actuator trajectories for tokamak plasma profile control. *Plasma Phys. Control. Fusion*, 54:025002.
- Felici, F., Sauter, O., Coda, S., Duval, B., Goodman, T., Moret, J.-M., Paley, J., and the TCV Team (2011). Real-time physics-model-based simulation of the current density profile in tokamak plasmas. *Nuclear Fusion*, 51:083052.
- Gahlawat, A., Peet, M. M., and Witrant, E. (August, 2011). Control and verification of the safety-factor profile in tokamaks using sum-of-squares polynomials. In *Proceedings of the 18th IFAC World Congress. Milan, Italy*.

- Gaye, O., Moulay, E., Brémond, S., Autrique, L., Nouailletas, R., and Orlov, Y. (2011). Sliding mode stabilization of the current profile in tokamak plasmas. In *Proceedings of the 50th IEEE Conference on Decision and Control and European Control Conference*, pages 2638–2643, Orlando, FL.
- Gilbert, W., Henrion, D., Bernussou, J., and Boyer, D. (2010). Polynomial LPV synthesis applied to turbofan engines. *Control Engineering Practice*, 18(9):1077–1083.
- Goniche, M. et al. (2005). Lower hybrid current drive efficiency on Tore Supra and JET. *16th Topical Conference on Radio Frequency Power in Plasmas. Park City, USA*.
- Gormezano, C. (1999). High performance tokamak operation regimes. *Plasma Phys. Control. Fusion*, 41:B367–80.
- Hinton, F. L. and Hazeltine, R. D. (1976). Theory of plasma transport in toroidal confinement systems. *Reviews of Modern Physics*, 48(2):239–308.
- Imbeaux, F. (1999). *Etude de la propagation et de l'absorption de l'onde hybride dans un plasma de tokamak par tomographie X haute énergie*. PhD thesis, Université Paris XI Orsay, Orsay, France.
- Imbeaux, F. et al. (2011). Real-time control of the safety factor profile diagnosed by magneto-hydrodynamic activity on the Tore Supra tokamak. *Nuclear Fusion*, 51:073033.
- ITER Organization (2010). Official iter site: <http://www.iter.org/>.
- Jayawardhana, B., Logemann, H., and Ryan, E. P. (2008). Infinite-dimensional feedback systems: the circle criterion and input-to-state stability. *Communications in Information and Systems*, 8(4):413–444.
- Kamen, E. W., Khargonekar, P. P., and Tannenbaum, A. (1989). Control of slowly-varying linear systems. *IEEE Transactions on Automatic Control*, 34:1283–1285.
- Kazarian-Vibert, F. et al. (1996). Full steady-state operation in Tore Supra. *Plasma Phys. Control. Fusion*, 38:2113–2131.
- Krstic, M. and Smyshlyaev, A. (2008). Adaptive boundary control for unstable parabolic PDEs—part I: Lyapunov design. *IEEE Transactions on Automatic Control*, 53(7):1575–1591.
- Laborde, L. et al. (2005). A model-based technique for integrated real-time profile control in the JET tokamak. *Plasma Phys. Control. Fusion*, 47:155–183.
- Leith, D. and Leithead, W. (2000). Survey of gain-scheduling analysis and design. *Int. J. Control*, 73(11):1001–1025.

- Löfberg, J. (2004). YALMIP : A toolbox for modeling and optimization in MATLAB. In *Proceedings of the CACSD Conference, Taipei, Taiwan*.
- Lunardi, A. (1995). *Analytic Semigroups and Optimal Regularity in Parabolic Problems*, volume 16 of *Progress in nonlinear differential equations and their applications*. Birkhäuser.
- Mazenc, F. and Prieur, C. (2011). Strict Lyapunov functions for semilinear parabolic partial differential equations. *Mathematical Control and Related Fields*, 1:231–250.
- Moreau, D. et al. (2011). Plasma models for real-time control of advanced tokamak scenarios. *Nucl. Fusion*, 51(6).
- Moreau, P. et al. (October 2009). Plasma control in Tore Supra. *Fusion Science and Technology*, 56:1284–1299.
- Ni, M. L. (2008). Existence condition on solutions to the algebraic riccati equation. *Acta Automatica Sinica*, 34:85–87.
- Ou, Y., Xu, C., and Schuster, E. (2010). Robust control design for the poloidal magnetic flux profile evolution in the presence of model uncertainties. *IEEE Transactions on Plasma Science*, 38(3):375–382.
- Ou, Y., Xu, C., Schuster, E., Luce, T. C., Ferron, J. R., Walker, M. L., and Humphreys, D. A. (2008). Design and simulation of extremum-seeking open-loop optimal control of current profile in the DIII-D tokamak. *Plasma Phys. Control. Fusion*, 50:115001.
- Ou, Y., Xu, C., Schuster, E., Luce, T. C., Ferron, J. R., Walker, M. L., and Humphreys, D. A. (2011). Optimal tracking control of current profile in tokamaks. *IEEE Transactions on Control Systems Technology*, 19(2):432–441.
- Peet, M. M., Papachristodoulou, A., and Lall, S. (2009). Positive forms and stability of linear time-delay systems. *SIAM Journal on Control and Optimization*, 47(6):3237–3258.
- Pironti, A. and Walker, M. (2005). Fusion, tokamaks, and plasma control: an introduction and tutorial. *IEEE Control Systems Magazine*, 25(5):30–43.
- Prieur, C. and Mazenc, F. (2012). ISS-Lyapunov functions for time-varying hyperbolic systems of conservation laws. *Math. Control Signals Systems*, 24(1):111–134.
- Rosenbrock, H. H. (1963). The stability of linear time-dependent control systems. *J. Electronics and Control*, 15:73–80.
- Rugh, W. and Shamma, J. (2000). Research on gain scheduling. *Automatica*, 36:1401–1425.



- SeDuMi (2011). Sedumi website: <http://sedumi.ie.lehigh.edu/>.
- Smyshlyaev, A. and Krstic, M. (2004). Closed-form boundary state feedback for a class of 1-D partial integro-differential equations. *IEEE Transactions on Automatic Control*, 49(12):2185–2201.
- Smyshlyaev, A. and Krstic, M. (2005). On control design for PDEs with space-dependent diffusivity or time-dependent reactivity. *Automatica*, 41:1601–1608.
- Smyshlyaev, A. and Krstic, M. (2007a). Adaptive boundary control for unstable parabolic PDEs—part II: Estimation-based designs. *Automatica*, 43(9):1543–1556.
- Smyshlyaev, A. and Krstic, M. (2007b). Adaptive boundary control for unstable parabolic PDEs—part III: Output feedback examples with swapping identifiers. *Automatica*, 43(9):1557–1564.
- Sontag, E. D. (2008). Input to state stability: Basic concepts and results. In *Nonlinear and Optimal Control Theory*, pages 163–220. Springer-Verlag, Berlin.
- Taylor, T. S. (1997). Physics of advanced tokamaks. *Plasma Phys. Control. Fusion*, 39:B47–73.
- Vazquez, R. and Krstic, M. (2006). Explicit integral operator feedback for local stabilization of nonlinear thermal convection loop PDEs. *Systems & Control Letters*, 55:624–632.
- Vazquez, R. and Krstic, M. (2008). *Control of Turbulent and Magnetohydrodynamic Channel Flows Boundary Stabilization and State Estimation*. Systems & Control: Foundations & Applications. Birkhäuser.
- Vazquez, R. and Krstic, M. (2010). Boundary observer for output-feedback stabilization of thermal-fluid convection loop. *IEEE Transactions on Control Systems Technology*, 18(4):789–797.
- Walker, M., Humphreys, D., Mazon, D., Moreau, D., Okabayashi, M., Osborne, T., and Schuster, E. (2006). Emerging applications in tokamak plasma control. *IEEE Control Systems Magazine*, 26(2):35–63.
- Walker, M. L., Schuster, E., Mazon, D., and Moreau, D. (2008). Open and emerging control problems in tokamak plasma control. In *Proceedings of the 47th IEEE Conference on Decision and Control*, pages 3125–3132, Cancún, Mexico.
- Wassink, M. G., Van de Wal, M., Scherer, C. W., and Bosgra, O. (2005). LPV control for a wafer stage: beyond the theoretical solution. *Control Engineering Practice*, 13:231–245.

- Wesson, J. (2004). *Tokamaks*. International Series of Monographs on Physics 118. Oxford University Press, third edition.
- Wijnands, T., Houtte, D. V., Martin, G., Litaudon, X., and Froissard, P. (1997). Feedback control of the current profile on Tore Supra. *Nucl. Fusion*, 37:777–791.
- Witrant, E., Joffrin, E., Brémond, S., Giruzzi, G., Mazon, D., Barana, O., and Moreau, P. (2007). A control-oriented model of the current control profile in tokamak plasma. *Plasma Phys. Control. Fusion*, 49:1075–1105.
- Wolf, R. C. (2003). Internal transport barriers in tokamak plasmas. *Plasma Phys. Control. Fusion*, 45:R1–91.

# Index

- actuator
  - ECCD, [97](#), [99](#)
  - LHCD, [33](#), [55](#), [86](#), [95](#)
- ARE, [41](#), [42](#)
- assumptions
  - $A_1$ , [72](#)
- CLF, [64](#)
- constrained control, [78](#)
- control
  - finite dimensional
  - LQR, [38](#)
- Convergence Rate Control, [66](#)
- delay, [99](#)
- disturbance
  - ECCD, [101](#)
  - ECRH, [104](#)
  - ICRH, [95](#), [96](#)
- equilibrium, [30](#)
- Global Exponential Stability, [66](#)
- ISS-Lyapunov function, [67](#)
- LMI, [49](#)
- LPV, [46](#)
- magnetic flux
  - poloidal, [27](#)
  - toroidal, [29](#)
- norm
  - $L^2([0, 1])$ , [59](#), [63](#)
  - $L^2(\Omega)$ , [59](#)
  - $f$ -norm, [63](#)
- poloidal field
  - effective, [27](#), [32](#)
- polytope, [48](#)
- properties
  - $P_1$ , [32](#)
  - $P_2$ , [32](#)
  - $P_3$ , [32](#)
  - $P_4$ , [67](#)
- regularity, [32](#)
- resistivity profiles, [116](#)
- robustness
  - actuation errors, [68](#)
  - boundary disturbances
    - D<sup>1</sup>-ISS, [72](#)
    - ISS, [90](#)
  - estimation errors
    - $\eta$ , [69](#)
    - $z$ , [69](#)
    - ISS, [67](#)
- rotational transform, [34](#)
- safety factor, [32](#), [34](#)
- simulation code
  - $\psi_{sim}$ , [78](#)
  - METIS, [92](#), [95](#), [97](#)
  - RAPTOR, [97](#)
- strict Lyapunov function, [58](#)
- TCV, [99](#)
- tracking, [81](#)
- variables
  - definition, [28](#)
- weighting function, [116](#)